PROGRESS REPORT (A)
Grant NGL 34-002-047
April 2, 1971

"STUDY OF RECTANGULAR-GUIDE-LIKE STRUCTURES FOR MILLIMETER WAVE TRANSMISSION"

to
The National Aeronautics and Space Administration, Washington, D. C.

DEPARTMENT OF ELECTRICAL ENGINEERING
NORTH CAROLINA STATE UNIVERSITY
RALEIGH, NORTH CAROLINA

PROGRESS REPORT (A)
Grant NGL 34-002-047
April 2, 1971

"STUDY OF RECTANGULAR-GUIDE-LIKE STRUCTURES FOR MILLIMETER WAVE TRANSMISSION"

to
The National Aeronautics and Space Administration, Washington, D. C.

North Carolina State University
Raleigh, North Carolina

Submitted: F J Tischer

Dr. Frederick J. Tischer, Professor
Principal Investigator

SUMMARY

This report represents the final report on work carried out under Grant NGL 34-002-047 during the period ending June 30, 1971. The report deals with the effects of surface roughness on conduction losses in waveguides and resonators at 35 GHz. The study was carried out by Lyles C. Adair under the direction of Dr. Frederick J. Tischer as dissertation research for the degree of Doctor of Philosophy at the North Carolina State University, Raleigh, North Carolina.

ABSTRACT

ADAIR, LYLES CORNWELL. Effects of Surface Roughness on the Conduction Losses at Millimeter Wavelengths. (Under the direction of FREDERICK JOSEPH TISCHER)

The effects of surface roughness on conduction losses were investigated by measuring roughness parameters of metallic surfaces by an optical technique and correlating them with the measured quality factors of two types of resonators at 35 GHz.

A new technique with improved accuracy for measuring the statistical parameters of a rough surface was developed. The reflectance of a rough surface illuminated by a laser was observed to contain all of the information needed to completely define the surface characteristics. Theoretical expressions used for the scattered light were derived on the assumption that the surface had a one-dimensional roughness, characterized by a Maxwell height density function and a Laplace correlation function. The measured intensity of light reflected from rough surfaces was found to be in good agreement with the theoretical values which were based on statistical parameters obtained for the surfaces by a microscopic study. The microscopic results for surfaces polished in one direction with abrasive papers showed that best approximations can be obtained by Maxwell density and Laplace functions for the statistical properties. Earlier models based on isotropic surfaces and Gaussian statistics were not in agreement with the light reflectance measurements.

Using a demountable rectangular structure for a conventional and a closed H-guide resonator, variations in surface losses with surface roughness were measured. The derivations of Q-values for the two resonators showed that the fields in the closed H-guide provided an improved method for measuring surface losses as a function of surface roughness. The side walls of the resonator were the only sections removed from the test structure, and the surface roughness created on the side walls by abrasive polishing was measured by the optical technique. By normalization of the Q of the side walls, the change of surface losses in per cent was shown to be greatly effected by the correlation factor of the surface roughness. No conclusive results by this evaluation could be found relating the losses to the rms height variation. The scattering of data was found to be much less for the closed H-guide resonator illustrating the improvement obtained by the use of this resonator. Included in the study were observations of the effects caused by electropolishing and other types of surface preparation.

TABLE OF CONTENTS

TABLE OF CONTENTS (continued)

LIST OF TABLES

LIST OF FIGURES

LIST OF FIGURES (continued)

LIST OF FIGURES (continued)

LIST OF FIGURES (continued)

1. INTRODUCTION

The increasing demands for high frequencies in communication has caused much concern in the millimeter wavelength region of the electromagnetic spectrum. Operations at these frequencies impose some serious problems. The conventional waveguide size is greatly reduced and causes serious manufacturing problems. Not only does size decrease the power handling capability but attenuation increases rapidly with frequency for such waveguides. Possible alternatives are other guide structures, such as the H-guide, but the major concern is that the depth of penetration of electromagnetic waves into the metallic surface is very small at these frequencies. Because of the small penetration, the surface conditions of the guide play an important role in the attenuation of the guide. Of course bulk properties, such as conductivity, provide a great contribution to losses, but chemical films and surface irregularities now produce major effects.

Many investigators have observed the discrepancy between the theoretical values and the measured values of losses in waveguide structures. Maxwell [15] attempted to show the difference by measuring the r-f and dc conductivity of drawn copper. Although he observed differences, the effects of surface roughness could not be properly evaluated because there were no reliable methods for measuring roughness.

Morgan [17] used models to illustrate the increase of losses due to surface roughness but his theoretical models could not satsifactorily be related to the actual case. Benson [5] investigated the effects of roughness in rectangular waveguides of drawn copper for TE field modes. Benson cut sections of waveguides and examined them microscopically to determine roughness. These microscopic examinations for determining roughness did not give well defined relationships to surface losses. Previous investigators who had used profilometer measurements knew such measurements were not accurate. Non only existed serious limitations for measuring roughness mechanically and microscopically, but improved measurement techniques for measuring losses were needed also. With these problems in mind, an investigation of surface effects on surface resistivity was initiated. The intent of the study was to clearly define surface roughness, both theoretically and experimentally, and then to find a meaningful relationship between surface roughness and surface resistance.

This investigation is concerned with first providing a means of determining an index of the surface irregularity for a one-dimensionally rough surface and then relating the index to the surface losses in waveguides in the 35 GHz frequency range. The index of the surface irregularity is based on the scattering theory of light from rough surfaces and the statistical properties of the surface. An apparatus

is developed for verifying a theoretical model of the surface by measuring the reflected light from it and is then used to measure the statistical parameters.

The characteristics of a shorted H-guide section indicate that properties of such a structure has the possibility of an improved technique for measuring losses. Two types of waveguides, H-guide and rectangular, are employed. The side walls of these shorted waveguide sections are used to determine the effects of the surface parameters on the losses. Wall losses, found by Q-value measurements, are then related to the surface parameters.

2. REVIEW OF LITERATURE

2.1 R-F Conductivity Measurements

As a result of the rapid advances of microwaves during World War II, some areas were not investigated in depth in order to achieve the short range goals. One of these areas dealt with losses and their causes in waveguide structures. It was observed that the losses in waveguides were higher than predicted by the dc conductivity of the metal. Accurate determination of the dc conductivity was needed to assure that variations in metals were not the source of the error. Arsenic and antimony are the two impurities likely to be found in refined copper which strongly decreases the dc conductivity; thus 0.0013 percent As or 0.0071 per cent Sb lowers it one per cent [9, 18]. Oxygen oxidizes the copper, forming Cu_2O which reduces the conductivity. Therefore the conductivity of copper, through oxidization, decreases by aging.

Many investigators in the 1940's studied the effects of increasing frequency on the conductivity of metals. Maxwell [15] in 1947 published the results of an investigation of r-f conductivity in the 1.25 cm region. He first measured the attenuation of a long, shorted section of waveguide. The attenuation of waves in the TE_{10} mode at 1.25 cm reduces to

$$\alpha = 299/\sigma^{1/2} \quad \text{nepers per meter} \qquad (2.1)$$

for a 0.17 in. by 0.42 in. waveguide. Maxwell used as a

second method the Q-values of a rectangular resonator with demountable sections. From the Q-values the effective conductivity was determined. As a result of his experiments, Maxwell found the effective conductivity of drawn copper was 4.0×10^7 mhos per meter at 1.25 cm where the dc value was 5.48×10^7 mhos per meter. He made many attempts to polish the walls both mechanically and electrolytically but with little effect. Maxwell believed that the primary difference in dc and r-f conductivity was surface roughness but at that time no realiable index of surface roughness was available.

Beck and Dawson [2] reported in 1950 the results of an investigation of conductivity measurements at microwave frequencies (9 GHz). The method used was to determine the Q-value of an open-ended coaxial line having as a center conductor the sample being tested. The measurements included samples which were polished by mechanical and electrolytical procedures. Their results indicate that surface roughness does play a role in the losses but the observations were by microscopic examination. These observations did not give an index of roughness but only a qualitative trend. The results of a prepared sample with a smooth 60° V thread on the surface showed a reduction of the Q-value to about 40 per cent of the smooth value, whereas a model proposed by Morgan [17] predicted 50 per cent of the smooth value.

Thorp [23] showed at 8 mm that surface roughness as well as stress in the metal surface affects the dc conductivity. He did not attempt to determine a relationship between surface roughness and conductivity. Lending [13] investigated the conductivity of metals at 3 GHz as a function of surface roughness but failed to indicate the method of determining surface roughness. Other investigators [8, 10] have acknowledged the influence of surface roughness on conductivity and used various methods to improve the loss characteristics.

2.2 Model for Predicting Roughness Effects

Morgan [17] in 1949 proposed surface models to predict the increased losses caused by rough surfaces. Studies at Bell Telephone Laboratories had revealed that losses in the neighborhood of 3 cm had material losses higher than calculated, by amounts ranging from 10 to 60 per cent. According to Morgan [17]

> these discrepancies cannot be explained as attributable to the deviations from Ohm's law which occur when the eddy current skin depth becomes less than the mean free path of electrons in the metal, or when the period of the electromagnetic oscillations becomes comparable with the mean time between collisions of an electron with the crystalline lattice, since it now appears that the latter effects will be encountered in good conductors at room temperature only if the wavelength is shorter than a few tenths of a millimeter.

Morgan used a two-dimensional model with periodic rectangular or triangular gooves transverse to the direction

of current flow (Figure 2.1). Since the grooves are small as compared to the dimensions of the apparatus, the fields within the groove do not vary appreciably with depth. By taking the H-field constant with z and having only a z component, the wave equation becomes

$$\frac{\partial^2 H_z}{\partial x^2} + \frac{\partial^2 H_z}{\partial y^2} = 2 \frac{j}{\delta^2} H_z \qquad (2.2)$$

where δ is the skin depth. The solution of (2.2) substituted into

$$P = \frac{1}{2\sigma} \int_V (\nabla \times \underline{H}) \cdot (\nabla \times \underline{H}^*) \, d V, \qquad (2.3)$$

where σ is the conductivity, gives the power dissipated by the current in the conducting surface. If a cell of width d equal to the periodic displacement, of unit length in the z direction, has infinite depth, the integral may be transformed for one period into

$$P = - \left(\frac{1}{\sigma \delta^2}\right) I_m H_o^* \int_o^d \int_{-\infty}^{f(x)} H_z \, dy \, dx. \qquad (2.4)$$

For a plane surface the dissipated power becomes

$$P_o = \frac{|H_o|^2 d}{2\sigma\delta} . \qquad (2.5)$$

Therefore the ratio of the variational surface to the plane surface becomes

$$\frac{P}{P_o} = - \frac{2}{|H_o|^2 d \, \delta} I_m H_o^* \int_o^d \int_{-\infty}^{f(x)} H_z \, dy \, dx. \qquad (2.6)$$

Morgan used the "relaxation method," a numerical technique,

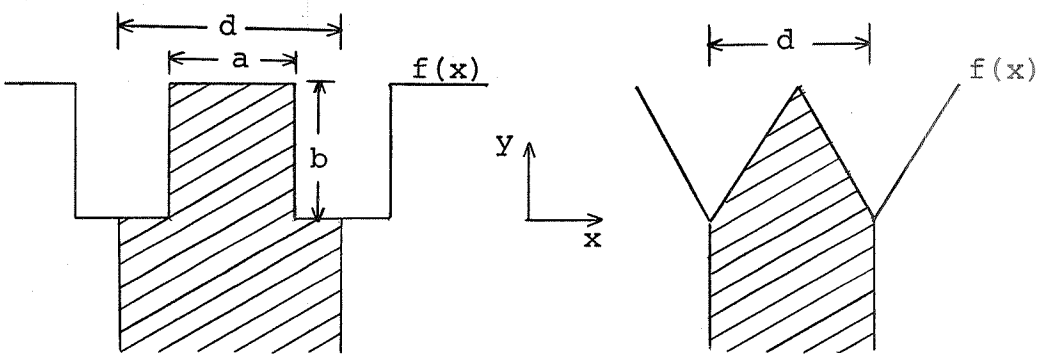

Figure 2.1. Cross sections of Morgan's surface profiles

to solve (2.2) in order to determine the relative power dissipation from (2.6). Morgan's model gave for different values of the ratio of rms roughness to skin depth the numerical values recorded in Table 2.1. It should be noted that for the dimensional restrictions used by Morgan the relative power dissipation will approach the asymptotic value of 2.0 for the three profiles given in the table.

2.3 A Model for Waveguide Attenuation as Affected by Roughness

In 1953 Benson [5] reported a modification to the attenuation formula derived by Kuhn [12]. The modification provided a correction for the additional surface area created by a rough surface. Benson used a long shorted section of rectangular waveguide to measure the attenuation. Using the VSWR of a shorted section, he found by these measurements the attenuation. Benson took samples cut from walls of the waveguides and mounted them in a Perspex mould. The composite sample was polished by standard techniques and then photographed through a projection microscope. The actual surface was observed and a ratio of the length of the actual surface to that of an ideally smooth surface was determined. Benson used the modified formula of Kuhn to verify his findings, and for the H_{01} mode the formula becomes

$$\alpha = \left[\frac{c}{\sigma} \frac{\mu_1}{\mu} \left(\frac{\varepsilon}{\mu}\right) \right]^{1/2} \frac{\lambda_g}{\lambda_e^{3/2}} \left(\frac{K_{T2} \lambda_e^2}{b \lambda_{cr}^2} + \frac{K_{T1}}{2a} \right) K_p \qquad (2.7)$$

Table 2.1 Relative power dissipation versus root-mean-square roughness for surface grooves transverse to current flow

Δ/δ [a]	Square a:b:d=1:1:2	Rectangular a:b:d=3:2:4	Triangular d=2δ/3
0.00	1.00	1.00	1.00
0.25	1.04	--	--
0.43	--	1.25	--
0.50	1.17	--	1.24
0.87	--	1.60	--
1.00	1.57	--	1.61
1.52	--	1.72	--
1.67	--	--	1.80
1.75	1.75	--	--

[a] Δ/δ ratio of rms roughness, Δ, to skin thickness, δ

where α = the attenuation

c = velocity of light

σ = conductivity of metal

μ = permeability of dielectric

ε = permittivity of dielectric

λ_g = guide wavelength

λ_e = wavelength in unbounded dielectric

λ_{cr} = critical guide wavelength (cut-off wavelength)

a = short dimension of waveguide

b = long dimension of waveguide

K_{T1} = ratio of length of actual surface to ideal for long dimension

K_{T2} = ratio of length of actual surface to ideal for short dimension

K_p = ratio of length of actual surface to ideal for longitudinal dimension

Although the Benson formulation gave a correct trend for increased attenuation resulting from roughness, he concluded [5]

> in view of the difficulty of determining accurate values for K_{T1}, K_{T2}, and K_p, it seems reasonable to conclude that the discrepancies between measured and calculated attenuation in waveguides are due solely to the roughness of the internal surface.

Benson doubted if any improvements in commercial waveguides at frequencies near or below 24 GHz were needed.

Allison and Benson [1] in 1954 updated Benson's previous report. The second report included a formula for any H mode,

$$\alpha = \left[\frac{c}{\mu}\frac{\mu_1}{\mu}\frac{\varepsilon}{\mu}^{1/2}\right]^{12}\frac{\lambda_g}{b\,\lambda_e}^{3/2}\left[(K_{T2}+\frac{b}{2a}K_{T1})\frac{\lambda_e^2}{\lambda_{cr}^2}+K_p\frac{b}{2a}(1-\frac{\lambda_e^2}{\lambda_{cr}^2})\right] \tag{2.8}$$

Although the models proposed by Benson gave the correct trend for increasing losses due to the surface roughness, the measured values were still greater than predicted. Later Benson explained the difference by saying that the surface contains cavity-like features caused during the manufacturing process of waveguides[1]. Such features would increase the losses more than the originally proposed increase of surface area due to roughness. But this explanation is limited to drawn waveguides.

2.4 A Statistical Model for Predicting Reflectance from a Rough Surface

Although much speculation has been done on the characteristic of the wall losses, correlation with the actual surface parameters has been limited to procedures such as that used by Benson. In optics many investigators have studied the reflection of light from rough surfaces.

Davies [7] in 1954 introduced the first statistical model for predicting reflection of electromagnetic waves from a rough surface. He assumed a perfectly conducting surface and used diffraction theory to illustrate the model.

---

[1] Personal communication between F. Benson and F. Tischer.

By considering a distribution of heights z being of the Gaussian form,

$$p(z) = \frac{1}{\sigma\sqrt{2\pi}} \exp\left(-\frac{z^2}{2\sigma^2}\right) \tag{2.9}$$

where σ is the height density parameter, he found the steady field reflected from the surface for the slightly rough case, $z/\lambda << 1$ and $\sigma/\lambda << 1$,

$$\langle\xi\rangle = \frac{A}{2\lambda r}(\cos\theta + \cos\psi)\frac{\sin\left[\frac{\pi\ell}{\lambda}(\sin\theta\cos\phi - \sin\psi)\right]}{\pi/\lambda(\sin\theta\cos\phi - \sin\psi)} \tag{2.10}$$

$$\frac{\sin\left(\frac{\pi m}{\lambda}\sin\theta\sin\phi\right)}{\pi/\lambda\sin\theta\sin\phi} \exp\left[-\frac{2\pi^2\sigma^2}{\lambda^2}(\cos\theta + \cos\psi)^2\right],$$

λ = wavelength of incident light

A = amplitude of incident light

ℓ, m = dimensions of reflectors

ψ = angle of incidence

θ, ψ = angles of scattering.

In order to determine the reflected intensity, the auto-correlation function is needed and Davies assumed one of the Gaussian form,

$$R(\tau) = \sigma^2 \exp\left\{-\frac{1}{a^2}\left[(\tau_x)^2 + (\tau_y)^2\right]\right. \tag{2.11}$$

where a = correlation parameter

τ_x = variation with x

τ_y = variation with y.

Using the Gaussian correlation model and the appropriate integration, the diffused reflected intensity becomes

$$\langle |\xi - \langle\xi\rangle|^2 \rangle = \frac{\pi^3 A^2 a^2 \sigma^2 \ell m}{\lambda^4 r^2} (\cos\theta + \cos\psi)^4$$

$$\cdot \exp\left\{-\frac{\pi^2 a^2}{\lambda^2}\left[(\sin\theta\cos\phi - \sin\psi)^2 + \sin^2\theta\sin^2\phi\right]\right\} \quad (2.12)$$

From this, Davies concluded that the diffused reflected intensity for the slightly rough case can be determined from the two statistical properties a and σ. His conclusions were based on the following assumptions: 1) a perfectly conducting surface, 2) a Gaussian density function for the height variation, and 3) a Gaussian auto-correlation function where the variation with x and y are identical.

2.5 Improved Reflectance Models

Bennett and Porteus [4] proposed in 1961 a modification to Davies' results for a finite conducting surface. The modification was confined to near normal incident light and rms roughness, σ, that met the requirement of $\sigma/\lambda \ll 1$. If one examines Davies' results for a slightly rough surface, the normal incident radiation reduces to

$$R_s = R_o \exp\left(-(4\pi\sigma/\lambda)^2\right) \quad (2.13)$$

where R_s = specular reflectance

R_o = specular reflectance from a smooth surface

σ = rms height variation.

The diffused reflectance becomes

$$R_d = R_o \frac{2^5\pi^4}{m^2} (\sigma/\lambda)^4 (\Delta\theta)^2 \quad (2.14)$$

where m = rms slope of the surface profile

$\Delta\theta$ = acceptance angle of measuring instrument.

The total reflected intensity is given by

$$R = R_o \exp\left[-(4\pi\sigma/\lambda)^2\right] + R_o \frac{2^5\pi^4}{m^2} (\sigma/\lambda)^4 (\Delta\theta)^2 \quad (2.15)$$

and if the condition that $\sigma/\lambda \ll 1$ is used then only the specular reflectance needs to be considered. Experimental data gathered by Bennett and Porteus verify the accuracy of the model for $\sigma/\lambda \ll 1$ but divergence occurs as $\sigma/\lambda \to 1$. The experimental concept of their program was, given a rough surface, what affect would result in the reflectance for a range of wavelengths of light.

The results of their experiment showed the increased accuracy of the reflectance method over the Profilometer for determining rms surface roughness. Since the Profilometer stylus tip has a radius of approximately 1000 μ in., it should not bottom in the grooves and therefore the light reflectance method would give the better accuracy.

Others [26,6], notably two groups at the University of Minnesota, Torrance and Sparrow, and Birkebak and Eckert, carried out experimental investigation of the reflection of light from rough surfaces, both metals and non-metals. Lacking other theoretical models for predicting reflectance, their results for metallic surfaces were in good agreement with Davies' model. The surfaces for both groups were considered isotropic in all directions.

3. REFLECTANCE THEORY

3.1 Introduction

The reflection from a metallic surface with a mirror-like finish is known to occur at an angle to the normal equal to the incident angle. The coefficient of reflection for such a case is determined by the bulk properties of the metal. For a surface containing irregularities, i.e. height variations about the mean, the reflected light contains both specular and diffused parts. The diffused part results from the many variations in the slopes of the surface and is scattered in all directions for a random rough surface. A statistical model first formulated by Davies [7] provides a tool for predicting the nature of the reflectance from such random rough surfaces. His model is for a surface having isotropic properties. The analysis of surfaces having parallel grooves in their surfaces are given in the following two sections. By normalization, it is shown that the model will provide a form of diffused reflectance that depends on only the auto-correlation parameter.

3.2 The Gaussian Density and Correlation Function Model

The surface is assumed to have parallel grooves along the y axis and the height variations of the surface irregularity is a function of only the x dimension. The coordinate system is illustrated in Figure 3.1. According to diffraction theory [7] and based on the coordinate system the reflected

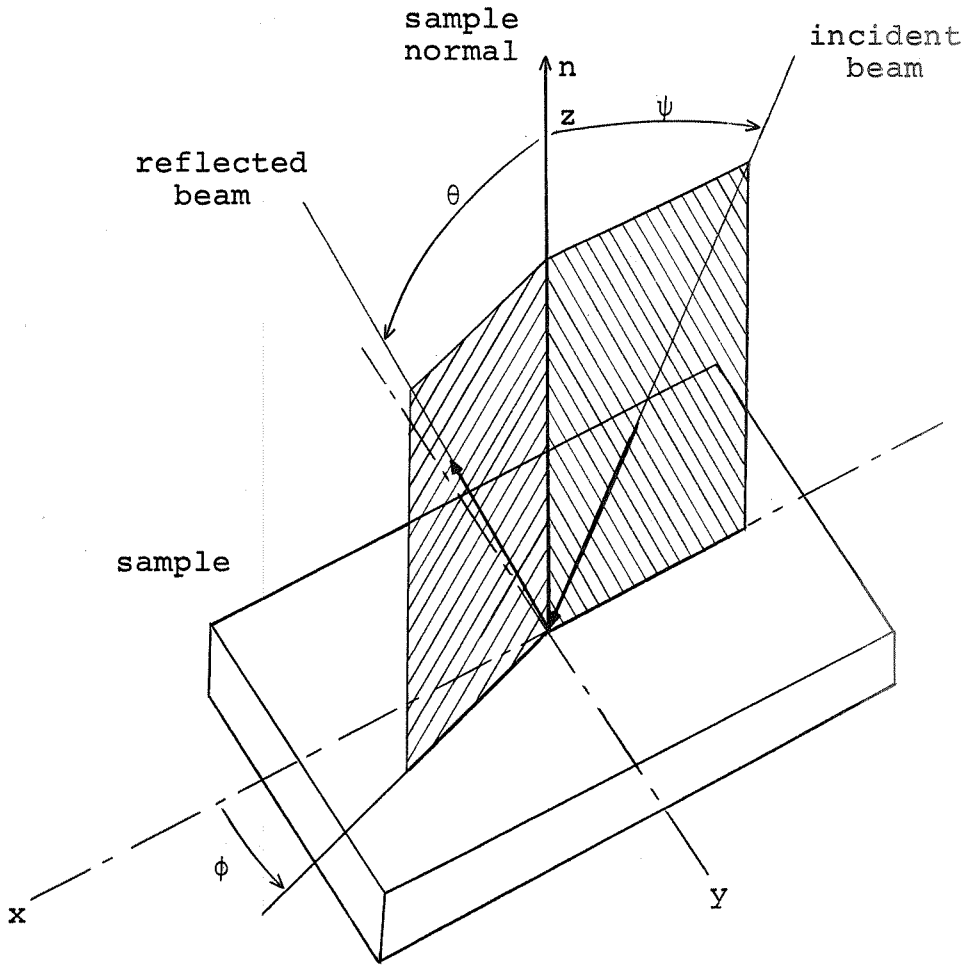

Figure 3.1. Basic coordinate system for reflectance theory

field, ξ is

$$\xi = \int_{-\ell/2}^{\ell/2}\int_{-m/2}^{m/2} dy\ dx\ \frac{A}{2\lambda r}\ (\cos\theta+\cos\psi)\ \exp\{\frac{2\pi}{\lambda}\ j\ [x(\sin\theta\cos\phi-\sin\psi) + y\ \sin\theta\sin\phi + z\ (\cos\theta+\cos\psi)]\} \qquad (3.1)$$

for a plane wave obliquely incident on an imperfectly smooth rectangular reflector of dimensions ℓ and m. The amplitude of the incident wave is given by A, and r represents the displacement from the reflector to the point of observation. In this integral z is a random, continuous function of position, i.e. of x, with certain statistical properties.

For the proposed surface, the variation in the y dimension is assumed to be zero, and therefore no light is reflected except in the direction indicated by ϕ being equal to zero. Thus (3.1) reduces to

$$\xi = \int_{-\ell/2}^{\ell/2}\int_{-m/2}^{m/2} dy\ dx\ \frac{A}{2\lambda r}\ (\cos\theta+\cos\psi)\exp\{\frac{2\pi}{\lambda}\ j\ [x(\sin\theta-\sin\psi) + z\ (\cos\theta+\ \cos\psi)]\}. \qquad (3.2)$$

If the surface is smooth, z=0, then

$$\xi = \frac{A}{2\lambda r}\ \ell\ m\ (\cos\theta+\cos\psi)\ \frac{\sin\ [\frac{\pi\ell}{\lambda}\ (\sin\theta-\sin\psi)]}{\pi\ell/\lambda\,(\sin\theta-\sin\psi)}\ . \qquad (3.3)$$

The important functions of ξ needed to define the diffused reflections are $\langle\xi\rangle$ and $\langle|\xi-\langle\xi\rangle|^2\rangle$. The term $\langle\xi\rangle$ is the steady field and $\langle|\xi-\langle\xi\rangle|^2\rangle$ is the diffused reflected intensity.

The total reflected intensity is

$$\langle|\xi|^2\rangle = \langle\xi\rangle^2 + \langle|\xi - \langle\xi\rangle|^2\rangle \ . \qquad (3.4)$$

In order to determine $\langle\xi\rangle$, the probability density function must be defined. Assuming the density function to be Gaussian, it is

$$p(z) = \frac{1}{\sigma\sqrt{2\pi}} \quad \exp\{-z^2/2\sigma^2\} \ . \qquad (3.5)$$

Now

$$\langle\xi\rangle = \frac{A}{2\lambda r}(\cos\theta+\cos\psi)\iint\langle\exp\{\frac{2\pi}{\lambda} j\, z\,(\cos\theta+\cos\psi)\}\rangle$$

$$\cdot \exp\{\frac{2\pi}{\lambda} j\, x\,(\sin\theta-\sin\psi)\}\ dx\ dy. \qquad (3.6)$$

Then it follows using the probability function

$$\langle\exp\{\frac{2\pi}{\lambda} j\, z(\cos\theta+\cos\psi)\}\rangle = \exp\{-\frac{2\pi^2\sigma^2}{\lambda^2}(\cos\theta+\cos\psi)^2\}. \qquad (3.7)$$

Therefore

$$\langle\xi\rangle = \frac{A}{2\lambda r}(\cos\theta+\cos\psi)\ \ell\ m\ \frac{\sin[\frac{\pi\ell}{\lambda}(\sin\theta-\sin\psi)]}{\pi\ell/\lambda\,(\sin\theta-\sin\psi)}$$

$$\cdot\exp\{-\frac{2\pi^2\sigma^2}{\lambda^2}(\cos\theta+\cos\psi)^2\} \ . \qquad (3.8)$$

The reflection is modified by a factor depending on σ/λ. Furthermore,

$$\xi - \langle\xi\rangle = \frac{A}{2\lambda r}(\cos\theta+\cos\psi)\iint\exp\{\frac{2\pi}{\lambda} j\, x\,(\sin\theta-\sin\psi)\}$$

$$[\exp\{\frac{2\pi}{\lambda} j\, z(\cos\theta+\cos\psi)\}-\exp\{-\frac{2\pi^2\sigma^2}{\lambda^2}(\cos\theta+\cos\psi)^2\}]\ dx\ dy. \qquad (3.9)$$

For a slightly rough surface, the following inequalities are assumed $z/\lambda \ll 1$, and $\sigma/\lambda \ll 1$. Then neglecting powers of z/λ and σ/λ beyond the first term

$$\xi-\langle\xi\rangle=\frac{j\pi A}{\lambda^2 r}(\cos\theta+\cos\psi)^2\iint z(x)\exp\{\frac{2\pi}{\lambda}jx(\sin\theta-\sin\psi)\}dxdy. \quad (3.10)$$

The intensity averaged over the ensemble of reflectors is

$$\langle|\xi-\langle\xi\rangle|^2\rangle = \frac{\pi^2A^2}{\lambda^4r^2}(\cos\theta+\cos\psi)^4\iiiint \langle z(x)\ z(x')\rangle$$

$$\exp\{\frac{2\pi}{\lambda}j(x-x')(\sin\theta-\sin\psi)\}dx\ dy\ dx'\ dy'. \quad (3.11)$$

Here, the important statistical factor is the auto-correlation function of the height of the surface. Assuming a Gaussian model, the auto-correlation is

$$\langle z(x)z(x')\rangle = \sigma^2\ \exp\{-\frac{(x-x')^2}{a^2}\} \quad (3.12)$$

where a is the correlation parameter. Then writing $x'=x+\tau$ gives

$$\langle|\xi-\langle\xi\rangle|^2\rangle = \frac{\pi^2A^2}{\lambda^4r^2}(\cos\theta+\cos\psi)^4\iiiint \sigma^2\ \exp\{-\frac{\tau^2}{a^2}\}$$

$$\exp\{\frac{2\pi}{\lambda}j\ \tau(\sin\theta-\sin\psi)\}\ dx\ dy\ d\tau\ dy'. \quad (3.13)$$

Then, consider the domain of integration

$$-\ell/2\le x\le\ell/2 \qquad -m/2\le y\le m/2$$
$$-\ell/2\le x+\tau\le\ell/2 \qquad -m/2\le y'\le m/2.$$

If $\ell>>a$, then the domain may be approximated by

$$-\ell/2\le x\le\ell/2 \qquad -m/2\le y\le m/2$$
$$-\infty\le\tau\le\infty \qquad -m/2\le y'\le m/2.$$

It then follows

$$\langle|\xi-\langle\xi\rangle|^2\rangle \frac{\pi^{5/2}A^2a\sigma^2\ell m^2}{\lambda^4r^2}(\cos\theta+\cos\psi)^4\exp\{-\frac{\pi^2a^2}{\lambda^2}(\sin\theta-\sin\psi)^2\}. \quad (3.14)$$

If the diffused reflected intensity is normalized with respect to the intensity at $\theta=\psi$, then

$$\langle|\xi-\langle\xi\rangle|^2\rangle_N=\left(\frac{\cos\theta+\cos\psi}{2\cos\psi}\right)^4 \exp\left\{-\frac{\pi^2a^2}{\lambda^2}(\sin\theta-\sin\psi)^2\right\}. \quad (3.15)$$

The normalized diffused intensity is a function of only one of the statistical parameters of the surface, designated by a.

3.3 The Maxwell Density and the Laplace Correlation Function Model

In the previous section, a symmetrical density function, Gaussian, was assumed. The density function selected for this section is asymmetric,

$$p(z) = \frac{1}{\alpha^3}\sqrt{\frac{2}{\pi}}\, z^2 \exp\left\{-\frac{z^2}{2\alpha^2}\right\}, \quad (3.16)$$

often referred to as a Maxwell density function. The second moment of the density function is often referred to as the rms value of the random variable z. For the Gaussian density function the rms value is σ. The Maxwell density function has a rms value equal to 0.674α. In most literature the symbol σ is used to represent the rms value.

Recalling (3.2),

$$\langle\xi\rangle=\frac{A}{2\lambda r}(\cos\theta+\cos\psi)\iint\left\langle\exp\left\{\frac{2\pi}{\lambda}j\,z\,(\cos\theta+\cos\psi)\right\}\right\rangle \exp\left\{\frac{2\pi}{\lambda}j\,x\,(\sin\theta-\sin\psi)\right\}\,dx\,dy, \quad (3.17)$$

then using the Maxwell density function

$$\left\langle\exp\left\{\frac{2\pi}{\lambda}j\,z\,(\cos\theta+\cos\psi)\right\}\right\rangle = \{1+\gamma^2\alpha^2\}\left\{1-\operatorname{erf}\left(\frac{\gamma\alpha}{\sqrt{2}}\right)\right\} \cdot \exp\left\{\frac{\gamma^2\alpha^2}{2}\right\} + \gamma\alpha\sqrt{2/\pi} \quad (3.18)$$

where $\gamma=\frac{2\pi}{\lambda}j\,(\cos\theta+\cos\psi)$.

Then for a slightly rough surface, the terms z/λ and α/λ to powers beyond the first are neglected. Therefore

$$\xi - \langle\xi\rangle = \frac{j\pi A}{\lambda^2 r} (\cos\theta+\cos\psi)^2 \iint z(x) \exp\{\frac{2\pi}{\lambda} jx(\sin\theta-\sin\psi)\} dx\, dy \tag{3.19}$$

This is the same expression obtained with the Gaussian density function for a slightly rough surface.

The diffused intensity averaged over the ensemble of reflectors is

$$\langle|\xi - \langle\xi\rangle|^2\rangle = \frac{\pi^2 A^2}{\lambda^4 r^2} (\cos\theta+\cos\psi)^4 \iiiint \langle z(x) z(x')\rangle \exp\{\frac{2\pi}{\lambda} j (x-x')(\sin\theta-\sin\psi)\} dx\, dy\, dx' dy' \tag{3.20}$$

As stated in the preceding section, the important statistical factor is the auto-correlation function. For this case, a Laplace model is used,

$$\langle z(x)\, z(x')\rangle = (0.674\alpha)^2 \exp\{ -\frac{|x-x'|}{2\beta} \}. \tag{3.21}$$

Then writing $x' = x + \tau$ gives

$$\langle|\xi - \langle\xi\rangle|^2\rangle = \frac{A^2\pi^2}{\lambda^4 r^2} (\cos\theta+\cos\psi)^4 (0.674\alpha)^2 \iiiint \exp\{-\frac{|\tau|}{2\beta}\} \exp\{-\frac{2\pi}{\lambda} j\tau(\sin\theta-\sin\psi)\} dx\, dy\, d\tau\, dy' \tag{3.22}$$

Considering the domain of integration where $\ell >> \beta$, then

$-\ell/2 \le x \le \ell/2$ $\qquad$ $-m/2 \le y \le m/2$

$-\infty \le \tau \le \infty$ $\qquad$ $-m/2 \le y' \le m/2$

Therefore,

$$\langle|\xi - \langle\xi\rangle|^2\rangle = \frac{A^2\pi^2\ell^2}{\lambda^4 r^2} (0.674\alpha)^2 \beta \frac{4(\cos\theta+\cos\psi)^4 \lambda^2}{\lambda^2+4\pi^2\beta^2(\sin\theta-\sin\psi)^2}. \tag{3.23}$$

If the diffused reflected intensity is normalized with respect to the intensity at $\theta=\psi$, then

$$\langle |\xi - \langle\xi\rangle|^2 \rangle_N = \left(\frac{\cos\theta+\cos\psi}{2\cos\psi}\right)^4 \frac{1}{1 + 4\pi^2\beta^2/\lambda^2(\sin\theta-\sin\psi)^2} . \tag{3.24}$$

Again the normalized diffused intensity is a function of only one of the statistical parameter of the surface, designated by β.

3.4 Comparison

For either case, the normalized diffused reflected intensity is a function of only one of the statistical parameters of the surface, the correlation factor. It is obvious that both normalized functions have the common factor

$$\left(\frac{\cos\theta + \cos\psi}{2\cos\psi}\right)^4 .$$

For a given case where $a=\beta$, the normalized diffused reflected intensity based on the Laplace model has a sharper peak and longer trailing ends with the angle of reflectance. Recalling that 0.674α is equal to the rms value of the heights for the Laplace model, the diffused reflected intensity in both models are directly proportional to the product of the correlation parameters and the square of the rms height.

From these two models, it is reasoned that the reflected intensity with angle or reflectance is greatly dependent on the nature of the auto-correlation function.

4. EXPERIMENTAL EVALUATIONS OF MODEL

4.1 Introduction

To verify the validity of the models used in the previous chapter, the analysis of actual copper surfaces prepared in a certain manner is given. Copper samples were prepared to give a range of height variations, and on these samples, light reflectance measurements were made. The samples were cut and examined microscopically. From the microscopic examination, the statistical properties of the surface were determined. The statistical properties and the light reflectance measurements were correlated to determine the model best suited for predicting diffused reflected intensity for a one dimensionally rough surface. Three samples (Emery G-2, Grit 320, Grit 400) are used throughout the chapter for purposes of illustration.

4.2 Sample Preparation

A sheet of 1/8 inch copper was cut into 1-1/2 by 2 inch sections. Grinders manufactured by Buchler Ltd. were used to prepare the samples. There were two types of grinder; one consists of a set of abrasive papers mounted on dry, hard, flat surfaces and the other having the same type of mounting but a continuous flow of water immediately washed away the loose abrasive material and fragments of metal. These metallurgical grinders, both dry and wet, are commonly used for preliminary preparation in polishing of metal surfaces.

The copper surfaces were prepared in the following manner. First, the sample was moved forth and back on the coarsest grade of paper until grooves were present in only one direction. It was important that the grooves appear in only one direction since the finer paper can only remove the grooves created by the next coarses paper. The forces on the samples were held to a minimum to prevent crushing the abrasive particles which could cause large variations in the grooves or cause smoother surfaces than intended. The forces were only those to keep the samples in a position to create parallel grooves. The sample was then rotated ninety degrees and placed on the next finer paper. The process was continued until the desired degree of polishing was obtained. In this study, six grades of abrasive paper were used. The grain size of each abrasive paper is given in Table 4.1.

After each grinding, the samples were rinsed under running water to remove any loose material from the surface. A stream of air with sufficient force was blown across the surface to rapidly remove residual water, thus minimizing water spots. The surfaces were carefully handled to prevent finger prints or other stains and were stored in nitrogen-filled containers until reflectance studies could be made.

4.3 Apparatus for Reflectance Studies

The reflectance measurement set up is illustrated in Figures 4.1 and 4.2. The light source was a Spectra-Physics Model 124 Helium-Neon Laser capable of supplying fifteen

Table 4.1 Abrasive paper grain size

Grade	Grain size in microns
Emery 2	62
Emery 1	38
Grit 240	48
Grit 320	30
Grit 400	24
Grit 600	15

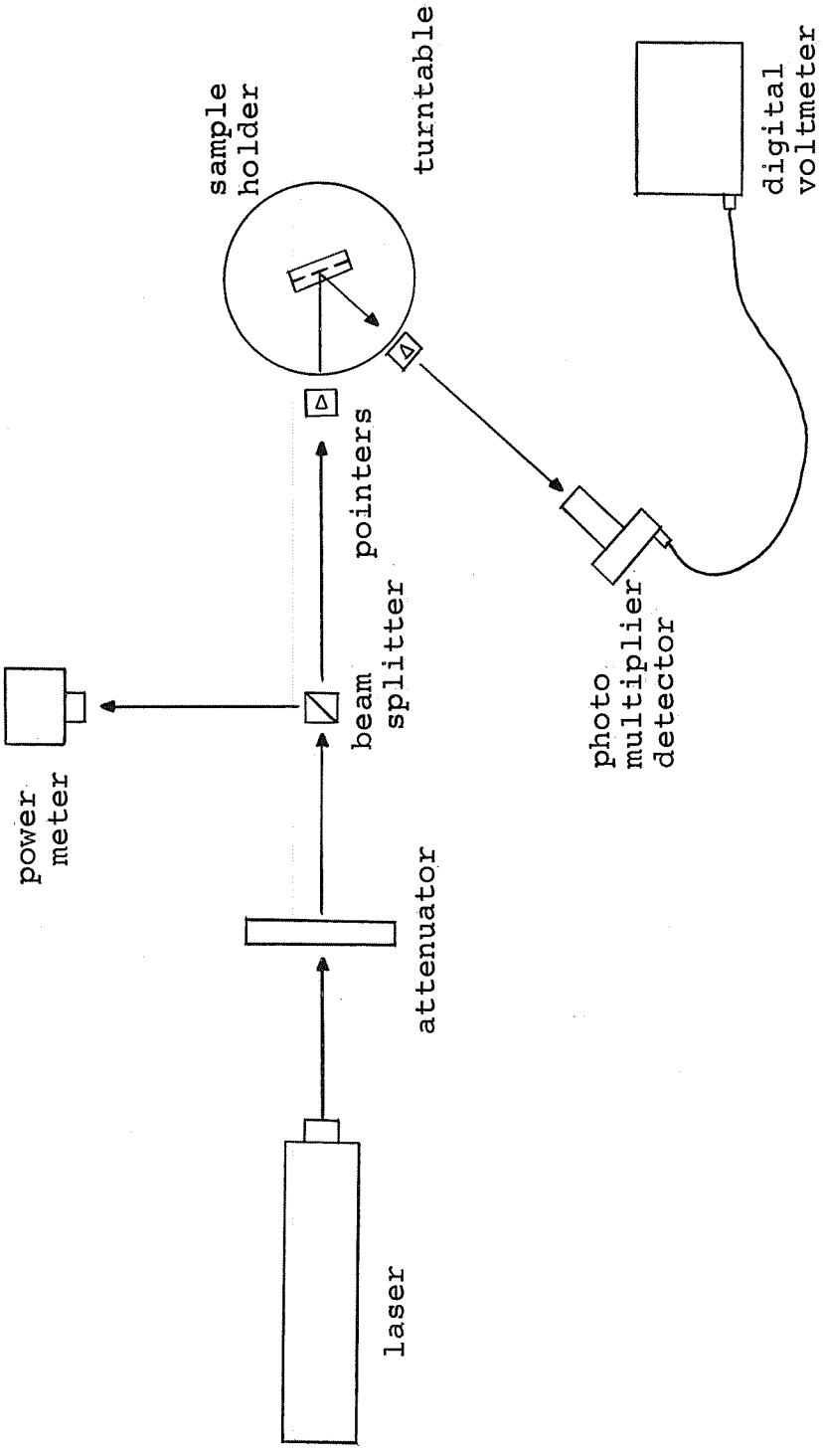

Figure 4.1. Schematic of reflectance measurement set up

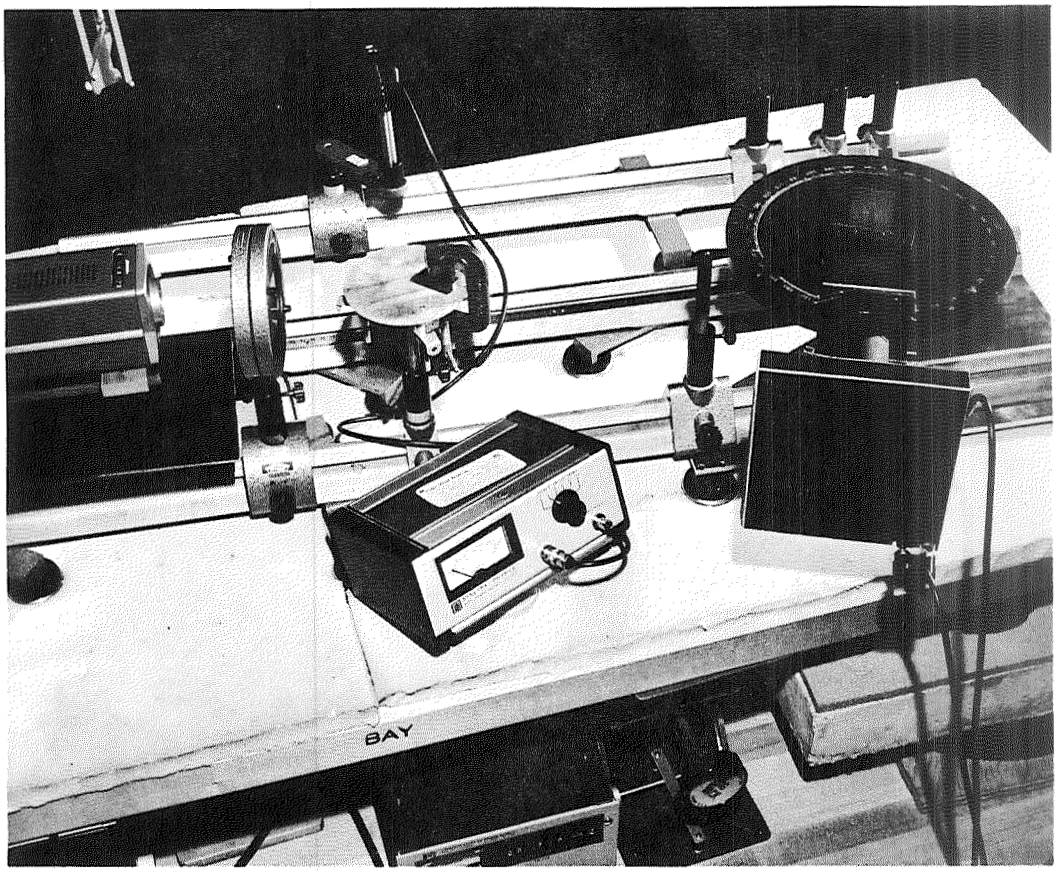

Figure 4.2 Photograph of the reflectance measurement bench

milliwatts of power at 6328 $\mathring{A}$. An adjustable attenuator with degree indicators along the circumference was used to regulate the light intensity that struck the test sample. The relative attenuation was determined by the angular displacement from a reference when applied to the sine square law. A continuous monitor of the source intensity was accomplished by a beam splitter which deflected part of the light into a Spectra-Physics 401 C power meter. If variation occurred during an experiment, the attenuation was adjusted to correct the change. A flat disc with a mounting stand located in the center was used to secure the test sample. The five inch radius disc had degrees marked off around the perimeter and with the aid of markers, the angles of incidence and reflectance were measured. An extension arm which pivoted about the center of the disc held a light detector which consisted of an RCA 7102 multiplier photo-tube and associated circuitry. The photo-tube was enclosed in a light tight cover with a one-eighth by one inch slit. The one-eighth inch slit which corresponded to less than one degree of arc measured the θ variation. The extension arm maintains the slit at a constant distance from the center of the disc and at a constant height above the plane of the disc. The power for the multiplier was supplied by a Hewlett-Packard Harrison 6516A DC power supply and the output of the detector was displayed on a Doric integrating microvoltmeter. The assembly, with the exception of the power supplies and the

voltmeter, was mounted on an optical rail which permitted accurate alighnment of the various components. The entire set-up was located in a dark room whose walls had been sprayed with a non-glossy black paint.

4.4 Reflectance Measurements

Three different sets of experimental data were taken from the set-up. For the first set, with the angle of incidence and incident light constant, and in a plane perpendicular to the surface, the intensity of the reflected light was measured at angles, θ, from the surface normal between 0 and 90 degrees. The output of a photomultiplier detector as a function of the angle of reflectance is illustrated in Figures 4.3, 4.4, and 4.5 for three prepared surfaces. The data were collected at three positions on the surface, in the center and plus and minus one-quarter of an inch from the center. The average output at each angle was computed and illustrated in the figures as a continuous curve.

By holding the incident angle constant and measuring the reflected intensity at the specular angle for various intensities of the incident light, a second set of data was collected. By adjustment of the precision attenuator (Figures 4.1 and 4.2), variations of the incident intensities were caused and detected by the power meter. The output of the photomultiplier detector as a function of the output of the power meter is shown in Figure 4.6. The results are illustrated as linear curves.

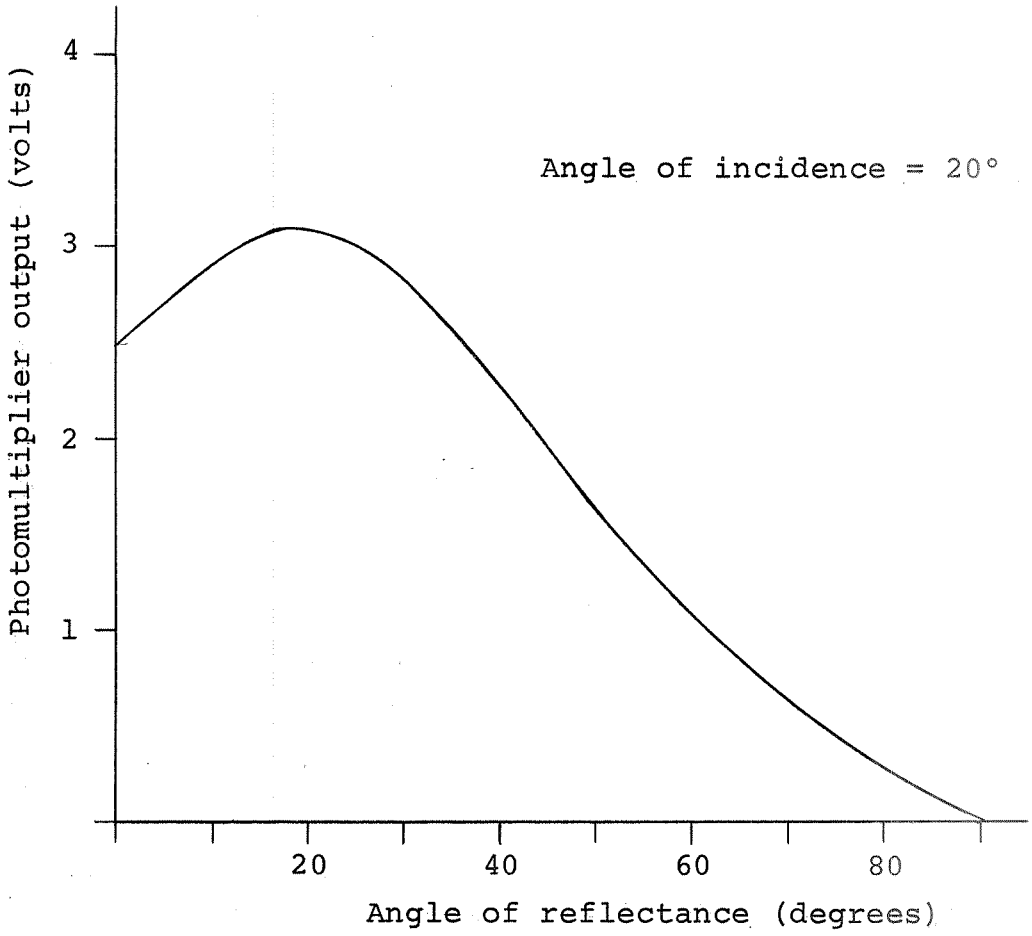

Figure 4.3. Reflected intensity of the Emery 2 (G-2) sample as a function of the angle of reflectance

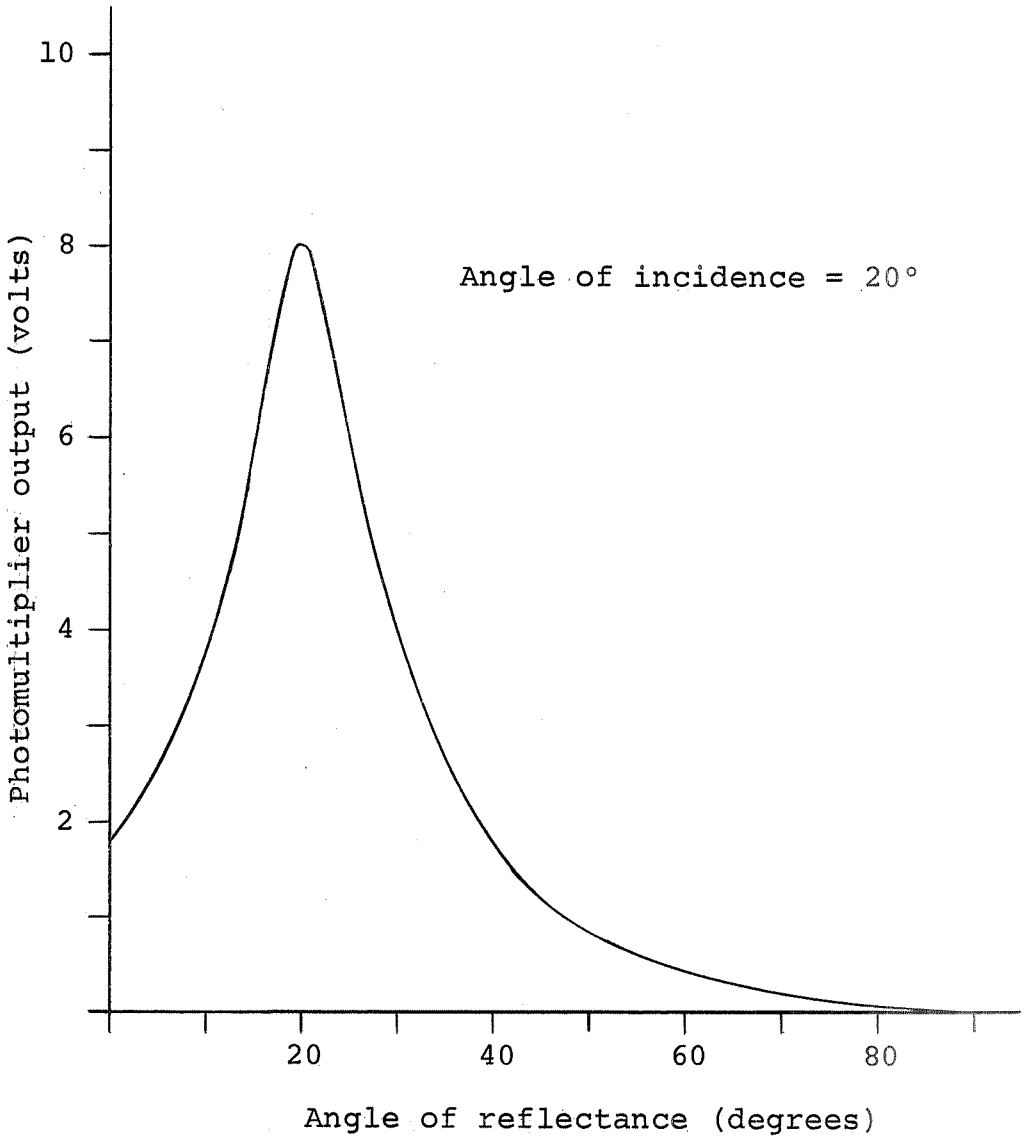

Figure 4.4. Reflected intensity of the Grit 320 (320) sample as a function of the angle of reflectance

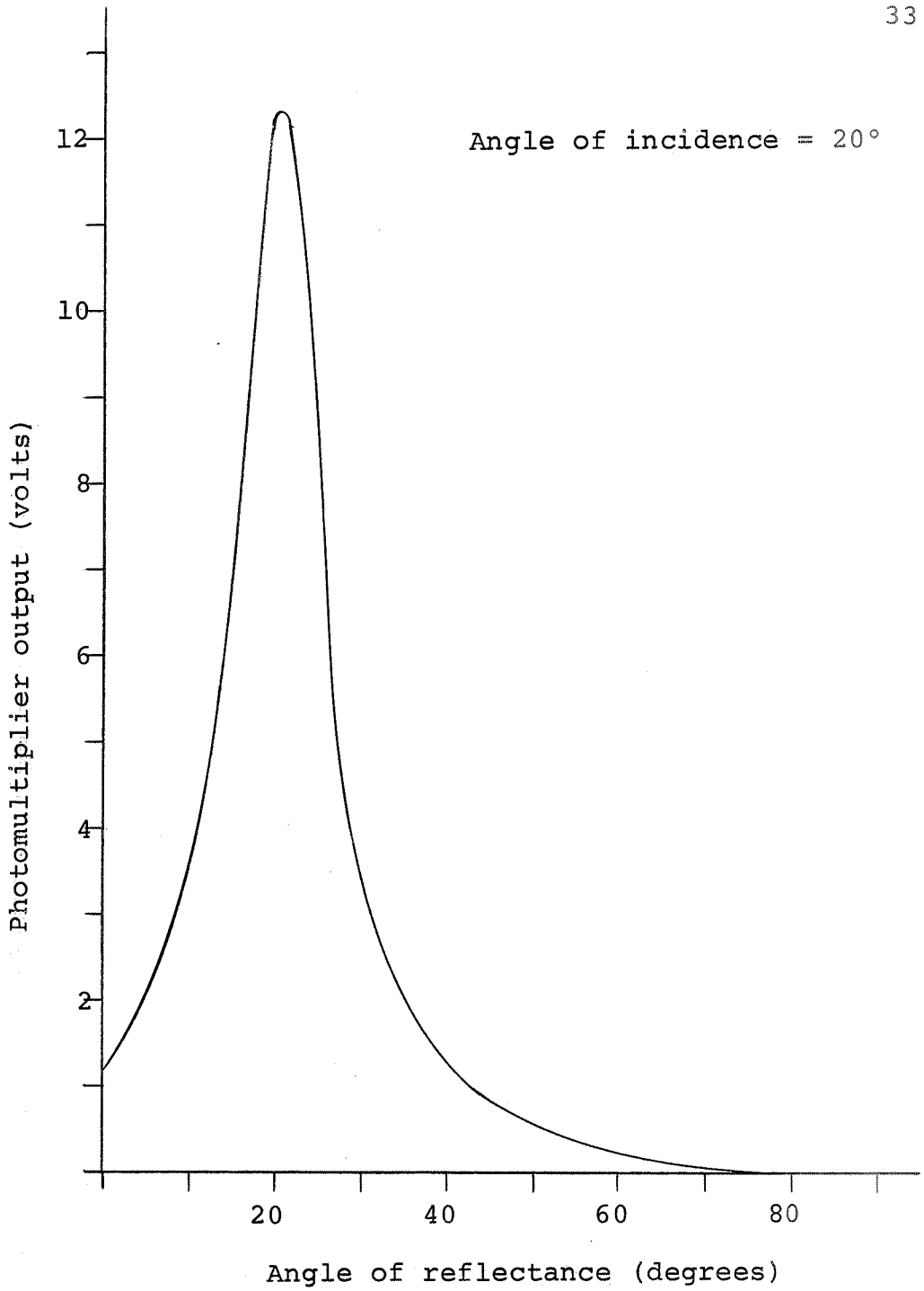

Figure 4.5. Reflected intensity of the Grit 400 (400) sample as a function of the angle of reflectance

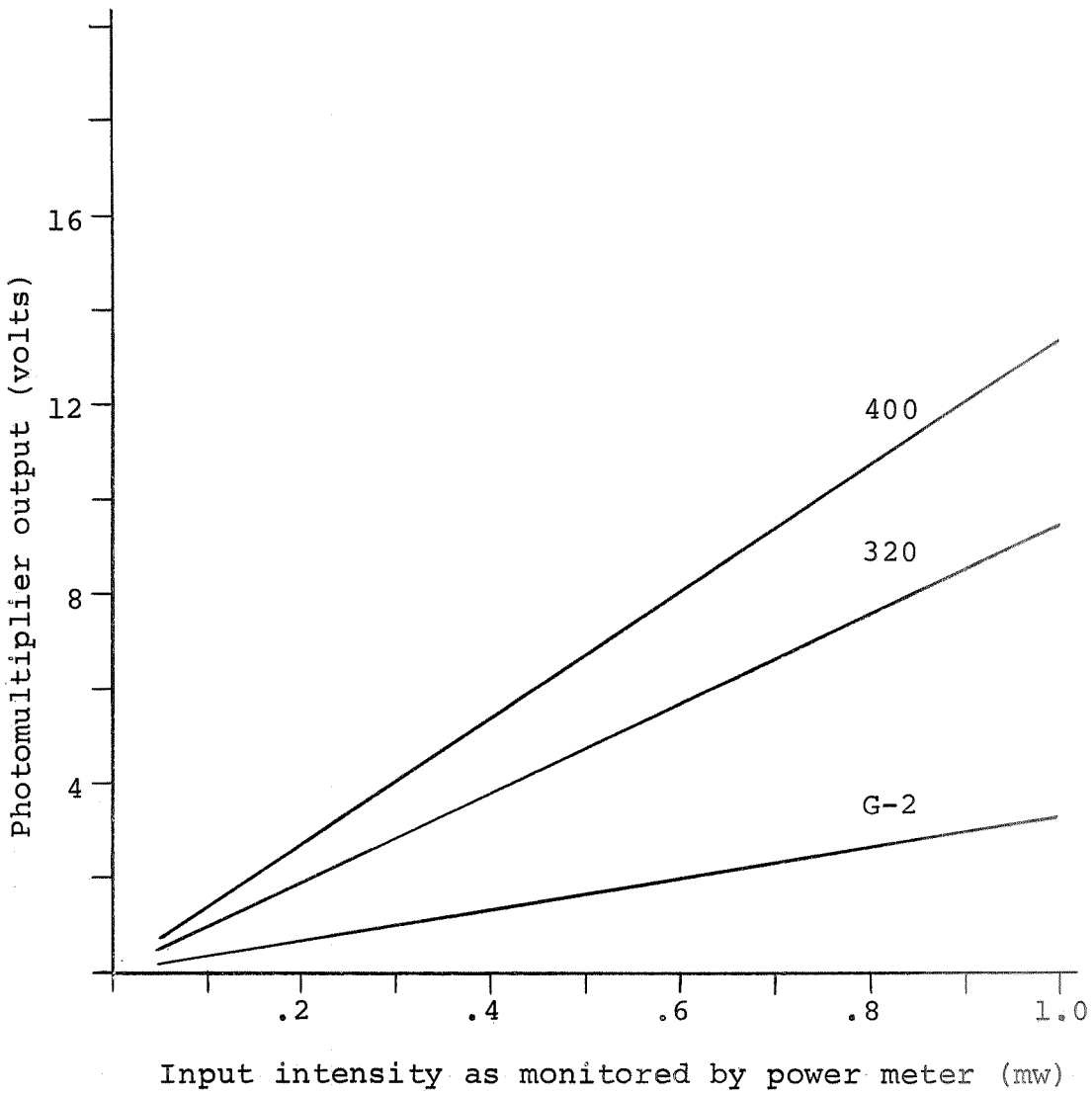

Figure 4.6. Reflected intensity at $\theta=\psi$ as a function of input intensity

A third variation of the three parameters, incident intensity, angle of incidence, and angle of reflectance, was possible. Holding the incident intensity constant, the angle of incidence was varied between 10 and 90 degrees while the reflected intensity was measured at the specular angle, $\theta=\psi$. The set-up was limited to angles of incidence equal to or greater than 10 degrees because of physical limitations of the system. The results are shown in Figure 4.7 as continuous curves of photomultiplier output versus angle of incidence.

4.5 Cross Sectional Surface Analysis

Each of the copper samples used in the reflectance measurements were cut cross-sectionally, revealing an edge view of the surface. To facilitate the observation, the cut specimens were molded into a cylinder of bakelit and the exposed surface polished. An example of a cylinder with the surfaces embedded in bakelit is seen in Figure 4.8. The polishing removed the foreign materials and fragmented metal caused by the cutting operation. The amount of material that was removed is between 0.4 and 0.5 mm. Then the surfaces are viewed through a microscope, which had a camera mounted on it for photographing the field of view. Sections of the surfaces were photographed with overlapping regions in order to provide an extended, continuous surface. A calibrated ten micron grid was placed in the same focal plane and photographed for scaling purposes. The negatives

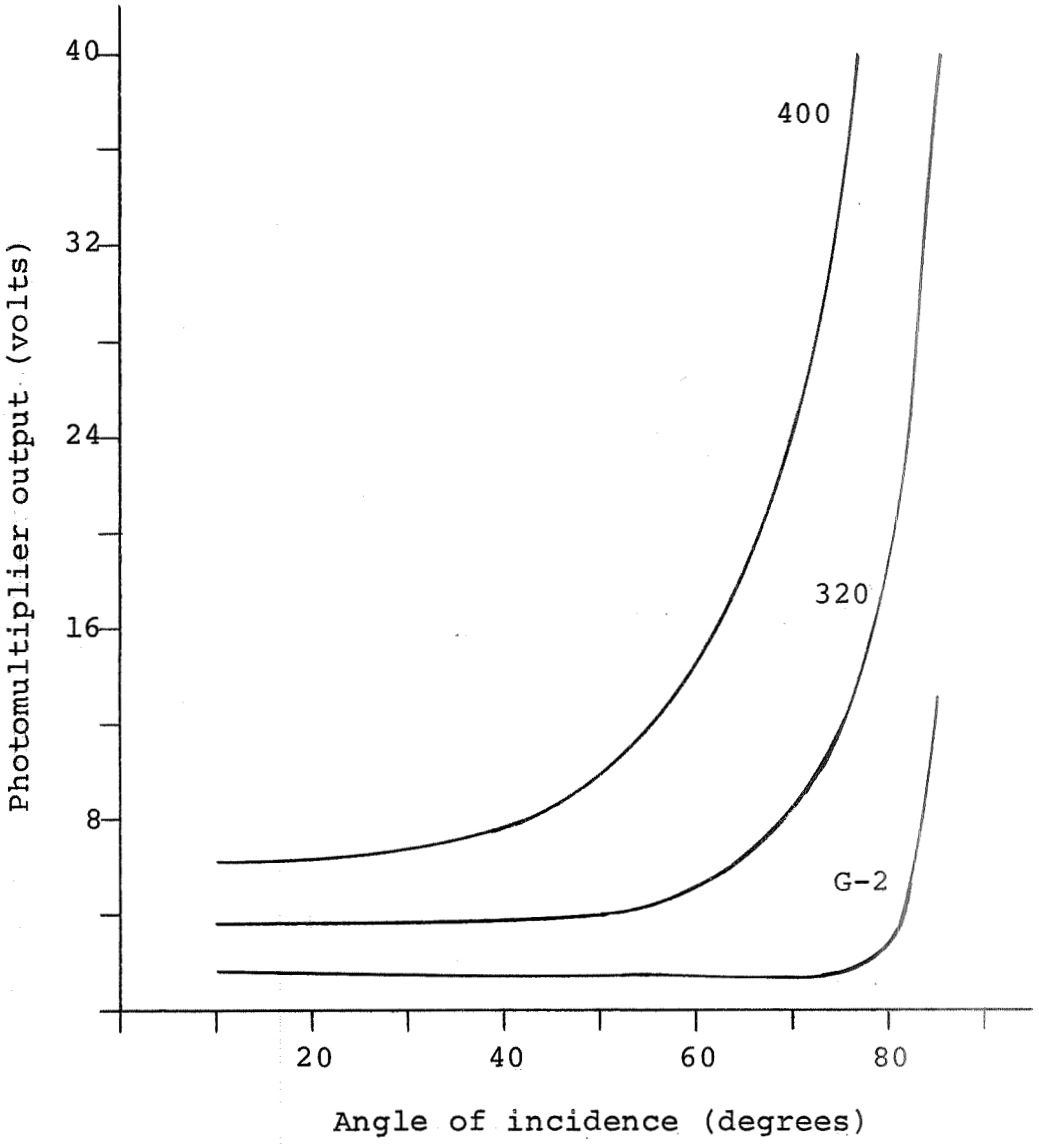

Figure 4.7. Reflected intensity at $\theta=\psi$ as a function of angle of incidence, ψ

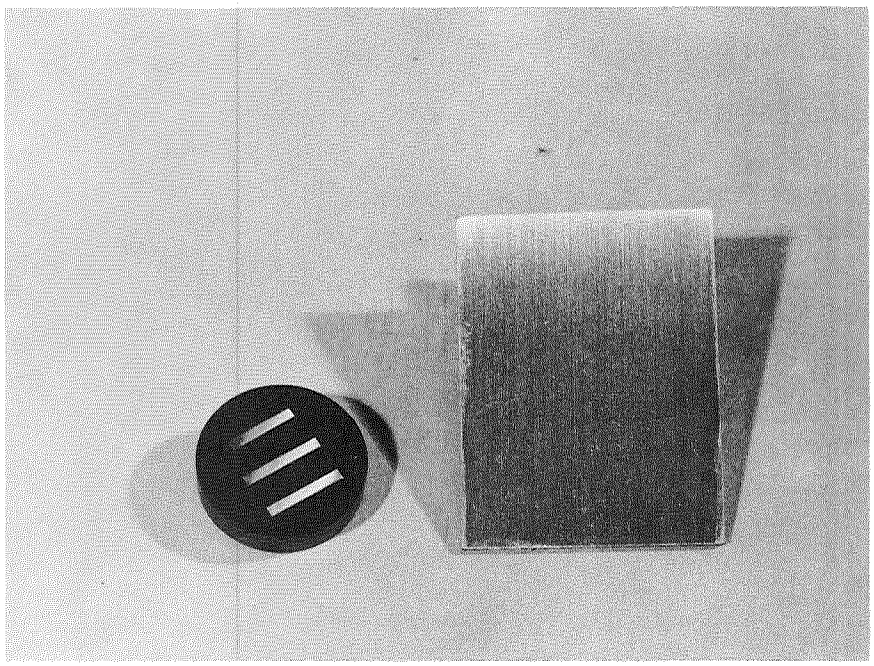

Figure 4.8. Photograph of test sample sheet and a cross section of the sample sheet embedded in a bakelit mold

were enlarged and photographic prints were made. A typical surface print is given in Figure 4.9. The total magnification of the prints used was between 850 and 900 times. The photographic prints were then aligned to give a continuous surface for each sample. The aligned prints are given in Figure 4.10. A reference line was then drawn on the print, and the perpendicular displacement from the reference to the surface was measured for each millimeter along the reference line. A computer program was used to count the number of surface points at each discrete level above the reference line. This information, often referred to as height density functions, is illustrated as bar graphs in Figures 4.11, 4.12, and 4.13.

The auto-correlation function was computed on the basis of the following formulation

$$R(\tau) = \frac{\sum_{i=1}^{N} z(x_i)\, z(x_i + \tau)}{\sum_{i=1}^{N} z^2(x_i)} \qquad (4.1)$$

where $z(x_i) = h(x_i) - z_o$ displacement from the mean surface

$h(x_i)$ = height above reference line at x_i

z_o = average height of surface above reference line.

A computer program was used to calculate the functional value of $R(\tau)$, and the results are given as continuous curves in Figures 4.14, 4.15, and 4.16.

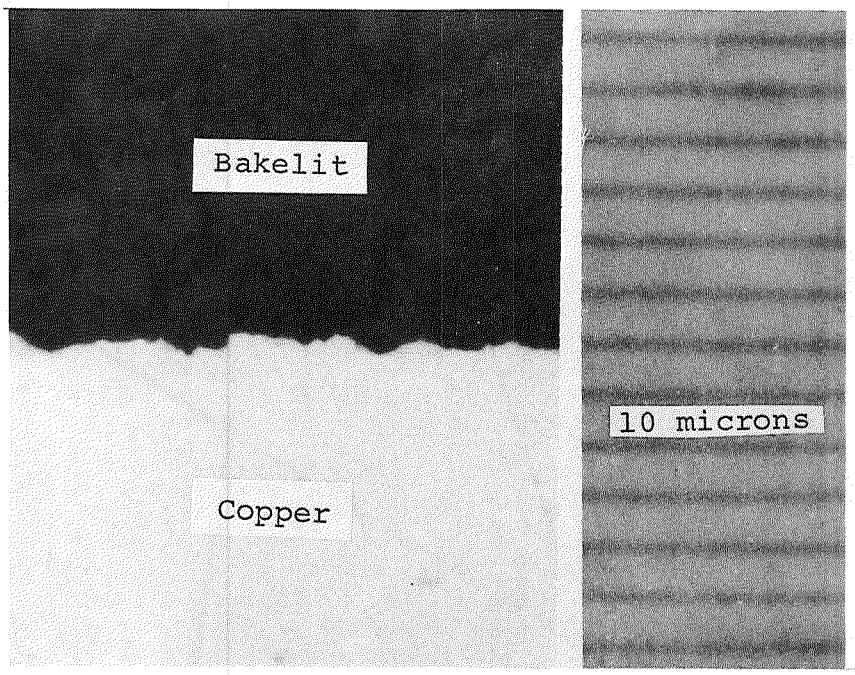

Figure 4.9. Photographic enlargement of a surface as viewed through a microscope with a 10 micron grid for scaling

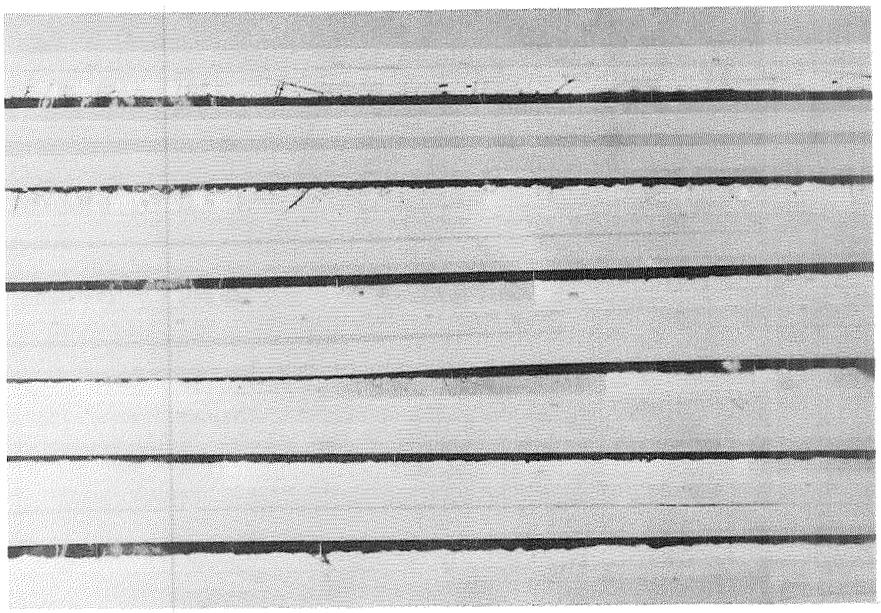

Figure 4.10. Aligned photographic prints

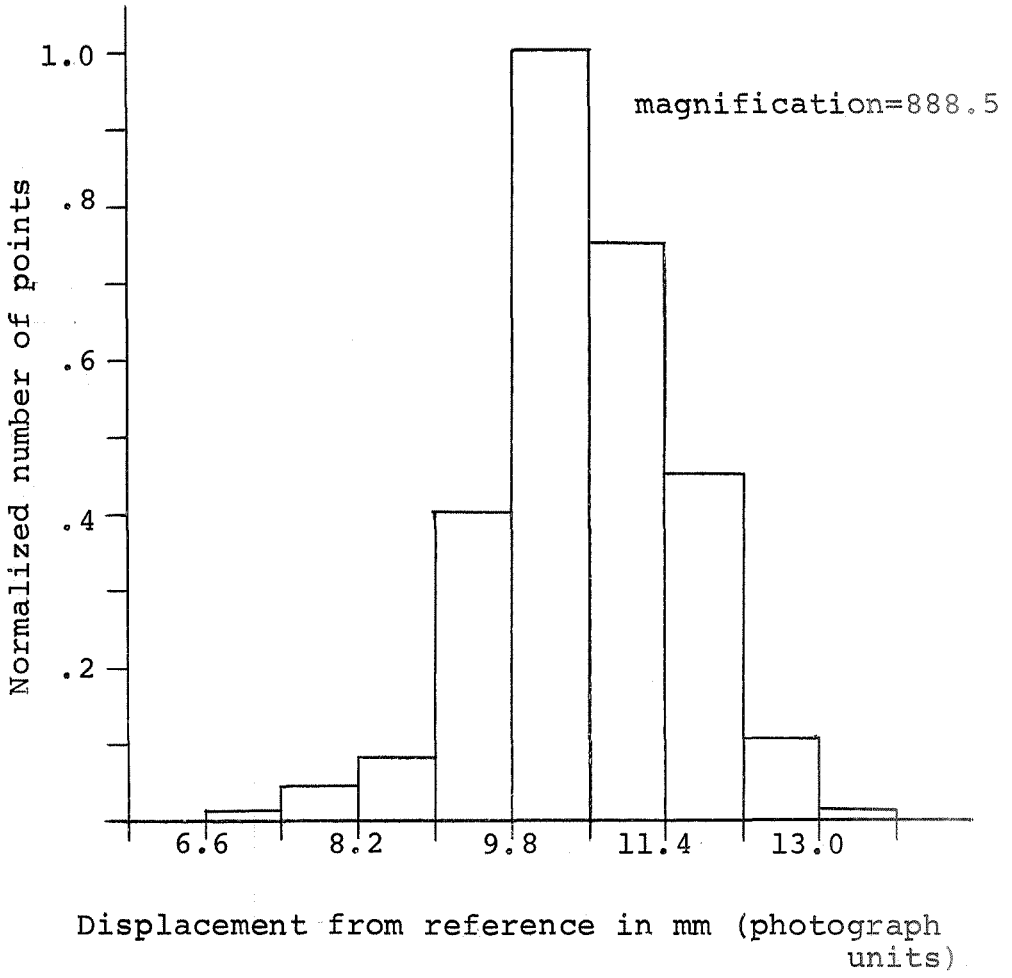

Figure 4.11. Normalized bar graph of surface points within each height band (0.8 mm wide) for Emery 2 sample

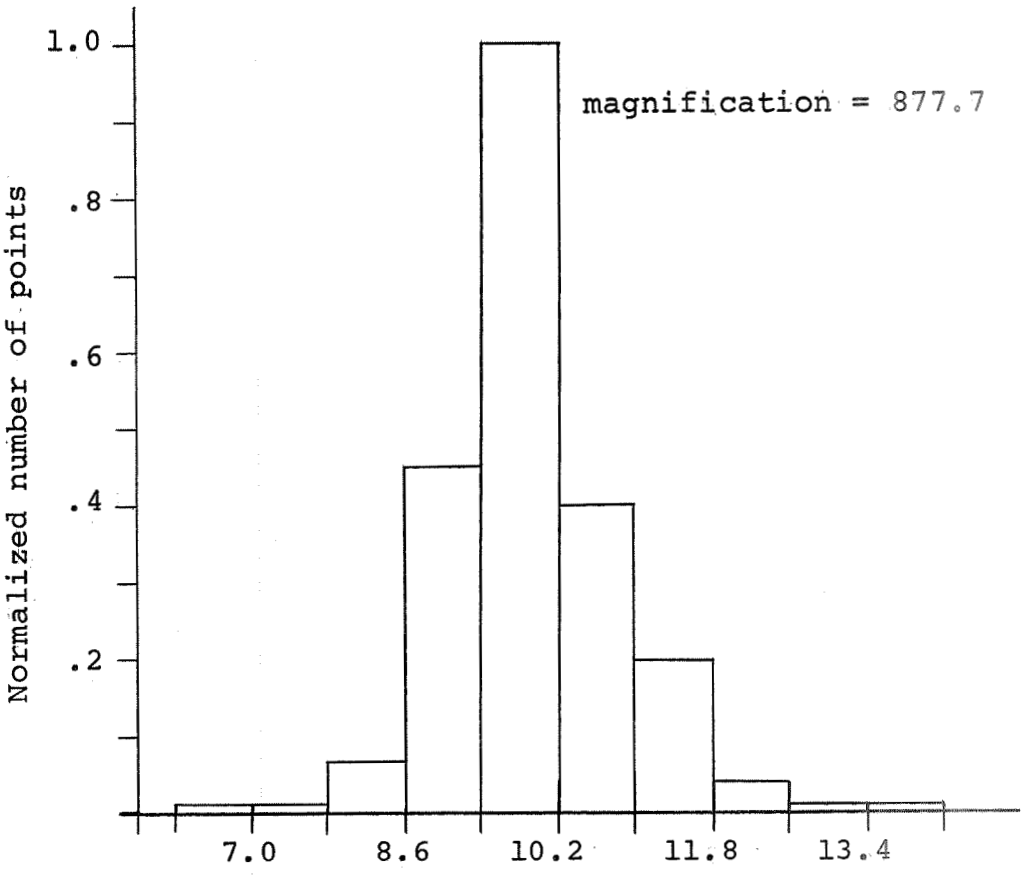

Figure 4.12. Normalized bar graph of surface points within each height band (0.8 mm wide) for Grit 320 sample

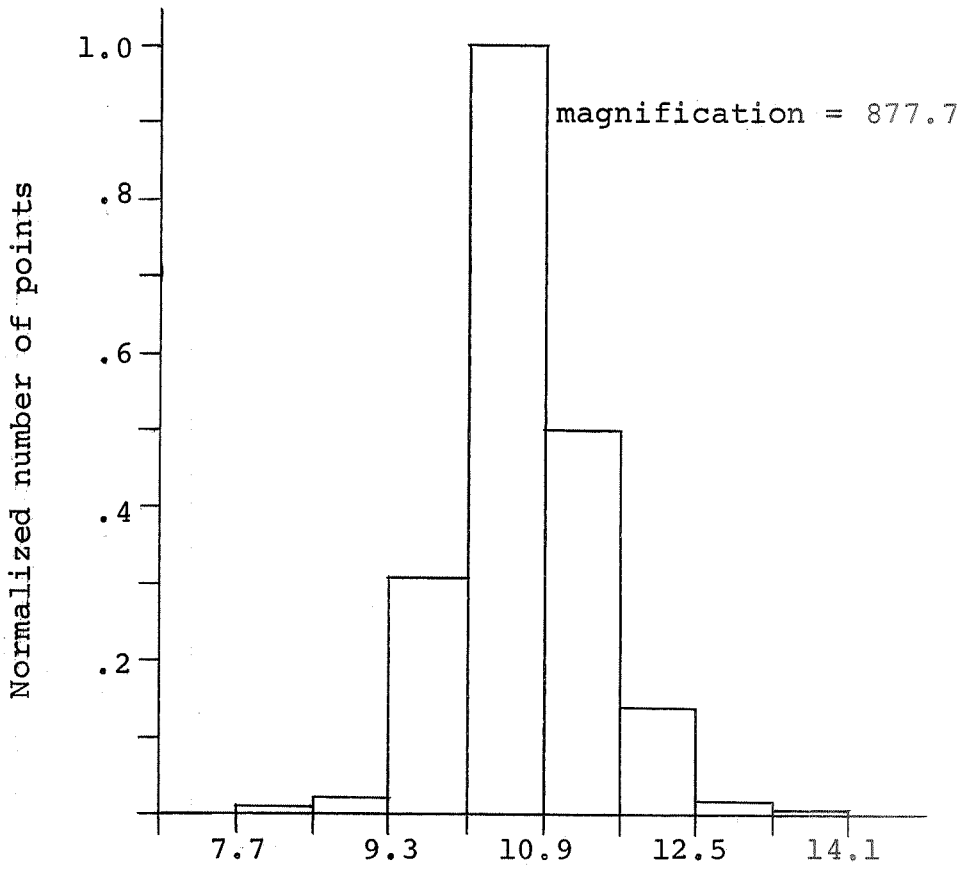

Figure 4.13. Normalized bar graph of surface points within each height band (0.8 mm wide) for Grit 400 sample

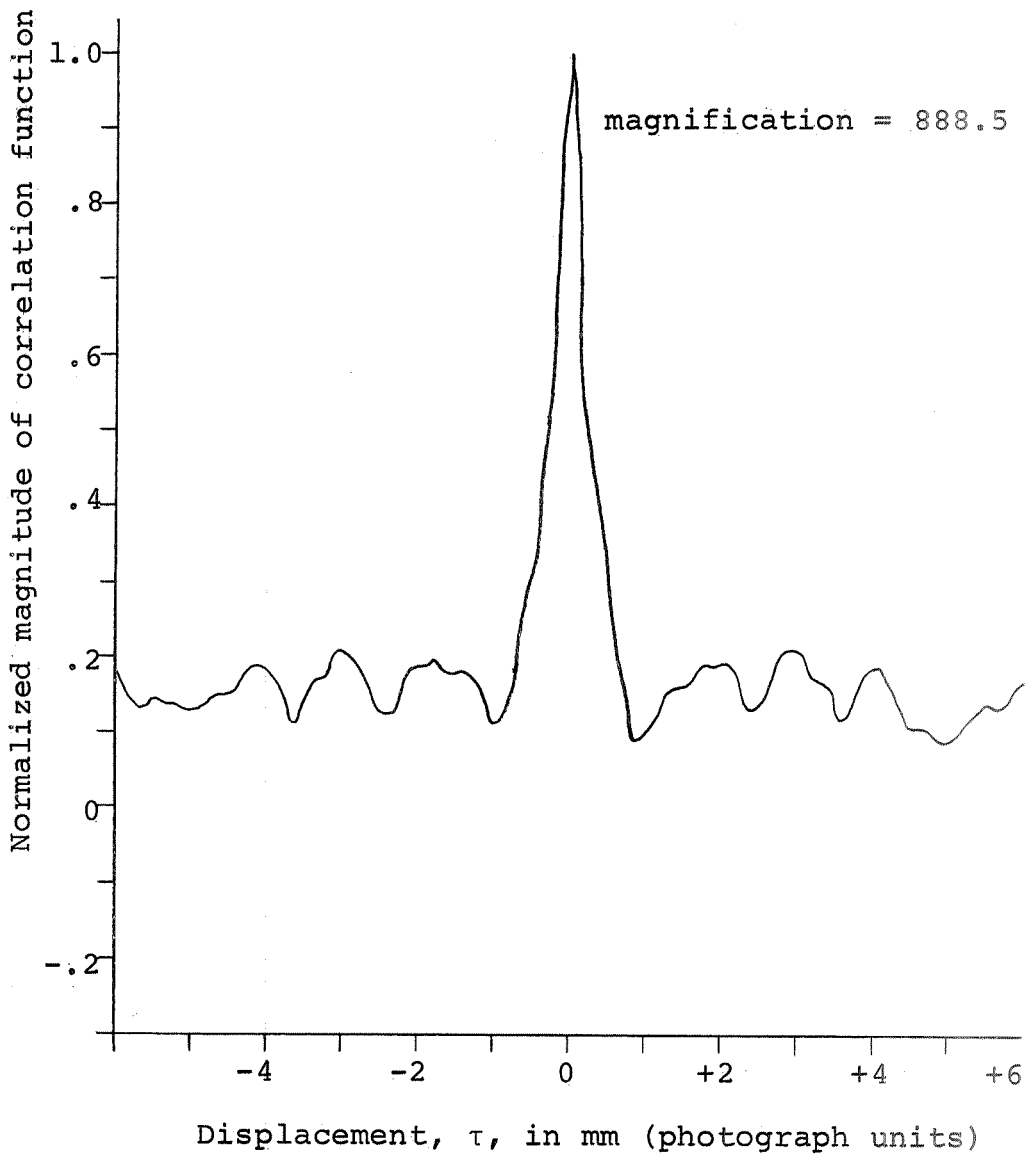

Figure 4.14. Auto-correlation function of the surface for the Emery 2 sample

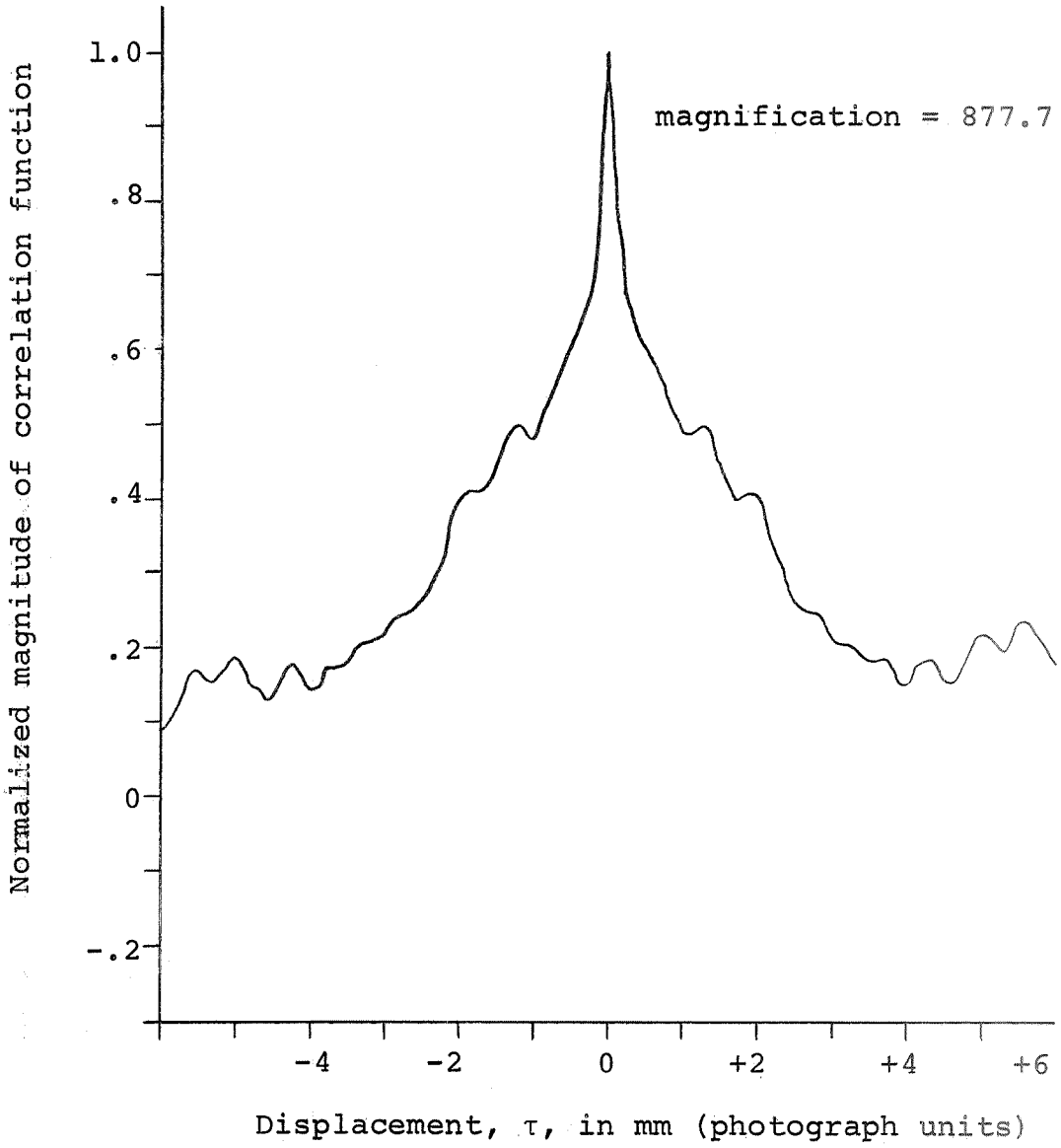

Figure 4.15. Auto-correlation function of the surface for the Grit 320 sample

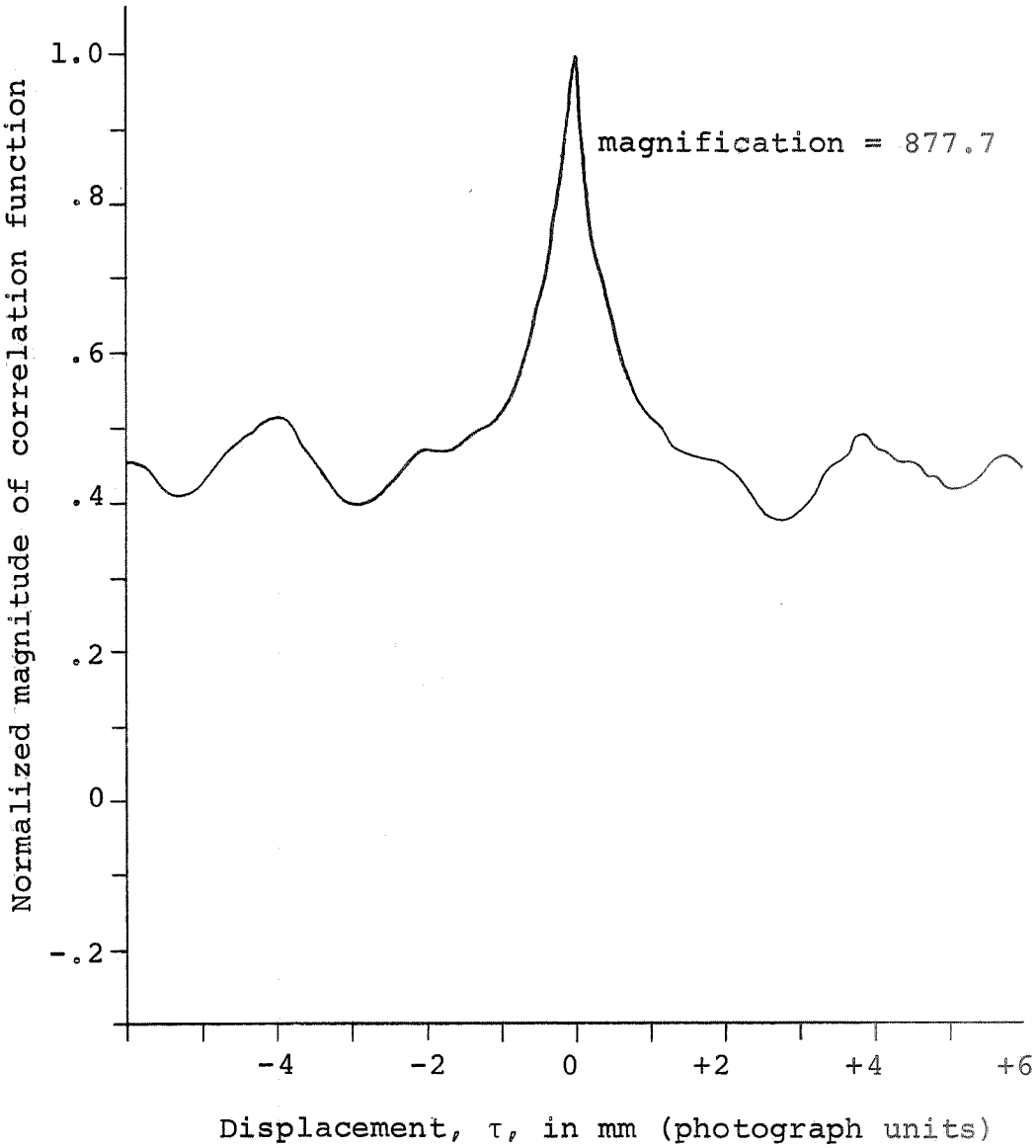

Figure 4.16. Auto-correlation function of the surface for the Grit 400 sample

4.6 Comparison of Theoretical and Experimental Data

It was obvious from the bar graphs of the height density (Figures 4.11, 4.12, and 4.13) that the density functions were asymmetric and that a Gaussian function was not the best model. A comparison of a Rayleigh and a Maxwell function to the graph is given in Figure 4.17. This illustrates that of the two functions, the Maxwell was the better. Then superimposing Maxwell functions on the bar graphs of the previous section, each surface density function was defined as shown in Figures 4.18, 4.19, and 4.20. A rms surface value was calculated based on the raw data for each surface and compared to the second moment (often used as the rms value) of the corresponding Maxwell function. Table 4.2 lists the results.

To compare the results of the reflected intensity as functions of the angle of reflectance, the magnitude of the experimentally determined reflected intensity was normalized with respect to the reflected intensity at $\theta=\psi$. The value of a and β which gave the best theoretical curve to match the experimental data of the Grit 400 sample was used in Figure 4.21. The Laplace correlation function model provided the best fit and was used to compare the experimental data to the theoretical model in Figures 4.22, 4.23, and 4.24. The value of β for which the best fit of the theoretical curve to the experimental data was used in the computation of the three Laplace correlation functions

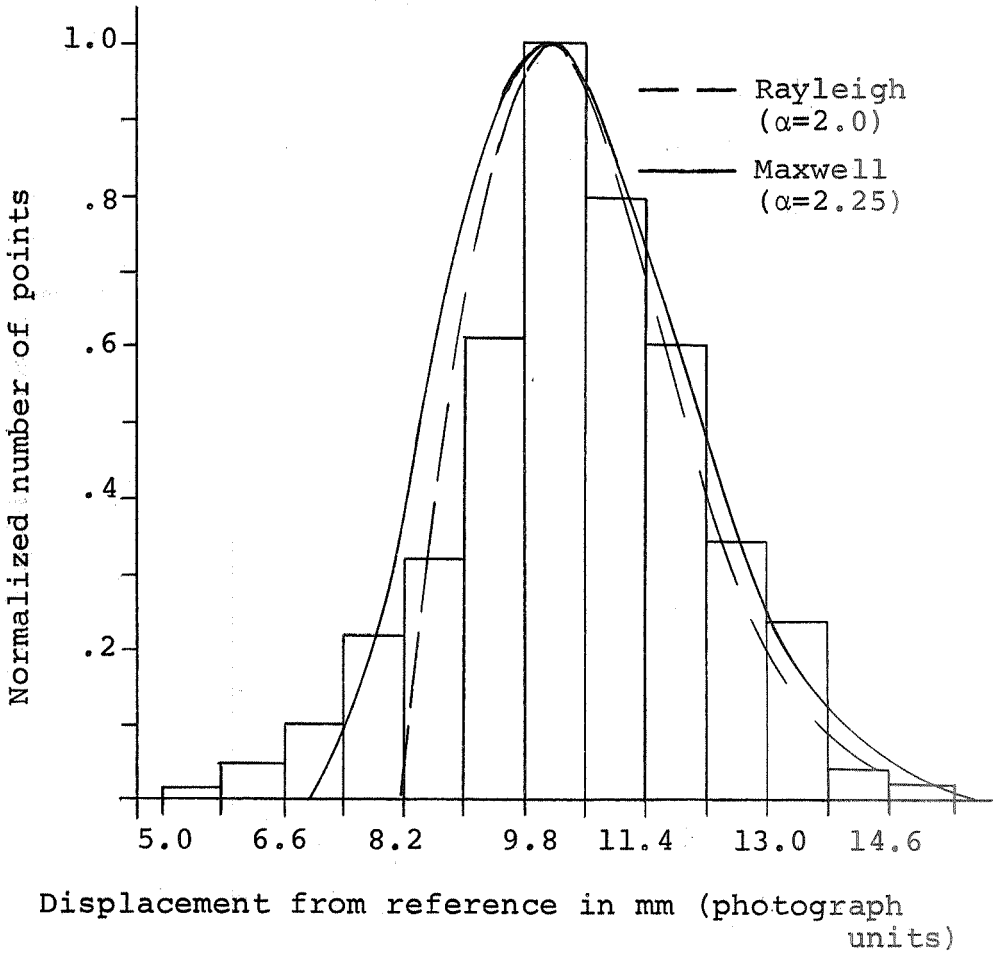

Figure 4.17. Comparison of Rayleigh and Maxwell density functions for the Emery 1 sample

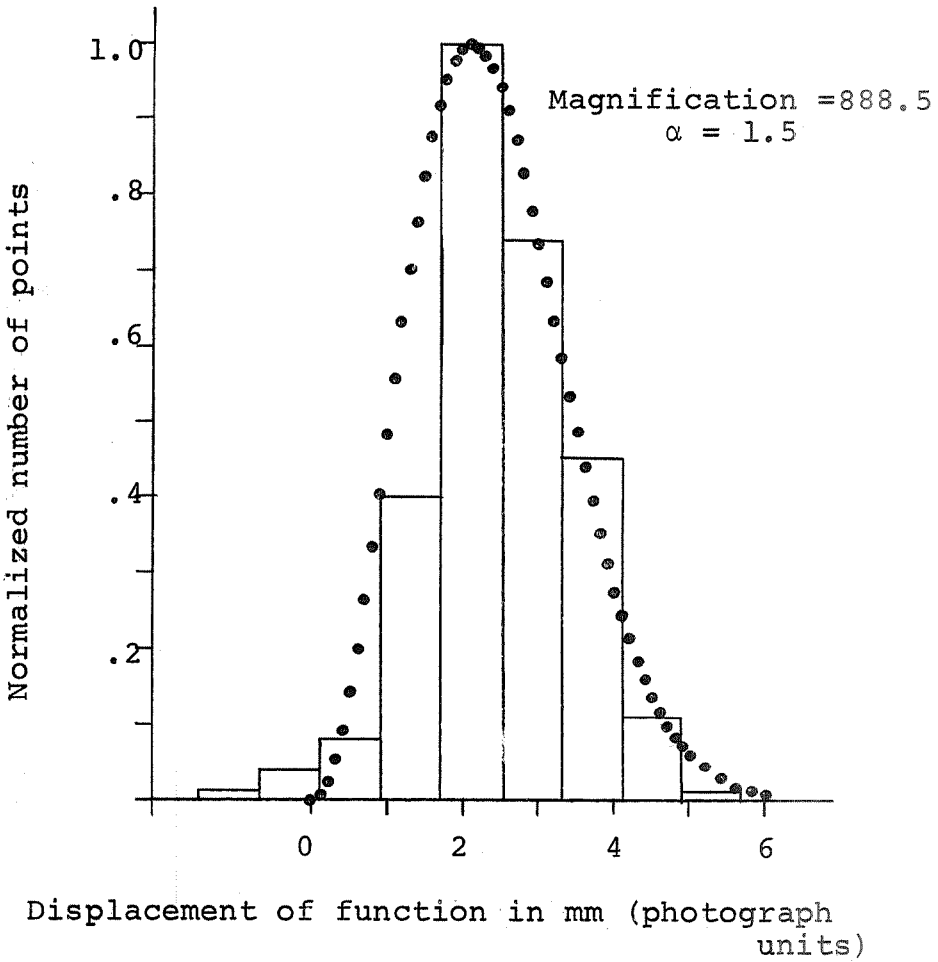

Figure 4.18. Maxwell density function superimposed on normalized bar graph of Emery 2 sample

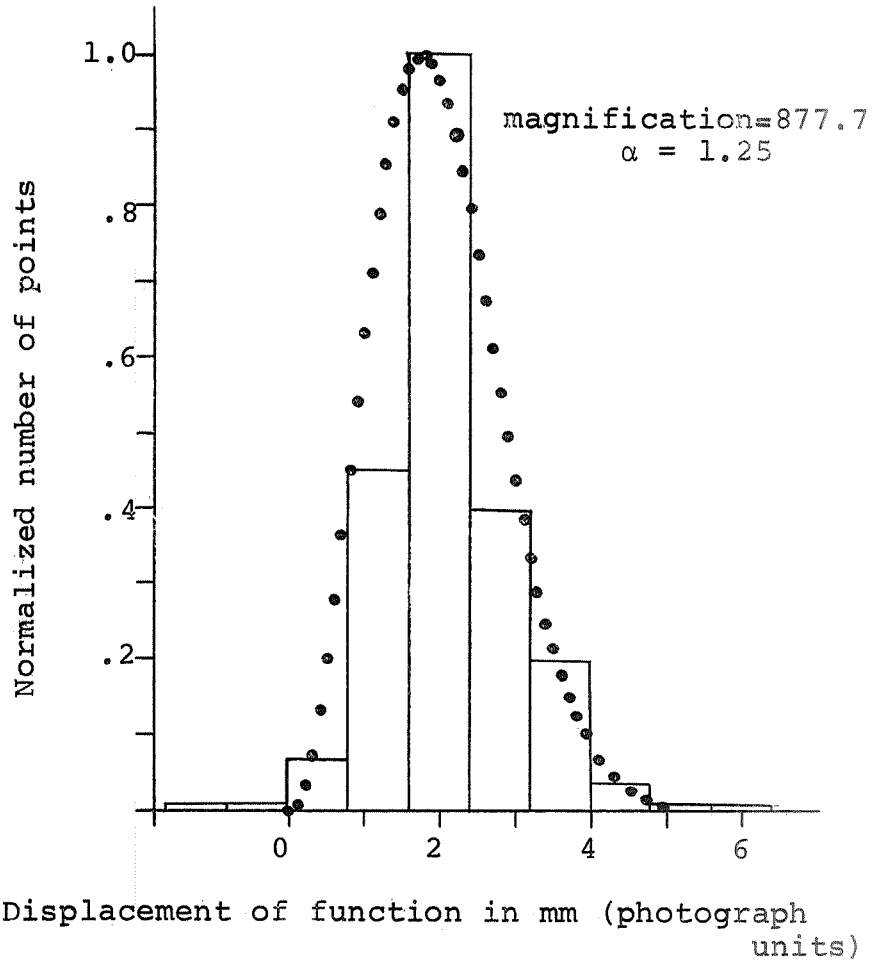

Figure 4.19. Maxwell density function superimposed on normalized bar graph of Grit 320 sample

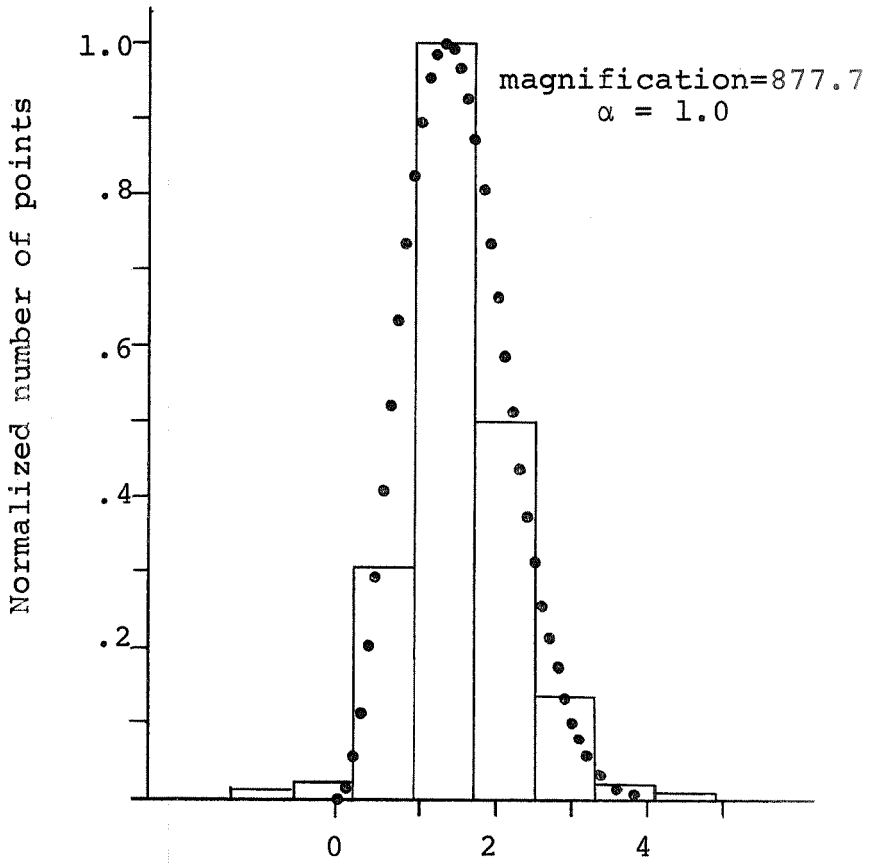

Figure 4.20. Maxwell density function superimposed on normalized bar graph of Grit 400 sample

Table 4.2 Measured rms heights as a result of polishing with different abrasive papers

Grade	Based on Maxwell density function	Based on the raw data
Emery 2	1.1378 μm	1.1344 μm
Emery 1	1.7065 μm	1.8152 μm
Grit 240	1.2478 μm	1.2645 μm
Grit 320	0.9500 μm	0.9300 μm
Grit 400	0.7680 μm	0.7800 μm

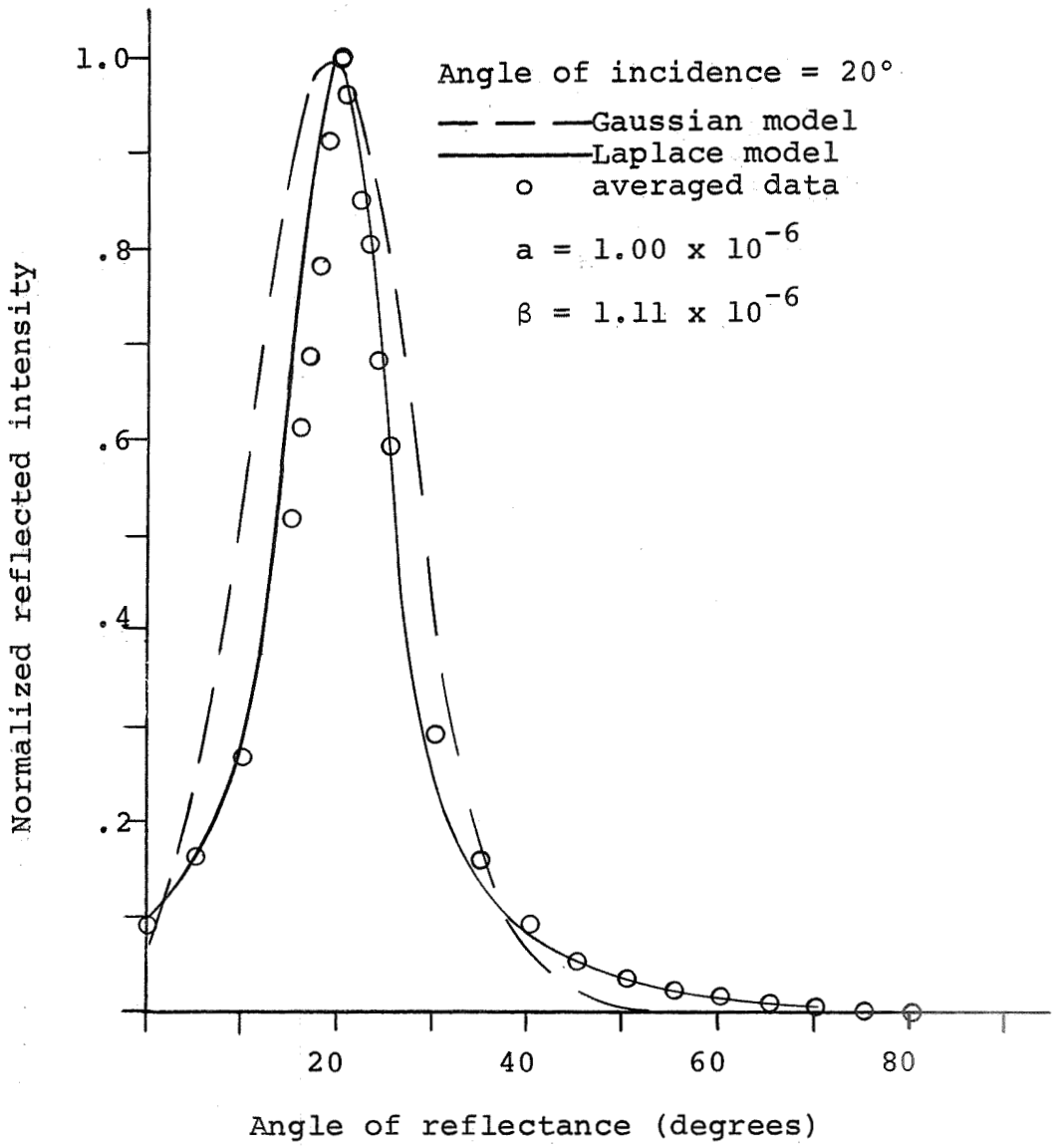

Figure 4.21. Comparison of Gaussian and Laplace correlation model values to Grit 400 sample values

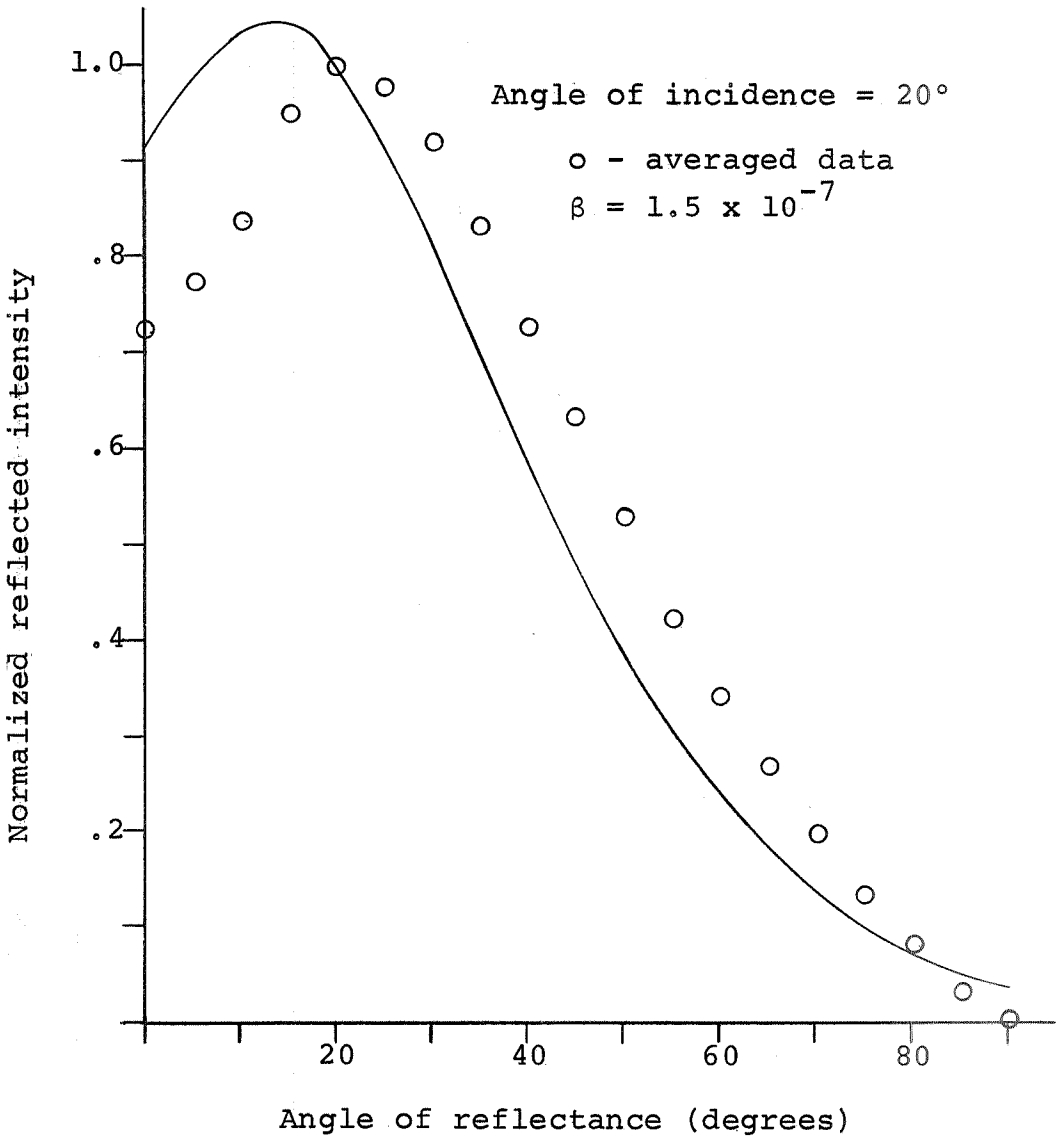

Figure 4.22. Laplace model of reflectance with Emery 2 sample data superimposed

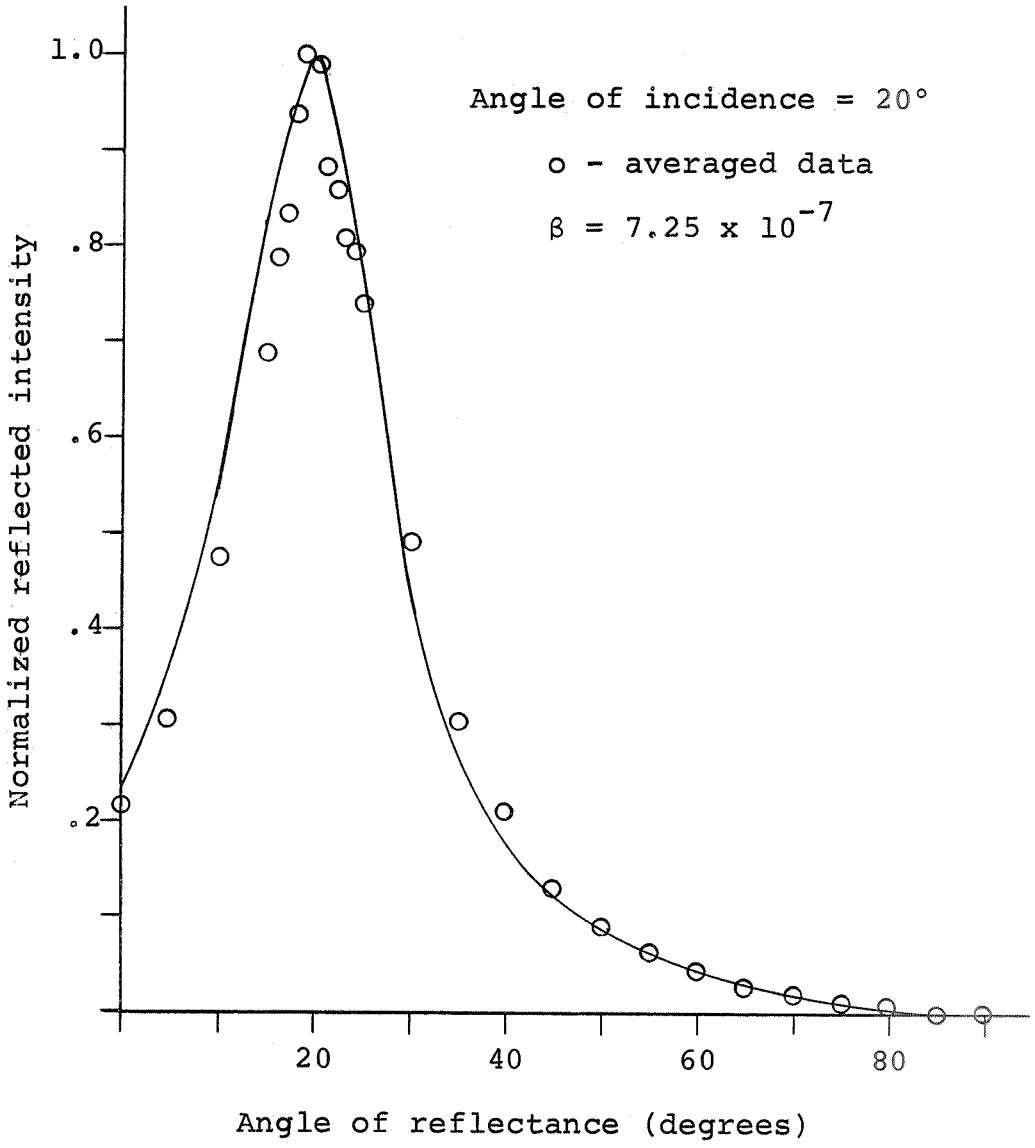

Figure 4.23. Laplace model of reflectance with Grit 320 sample data superimposed

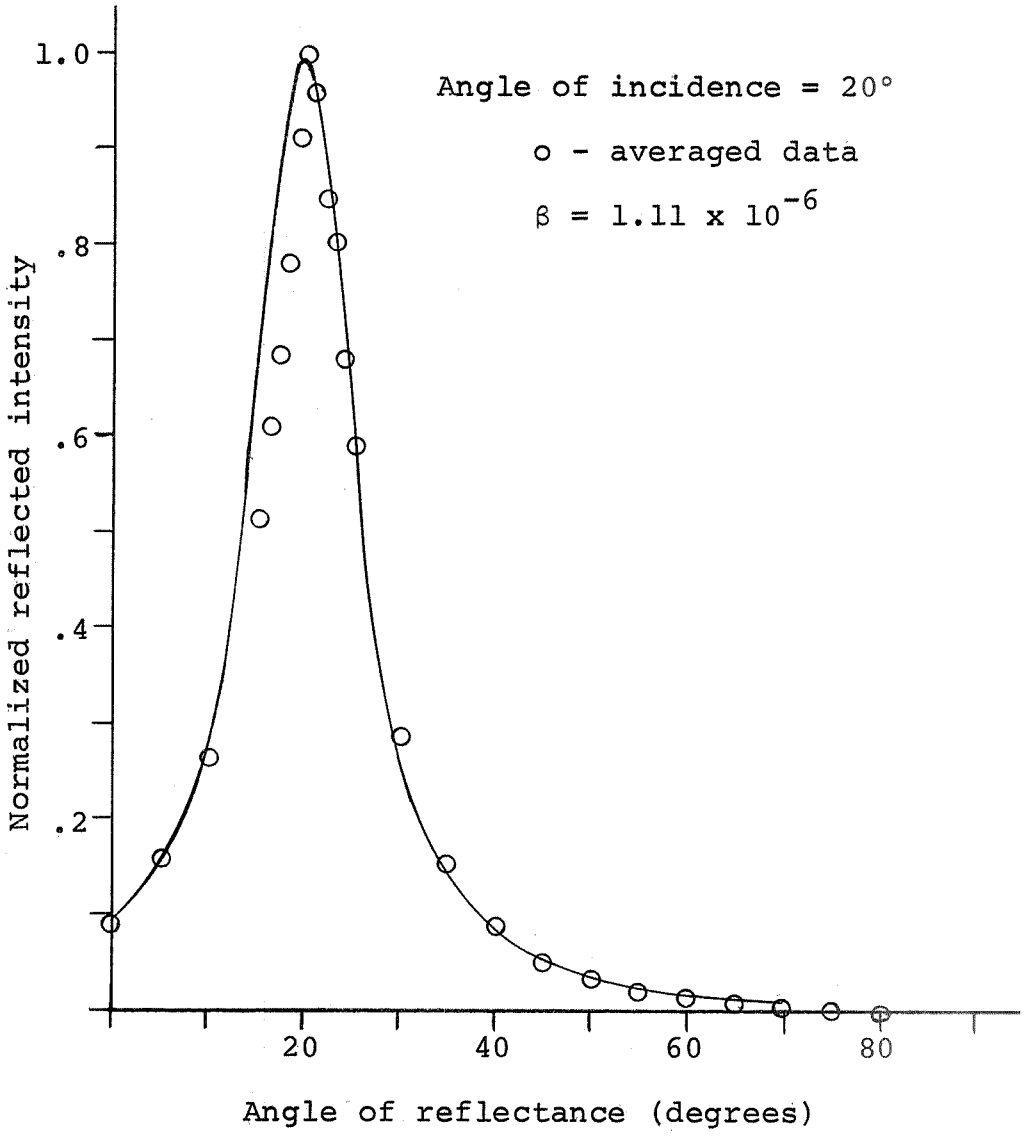

Figure 4.24. Laplace model of reflectance with Grit 400 sample data superimposed

illustrated in Figure 4.25. When compared to the auto-correlation curves found from the actual surface, Figures 4.14, 4.15, and 4.16, these curves were in remarkable agreement. Although the curves found from the actual surface were based on sampled points, together with theoretical curves, the Laplace function was shown to be a very good model for the auto-correlation function.

Table 4.3 was compiled from the rms height variation σ of the density function and the correlation parameter β of the auto-correlation function. Recalling (3.23), the diffused reflectance was proportional to the product $\sigma^2\beta$. Therefore using the value of the photomultiplier voltage output for the reflectance at the point $\theta=\psi$, the reflectance was given as a function of $\sigma^2\beta$ in Figure 4.26. The results were linear curves in agreement with the theoretical model.

4.7 Model Selection

From the analysis of a one-dimensional rough metallic surface, the model based on the Laplace correlation function outlined in Section 3.3 was a better representation of the statistical surface properties than the model based on the Gaussian function. The normalized reflected intensity was then a function of the correlation parameter only and the set-up described in Section 4.3 was a useful tool for determining the correlation parameter of the surface. When the experimental set-up was properly calibrated with actual surface parameters, the magnitude of the reflected intensity

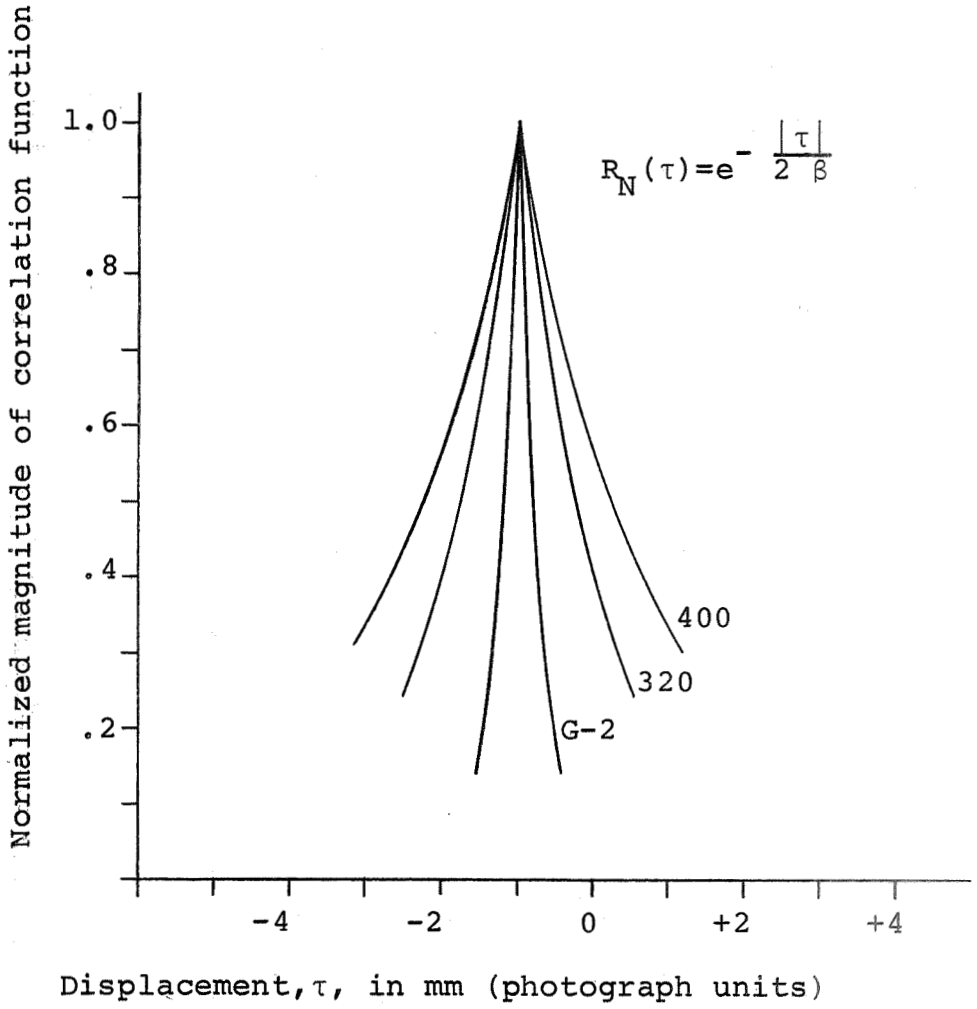

Figure 4.25. Laplace correlation functions for the three samples illustrated

Table 4.3 Measured surface characteristics as based on Laplace model

Grade	σ in μm	β in m	$\sigma^2\beta x10^{19}$ in m^3	Detector output in volts
Emery 1	1.80	$1.00x10^{-8}$	0.324	2.5
Emery 2	1.10	$1.50x10^{-7}$	1.815	3.0
Grit 240	1.20	$3.00x10^{-7}$	4.310	5.8
Grit 320	0.93	$7.25x10^{-7}$	6.270	8.8
Grit 400	0.77	$1.11x10^{-6}$	6.581	12.4
Grit 600	0.78	$2.00x10^{-6}$	12.150	17.0

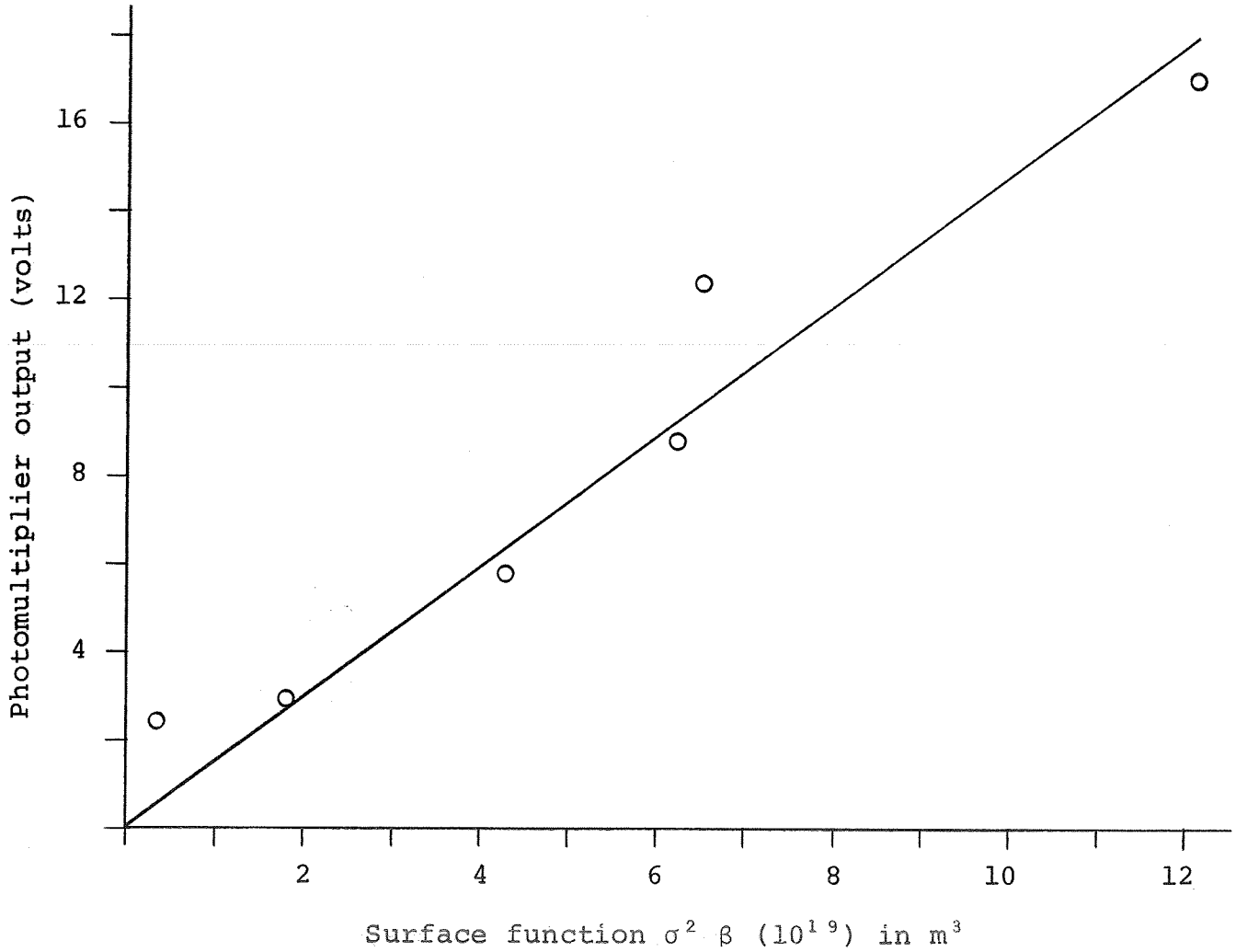

Figure 4.26. Reflected intensity as a function of surface parameter, $\sigma^2\beta$

at the specular angle was a function of $\sigma^2\beta$. From this type of calibration curve the surface rms height variation can be determined. Therefore, the derived model provided a satisfactory method to find both of the important surface parameters.

The curves of Figure 4.6 were easily explained by this model. The slope of each curve was proportional to $\sigma^2\beta$ or to the rate of change of the reflected intensity per change in input intensity.

The Rayleigh criterion for rough surfaces is given by assuming light strikes a maximum and minimum height of the surface and is reflected in the same direction. The phase difference between the two paths is

$$\Delta \phi = \frac{4\pi h}{\lambda} \cos \psi$$

where h is the total height difference and ψ is the angle of incidence. If $\Delta \phi = \pi$, then cancellation occurs and no energy flows in this direction. If $\Delta \phi = 0$, it reflects specularly and is considered smooth. A value between the two extremes is more often used as an indication of roughness, then for a smooth surface

$$h < \frac{\lambda}{8 \cos \psi} \quad .$$

From the simple formulation it is obvious that as the angle approaches ninety degrees a moderately rough surface appears smooth. This effect was measured experimentally by varying the angle of incidence, ψ, for each surface, and then

measuring the reflected intensity at the angle of reflectance equal to the angle of incidence ($\theta=\psi$). The result is given in Figure 4.7. The rougher surfaces required large angles of incidence before they began to show characteristics of a smooth surface as predicted by the Rayleigh criterion.

5. WAVEGUIDE THEORY

5.1 Introduction

For finding Q-values of resonators, one uses customarily the procedure of first assuming perfect conducting walls to determine the fields and then using the surface resistance of the walls to find the losses. The Q-value is defined as

$$Q = \omega U/P_L \tag{5.1}$$

where ω is the resonant frequency

U is the stored energy

and P_L is the power dissipated in the walls.

For good conductors such as silver, gold, and copper, this is a useful approximation.

The fields within the conventional rectangular resonator with perfectly conducting walls are well known and are given in many references [21]. The fields within the H-guide (Figure 5.1) have been derived by Tischer [24,25]. Propst [19] derived the fields for the H-guide by the method of field matching for symmetry about an artificial dielectric strip (x-direction). For later development, the fields are given with respect to a unit magnitude for the electric field in the x-direction. The fields are based on the H-guide having infinite walls in the x-direction. For the air region:

$$E_x = e^{-\alpha_x x} \cos (k_y y)\ e^{-jk_z z}\ , \tag{5.2}$$

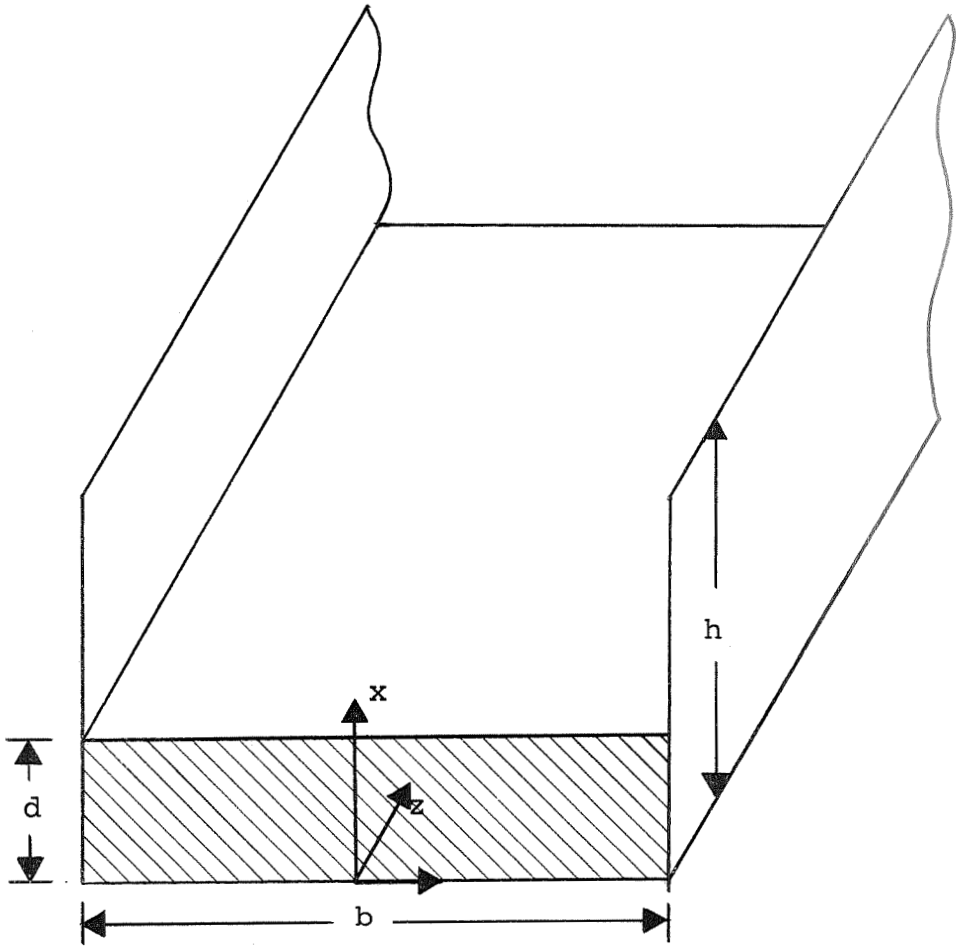

Figure 5.1. Upper half of dielectric H-guide

$$E_y = \frac{\alpha_x k_y}{k_c^2} \; e^{-\alpha_x x} \; \sin(k_y y) \; e^{-jk_z z}, \tag{5.3}$$

$$E_z = \frac{-\alpha_x k_z}{k_c^2} \; j \; e^{-\alpha_x x} \; \cos(k_y y) \; e^{-jk_z z}, \tag{5.4}$$

$$H_x = 0, \tag{5.5}$$

$$H_y = \frac{1}{\omega\mu_o} \frac{k_z k_o^2}{k_c^2} \; e^{-\alpha_x x} \; \cos(k_y y) \; e^{-jk_z z}, \tag{5.6}$$

and $$H_z = \frac{j}{\omega\mu_o} \frac{k_y k_o^2}{k_c^2} \; e^{-\alpha_x x} \; \sin(k_y y) \; e^{-j\,k_z z}. \tag{5.7}$$

For the dielectric region:

$$E_x = \frac{e^{-\alpha_x d}}{\varepsilon_r \cos(k_x d)} \; \cos(k_x x) \; \cos(k_y y) \; e^{-jk_z z}, \tag{5.8}$$

$$E_y = \frac{\alpha_x k_y \; e^{-\alpha_x d}}{k_c^2 \sin(k_x d)} \; \sin(k_x x) \; \sin(k_y y) \; e^{-j\,k_z z}, \tag{5.9}$$

$$E_x = \frac{-j\alpha_x k_z e^{-\alpha_x d}}{k_c^2 \sin(k_x d)} \; \sin(k_x x) \; \cos(k_y y) \; e^{-jk_z z}, \tag{5.10}$$

$$H_x = 0 \; , \tag{5.11}$$

$$H_y = \frac{1}{\omega\mu_o} \; \frac{k_z k_o^2 e^{-\alpha_x d}}{k_c^2 \cos(k_x d)} \; \cos(k_x x) \; \cos(k_y y) e^{-jk_z z}, \tag{5.12}$$

and $$H_z = \frac{j}{\omega\mu_o} \; \frac{k_y k_o^2 e^{-\alpha_x d}}{k_c^2 \cos(k_x d)} \cos(k_x x) \; \sin(k_y y) e^{-jk_z z}. \tag{5.13}$$

The characteristic equations are:

for the air region $$k_o^2 = -\alpha_x^2 + k_y^2 + k_z^2 \tag{5.14}$$

for the dielectric region $$k_o^2 \, \varepsilon_r = k_x^2 + k_y^2 + k_z^2 \tag{5.15}$$

The field matching at the interface of the electric and

the air region imposes the requirement

$$\varepsilon_r \alpha_x = k_x \tan (k_x d). \tag{5.16}$$

The equation parameters are defined as follows:

$$k_c^2 = k_y^2 + k_z^2$$

k_y, k_z = wave propagation constants,

k_x = wave propagation constant in the dielectric region ($|x| \leq d$),

α_x = field distribution constant in the air region ($|x| \leq d$),

k_o = free space propagation constant,

ε_r = relative dielectric constant of the dielectric strip,

and μ_o = permeability.

These fields are needed to investigate the properties of the H-guide resonator. First derivations are found relating attenuation and the Q-value of waveguides. The Q-values and resonant frequencies of three types of resonators are determined. The three resonators are compared and the loss factors are discussed.

5.2 Relation of α and Q

The attenuation of a shorted section of waveguide is given by

$$\alpha = \frac{P_L}{2 P_T} \tag{5.17}$$

$$P_L = \frac{R_S}{2} \oint_C |H_t|^2 \, d\ell \, , \tag{5.18}$$

$$P_T = \frac{1}{2} R_e \int_{S_c} (\underline{E} \times \underline{H}^*) \cdot \underline{n} \, dS, \tag{5.19}$$

and where C is the contour enclosing the cross-sectional area S_c.

The Q-value for the shorted section is

$$Q = \omega \frac{W_{E(max)}}{P_L'} \tag{5.20}$$

where $$W_{E(max)} = \frac{\varepsilon}{2} \int_V \underline{E} \cdot \underline{E}^* \, d\, V \tag{5.21}$$

$$P_L' = \frac{R_S}{2} \int_{S'} |H_t|^2 \, d\, S \tag{5.22}$$

and where S' is the internal surface area, the end plates are excluded, and where V is the enclosed volume.

For a shorted section of length d, P_L and P_L' can be related since

$$dS = d\ell \, dz. \tag{5.23}$$

The elementary length dz is the differential length in the direction of propagation. From this relation follows

$$P_L' = P_L \, d. \tag{5.24}$$

By letting U equal the energy density in the shorted section and $\underline{v}_t$ the velocity of energy propagation, (5.19) can be rewritten as

$$P_T = \int U \, \underline{v}_t \cdot \underline{n} \, \, d\, S, \tag{5.25}$$

and (5.21) as

$$W_{E(max)} = \int_V U \, \, d\, V \, . \tag{5.26}$$

The incremental volume element can be written as

$$dV = dz \, dS$$

and, upon suitable intergration, (5.26) becomes

$$W_{E(max)} = d \int U \, d S \, . \tag{5.27}$$

The product of α and Q is now formed,

$$\alpha Q = \frac{\omega P_L}{2 P_T} \quad \frac{W_{E(max)}}{P'_L} \, . \tag{5.28}$$

Substituting (5.24), (5.25), and (5.27) yields

$$\alpha Q = \frac{\omega}{2} \quad \frac{1}{|v_t|} \, . \tag{5.29}$$

In the case of a normal dispersive medium, the velocity of energy propagation equals the group velocity. The group velocity is given by

$$v_g = \frac{d\omega}{dk_z} = \frac{1}{\sqrt{\mu_o \varepsilon_o}} \quad \frac{dk}{dk_z} \tag{5.30}$$

where k_z is the propagation constant. For conventional rectangular waveguides the characteristic equation is

$$k^2 = k_x^2 + k_y^2 + k_z^2 \, , \tag{5.31}$$

where k_x and k_y are field constants specified by boundary conditions. For a waveguide filled with air, (5.31) gives for the group velocity

$$v_g = \frac{k_z}{k_o \sqrt{\mu_o \varepsilon_o}} \, . \tag{5.32}$$

Therefore, the relationship for the conventional guide using (5.29) and (5.32) gives

$$\alpha Q = \frac{k_o^2}{2 k_z} \, . \tag{5.33}$$

For the H-guide there are two characteristic equations and a relationship between field constants imposed by

boundary conditions. The only constant field parameter is k_y. The equations are:

in air $$k_o^2 = -\alpha_x^2 + k_y^2 + k_z^2 \quad , \tag{5.34}$$

in dielectric $$k_o^2 \varepsilon_r = k_x^2 + k_y^2 + k_z^2 \quad , \tag{5.35}$$

boundary condition $$\varepsilon_r \alpha_x = k_x \tan(k_x d) \tag{5.36}$$

where 2d is the thickness of the dielectric strip.

By differentiation and solving the three simultaneous equations, the group velocity for the H-guide is found. First, from (5.36) $\frac{d}{dk_z} x$ is given as

$$\frac{d\alpha_x}{dk_z} = \frac{1}{\varepsilon_r} \left[\tan(k_x d) + \frac{k_x d}{\cos^2(k_x d)} \right] \frac{d\, k_x}{d\, k_z} \quad , \tag{5.37}$$

and, using the following identities,

$$\cos(k_x d) = \frac{k_x}{g} \quad \text{and} \quad g^2 = k_x^2 + \varepsilon_r^2 \quad \alpha_x^2 \quad ,$$

(5.37) yields

$$\frac{d\alpha_x}{dk_z} = \frac{1}{\varepsilon_r k_x} \quad (\alpha_x \ \varepsilon_r + g^2 d) \ \frac{d\, k_x}{d\, k_z} \quad . \tag{5.38}$$

Differentiating (5.34) and (5.35) with respect to k_z gives

$$\frac{dk_o}{dk_z} = - \frac{\alpha_x}{k_o} \ \frac{d\alpha_x}{dk_z} + \frac{k_z}{k_o} \quad , \tag{5.39}$$

$$\frac{dk_o}{dk_z} = \frac{k_x}{\varepsilon_r k_o} \ \frac{dk_x}{dk_z} + \frac{k_z}{\varepsilon_r k_o} \quad , \tag{5.40}$$

and using (5.38) gives

$$v_g = \frac{1}{\sqrt{\mu_o \varepsilon_o}} \frac{k_z}{k_o} \left[\frac{k_x + \frac{\alpha_x}{\varepsilon_r k_x} (\varepsilon_r \alpha_x + g^2 d)}{k_x + \frac{\alpha_x}{k_x} (\varepsilon_r \alpha_x + g^2 d)} \right] . \qquad (5.41)$$

The relationship for the H-guide using (5.29) and (5.41) becomes finally

$$\alpha Q = \frac{k_o^2}{2 k_z} K \quad ; \qquad (5.42)$$

$$K = \frac{k_x + \frac{\alpha_x}{k_x} (\varepsilon_r \alpha_x + g^2 d)}{k_x + \frac{\alpha_x}{\varepsilon_r k_x} (\varepsilon_r \alpha_x + g^2 d)} \quad . \qquad (5.43)$$

5.3 Conventional Resonator

It has been shown [21] that the TE_{mnp} mode fields of the rectangular cavity as in Figure 5.2 are,

$$E_x = 0 \quad , \qquad (5.44)$$

$$H_z = H_o \cos\left(\frac{m\pi x}{b}\right) \cos\left(\frac{n\pi y}{h}\right) \sin\left(\frac{p\pi z}{d}\right) , \qquad (5.45)$$

$$H_x = - \frac{H_o}{k_c^2} \left(\frac{p\pi}{d}\right) \left(\frac{m\pi}{b}\right) \sin\left(\frac{m\pi x}{b}\right) \cos\left(\frac{n\pi y}{h}\right) \cos\left(\frac{p\pi z}{d}\right) , \qquad (5.46)$$

$$H_y = - \frac{H_o}{k_c^2} \left(\frac{p\pi}{d}\right) \left(\frac{n\pi}{h}\right) \cos\left(\frac{m\pi x}{b}\right) \sin\left(\frac{n\pi y}{h}\right) \cos\left(\frac{p\pi z}{d}\right) , \qquad (5.47)$$

$$E_x = \frac{j\omega\mu_o H_o}{k_c^2} \left(\frac{n\pi}{h}\right) \cos\left(\frac{m\pi x}{b}\right) \sin\left(\frac{n\pi y}{h}\right) \sin\left(\frac{p\pi z}{d}\right) , \qquad (5.48)$$

$$E_y = - \frac{j\omega\mu_o H_o}{k_c^2} \left(\frac{m\pi}{b}\right) \sin\left(\frac{m\pi x}{b}\right) \cos\left(\frac{n\pi y}{h}\right) \sin\left(\frac{p\pi z}{d}\right) , \qquad (5.49)$$

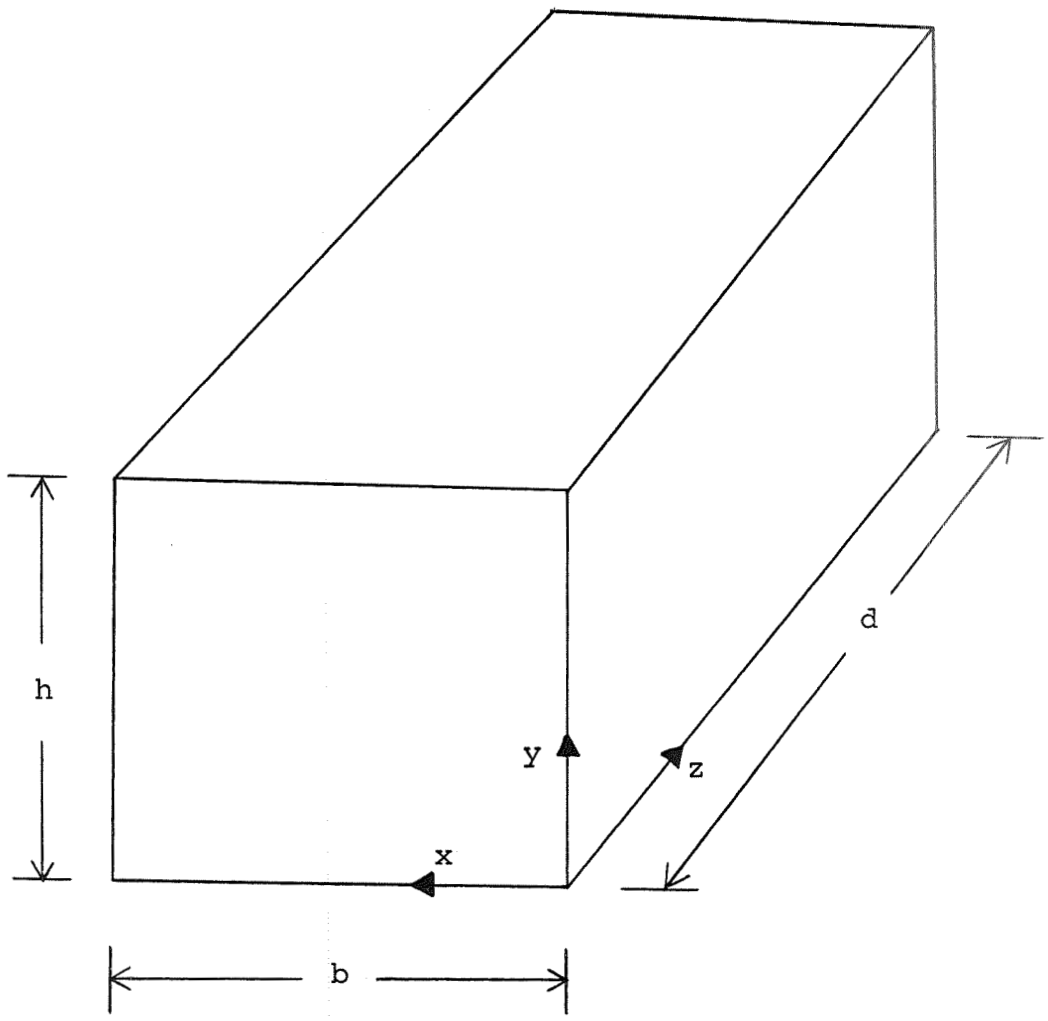

Figure 5.2. Conventional rectangular resonator

where

$$k_c^2 = \left(\frac{m\pi}{b}\right)^2 + \left(\frac{n\pi}{h}\right)^2 \quad ;$$

$$k = \frac{2\pi}{\lambda} = \left[\left(\frac{m\pi}{b}\right)^2 + \left(\frac{n\pi}{h}\right)^2 + \left(\frac{p\pi}{d}\right)^2 \right]^{1/2} . \tag{5.50}$$

The resonant frequency is given by

$$f_o = \frac{1}{2\pi \sqrt{\mu_o \varepsilon_o}} \left[\left(\frac{m\pi}{b}\right)^2 + \left(\frac{n\pi}{h}\right)^2 + \left(\frac{p\pi}{d}\right)^2 \right]^{1/2} . \tag{5.51}$$

The modes of major interest are for no variations in the y-direction, i.e. n=0. The fields then become

$$E_z = 0 \quad , \tag{5.52}$$

$$H_z = H_o \cos\left(\frac{m\pi x}{b}\right) \sin\left(\frac{p\pi z}{d}\right) , \tag{5.53}$$

$$H_y = 0 \quad , \tag{5.54}$$

$$H_x = - \frac{H_o}{k_c^2} \left(\frac{p\pi}{d}\right) \left(\frac{m\pi}{b}\right) \sin\left(\frac{m\pi x}{b}\right) \cos\left(\frac{p\pi z}{d}\right) , \tag{5.55}$$

$$E_x = 0 \quad , \tag{5.56}$$

$$E_y = \frac{-j\omega\mu_o H_o}{k_c^2} \left(\frac{m\pi}{b}\right) \sin\left(\frac{m\pi x}{b}\right) \sin\left(\frac{p\pi z}{d}\right) . \tag{5.57}$$

These modes produce currents in only one direction on the side walls of the y-z plane. At resonants the energy oscillates between the electric and magnetic fields, and at the instant the energy stored in the electric field is a maximum, the energy in the magnetic field is zero. The stored energy then is

$$U = U_{E(max)} = \frac{\varepsilon}{2} \iiint |E|^2 \, dV. \tag{5.58}$$

Therefore for the $TE_{m,o,p}$ modes

$$U = \frac{\omega^2 \mu^2 \varepsilon}{2 k_c^4} H_o^2 \left(\frac{m\pi}{b}\right)^2 \left(\frac{b}{2}\right) (h) \left(\frac{d}{2}\right) . \tag{5.59}$$

To obtain the approximate value of the power loss in the walls, the wall current is given by the tangential magnetic field at the surface. The power loss of each wall is given by

$$P_L = \frac{R_s}{2} \int\int |H|^2 \, dS \tag{5.60}$$

where H is evaluated at the surface, dS is the surface area and R_s is the surface resistivity. Then the power losses for each set of walls is

$$P_{L\ x\text{-}y\ plane} = \frac{R_s}{2} \frac{H_o^2}{k_c^4} \left(\frac{p\pi}{d}\right) \left(\frac{m\pi}{b}\right) h\, b \ , \tag{5.61}$$

$$P_{L\ x\text{-}z\ plane} = \frac{R_s}{4} H_o^2 bd \left\{1 + \frac{1}{k_c^4} \left(\frac{p\pi}{d}\right)^2 \left(\frac{m\pi}{b}\right)^2\right\}, \tag{5.62}$$

$$P_{L\ y\text{-}z\ plane} = \frac{R_s}{2} H_o^2 \, h\, d \ , \tag{5.63}$$

Therefore the total power loss is

$$P_L = \frac{R_s H_o^2}{4 k_c^4} \left\{\left(\frac{p\pi}{d}\right)^2 \left(\frac{m\pi}{b}\right)^2 b(d+2h) + k_c^4 d(b+2h)\right\}. \tag{5.64}$$

The Q of the resonator is given by

$$Q = \omega_o \, U/P_L \tag{5.65}$$

therefore

$$Q = \frac{k_o^3 \eta}{\varepsilon R_s \left\{\left(\frac{p\pi}{d}\right)^2 \left(\frac{d+2h}{dh}\right) + \left(\frac{m\pi}{b}\right)^2 \left(\frac{b+2h}{bh}\right)\right\}} \tag{5.66}$$

where $k_c^2 = (\frac{m\pi}{b})^2$;

$$k_o^2 = (\frac{m\pi}{b})^2 + (\frac{p\pi}{d})^2 \ .$$

Then for the $TE_{m,o,p}$ modes

$$f_o = \frac{1}{2\pi\sqrt{\mu_o \varepsilon_o}} \left[(\frac{m\pi}{b})^2 + (\frac{p\pi}{d})^2 \right]^{1/2} \qquad (5.67)$$

The fractional part of the total losses for each set of walls is

$$\frac{P_{L\ x=y\ plane}}{P_L} = \frac{2\ (\frac{p\pi}{d})^2\ hb}{D} \ , \qquad (5.68)$$

$$\frac{P_{L\ x-z\ plane}}{P_L} = \frac{(\frac{m\pi}{b})^2 + (\frac{p\pi}{d})^2\ bd}{D} \ , \qquad (5.69)$$

$$\frac{P_{L\ y-z\ plane}}{P_L} = \frac{2\ (\frac{p\pi}{d})^2\ hb}{D} \ ; \qquad (5.70)$$

where $D = (\frac{p\pi}{d})^2\ b\ (d+2h) + (\frac{m\pi}{b})^2\ d\ (b+2h)$.

The Q of the resonator is related to each of these ratios as

$$Q = \frac{P_{L\ x-y\ plane}}{P_L}\ Q_{x-y\ plane} \ , \qquad (5.71)$$

$$Q = \frac{P_{L\ x-z\ plane}}{P_L}\ Q_{x-z\ plane} \ , \qquad (5.72)$$

$$Q = \frac{P_{L\ y-z\ plane}}{P_L}\ Q_{y-z\ plane} \ . \qquad (5.73)$$

5.4 The Open H-guide Resonator

A shorted section of H-guide acts as a resonator. Under such conditions the field equations within the resonator are as follows, where the superscript refers to the region (a for air, d for dielectric) and the subscript for the vector component:

$$E_x^a = e^{-\alpha_x x} \cos(k_y y) \sin(k_z z) , \tag{5.74}$$

$$E_y^a = \frac{\alpha_x k_y}{k_c^2} e^{-\alpha_x x} \sin(k_y y) \sin(k_z z) , \tag{5.75}$$

$$E_z^a = \frac{-\alpha_x k_z}{k_c^2} e^{-\alpha_x x} \cos(k_y y) \cos(k_z z), \tag{5.76}$$

$$H_x^a = 0 , \tag{5.77}$$

$$H_y^a = \frac{j}{\omega\mu_o} \frac{k_z k_o^2}{k_c^2} e^{-\alpha_x x} \cos(k_y y) \cos(k_z z), \tag{5.78}$$

$$H_z^a = \frac{j}{\omega\mu_o} \frac{k_y k_o^2}{k_c^2} e^{-\alpha_x x} \sin(k_y y) \sin(k_z z), \tag{5.79}$$

$$E_x^d = \frac{e^{-\alpha_x d}}{\varepsilon_r \cos(k_x d)} \cos(k_x x) \cos(k_y y) \sin(k_z z), \tag{5.80}$$

$$E_y^d = \frac{\alpha_x k_y e^{-\alpha_x d}}{k_c^2 \sin(k_x d)} \sin(k_x x) \sin(k_y y) \sin(k_z z), \tag{5.81}$$

$$E_z^d = \frac{-\alpha_x k_x e^{-\alpha_x d}}{k_c^2 \sin(k_x d)} \sin(k_x x) \cos(k_y y) \cos(k_z z), \tag{5.82}$$

$$H_x^d = 0 , \tag{5.83}$$

$$H_y^d = \frac{j}{\omega\mu_o} \frac{k_z k_o^2 e^{-\alpha_x d}}{k_c^2 \cos(k_x d)} \cos(k_x x) \cos(k_y y) \cos(k_z z), \quad (5.84)$$

$$H_z^d = \frac{j}{\omega\mu_o} \frac{k_y k_o^2 e^{-\alpha_x d}}{k_c^2 \cos(k_x d)} \cos(k_x x) \sin(k_y y) \sin(k_z z), \quad (5.85)$$

The definitions for the parameters are given in Section 5.1.

The Q-value for the resonator is given by

$$Q = \omega U / P_L \quad . \quad (5.86)$$

The stored energy is

$$U = \mu/2 \iiint (\underline{H} \cdot \underline{H}^*) \, dV \quad (5.87)$$

which gives

$$U = \frac{b\ell\varepsilon_o k_o^2}{16 k_c^2} e^{-\alpha_x d} \left[\frac{1}{\alpha_x} + \frac{1}{k_x^2} (g^2 d + \varepsilon_r \alpha_x) \right] \quad (5.88)$$

The power dissipated in each wall is given by

$$P = \frac{R_s}{2} \iint (\underline{H} \cdot \underline{H}^*)_{\text{at wall}} \, d S_s \quad (5.89)$$

where dS_s is the differential element of the wall surface area. The losses in the side walls are

$$P_s = \frac{R_s \varepsilon_o \ell k_o^2 k_y^2}{4 \mu_o k_c^4} e^{-2\alpha_x d} \left[\frac{1}{\alpha_x} + \frac{1}{k_x^2} (g^2 d + \varepsilon_r \alpha_x) \right] \quad (5.90)$$

and losses in the shorting plates are

$$P_e = \frac{R_s \varepsilon_o b k_o^2 k_z^2}{4 \mu_o k_c^4} e^{-2\alpha_x d} \left[\frac{1}{\alpha_x} + \frac{1}{k_x^2} (g^2 d + \varepsilon_r \alpha_x) \right] . \quad (5.91)$$

The losses in the dielectric are given by

$$P_d = \frac{\omega \varepsilon_o \varepsilon_r \tan\delta}{2} \iiint (\underline{E} \cdot \underline{E}^*) \, d V_d \quad (5.92)$$

where dV_d is the differential volume element of the dielectric strip, which gives

$$P_d = \frac{\tan}{16} \frac{k_o \varepsilon_o \, b \, \ell}{\sqrt{\mu_o \, \varepsilon_o}} \left[k_o^2 g^2 d - (k_x^2 - k_c^2) \alpha_x \right] \frac{e^{-2\alpha_x d}}{k_x^2 k_c^2} \quad . \tag{5.93}$$

The propagation constants in the z-direction and the y-direction are

$$k_z = \frac{n \pi}{\ell} \quad \text{and} \quad k_y = \frac{m \pi}{b} \, .$$

Of major interest is the modes with one-half period variation in the y-direction, i.e. m=1. Then the Q-value of the side walls and the shorting plates are respectively

$$Q_s = \frac{k_o \eta}{4 R_s} \quad b^3 \quad \frac{k_o^2 + \alpha_x^2}{\pi^2} \tag{5.94}$$

and

$$Q_e = \frac{k_o \eta}{4 R_s} \quad \frac{\ell^3}{n^2} \quad \frac{k_o^2 + \alpha_x^2}{\pi^2} \tag{5.95}$$

The Q-value of the dielectric is given by

$$Q_d = \frac{k_x^2 + \alpha_x (g^2 d + \varepsilon_r \alpha_x)}{\alpha_x \tan\delta \left[g^2 d - \frac{\alpha_x}{k_o^2} (k_x^2 - k_c^2) \right]} \quad . \tag{5.96}$$

The Q-value of the open H-guide is

$$\frac{1}{Q} = \frac{1}{Q_s} + \frac{1}{Q_e} + \frac{1}{Q_d} \quad . \tag{5.97}$$

The resonant frequency is determined by the solution to the simultaneous equations

$$k_o^2 \varepsilon_r = k_x^2 + k_y^2 + k_z^2 \tag{5.98}$$

and

$$k_o^2\,\varepsilon_r^2 = -k_x^2\tan^2(k_x d) + \varepsilon_r^2\,(k_y^2 + k_z^2). \quad (5.99)$$

5.5 Closed H-guide Resonator

The structure of the closed H-guide is illustrated in Figure 5.3. The closed H-guide is the conventional H-guide with a conducting plane placed equal distance above and below the dielectric strip. The presence of the conducting plane produces new boundary conditions for the solutions of fields within such a structure. The H-guide required the fields to go to zero at infinity in the X-direction but with a conducting plane the standard boundary condition at this interface must be satisfied. The resulting field expressions are modifications of the open H-guide fields. Again the script notation is used as given in Section 5.4.

$$E_x^a = 2\,e^{-\alpha_x h}\cosh(\alpha_x x - \alpha_x h)\cos(k_y y)\sin(k_z z), \quad (5.100)$$

$$E_y^a = \frac{-2\alpha_x k_y}{k_c^2}\,e^{-\alpha_x h}\sinh(\alpha_x[x-h])\sin(k_y y)\sin(k_z z), \quad (5.101)$$

$$E_z^a = \frac{2\alpha_x k_z}{k_c^2}\,e^{-\alpha_x h}\sinh(\alpha_x[x-h])\cos(k_y y)\cos(k_z z), \quad (5.102)$$

$$H_x^a = 0, \quad (5.103)$$

$$H_y^a = \frac{j}{\omega\mu_o}\,\frac{2k_z k_o^2}{k_c^2}\,e^{-\alpha_x h}\cosh(\alpha_x[x-h])\cos(k_y y)\cos(k_z z), \quad (5.104)$$

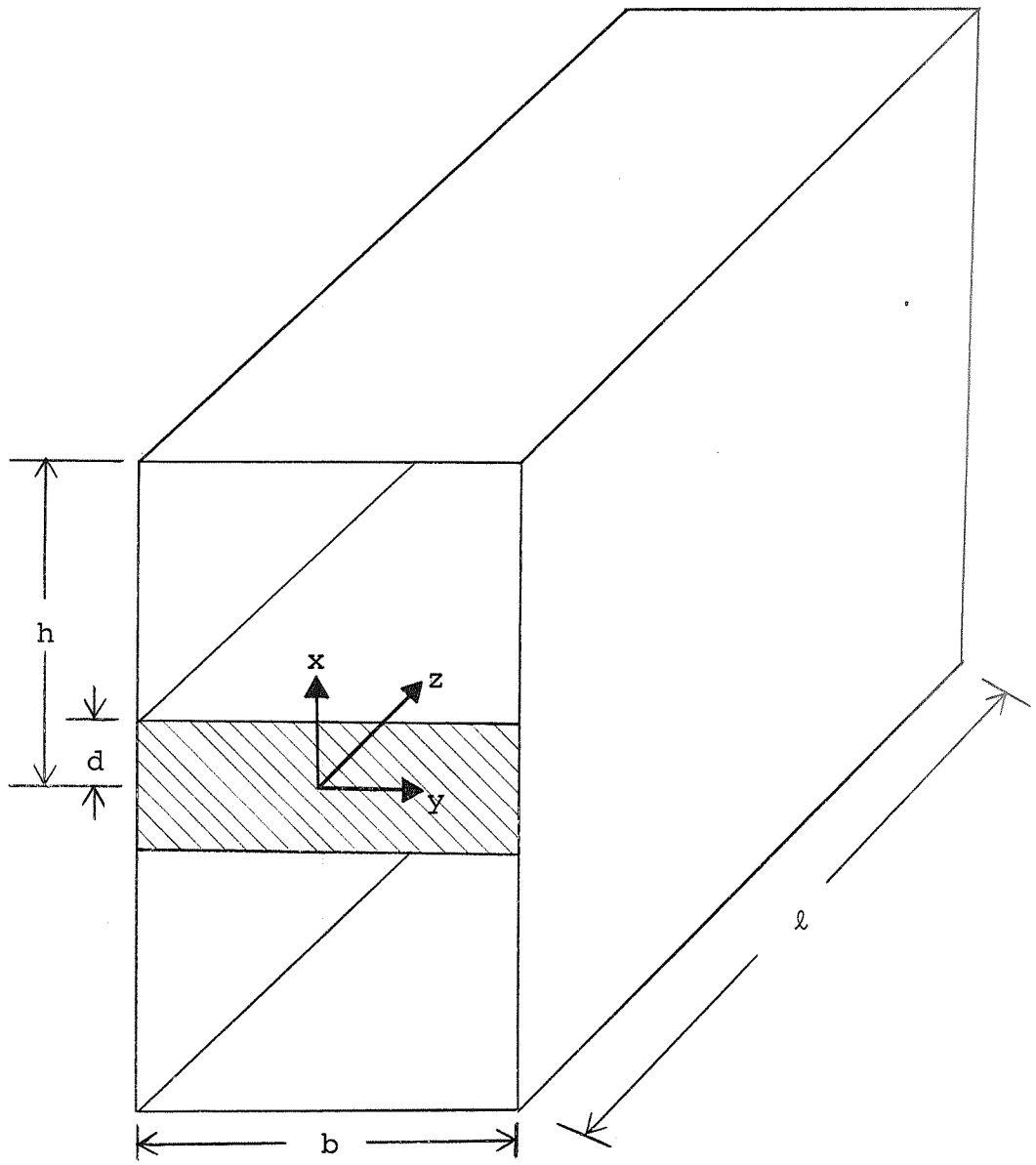

Figure 5.3. Closed H-guide resonator

$$H_z^a = \frac{j}{\omega\mu_o}\frac{2k_y k_o^2}{k_c^2} e^{-\alpha_x h}\cosh(\alpha_x[x-h])\sin(k_y y)\sin(k_z z), \quad (5.105)$$

$$E_x^d = \frac{2}{\varepsilon_r \cos(k_x d)} e^{-\alpha_x h}\cosh(\alpha_x[d-h])\cos(k_x x)$$
$$\cos(k_y y)\sin(k_z z), \quad (5.106)$$

$$E_y^d = \frac{2\alpha_x k_y}{k_c^2 \sin(k_x d)} e^{-\alpha_x h}\cosh(\alpha_x[d-h])\sin(k_x d)$$
$$\sin(k_y y)\sin(k_z z), \quad (5.107)$$

$$E_z^d = \frac{2\alpha_x k_z^2}{k_c^2 \sin(k_x d)} e^{-\alpha_x h}\sinh(\alpha_x[d-h])\sin(k_x x)$$
$$\cos(k_y y)\cos(k_z z), \quad (5.108)$$

$$H_x^d = 0, \quad (5.109)$$

$$H_y^d = \frac{j\,2\,k_z k_o^2}{\omega\mu_o k_c^2 \cos(k_x d)} e^{-\alpha_x h}\cosh(\alpha_x[d-h])$$
$$\cos(k_x x)\sin(k_y y)\sin(k_z z), \quad (5.110)$$

$$H_z^d = \frac{j\,2\,k_y k_o^2}{\omega\mu_o k_c^2 \cos(k_x d)} e^{-\alpha_x h}\cosh(\alpha_x[d-h])$$
$$\cos(k_x x)\sin(k_y y)\sin(k_z z), \quad (5.111)$$

The characteristic equations are the same as for the open H-guide,

$$k_o^2 \varepsilon_r = k_x^2 + k_y^2 + k_z^2 \quad (5.112)$$

and

$$k_o^2 = -\alpha_x^2 + k_y^2 + k_z^2, \quad (5.113)$$

but field matching at the interface of the dielectric strip

and air gives a modified expression,

$$\alpha_x \varepsilon_r = k_x \tan(k_x d) \coth(\alpha_x[h-d]) \quad . \tag{5.114}$$

In the same manner as in Section 5.4, the stored energy is

$$U = \frac{\varepsilon_o b \ell k_o^2}{16 \alpha_x k_x^2 k_c^2} \left[k_x^2 \{ e^{-2\alpha_x d} - e^{-2\alpha_x (h-d)} + 4\alpha_x (h-d) e^{-2\alpha_x h} \} \right.$$

$$\left. + \alpha_x \{ e^{-\alpha_x d} + e^{-\alpha_x (2h-d)} \} \{ g^2 d + \varepsilon_r \alpha_x \} \right] \tag{5.115}$$

The losses in the side walls are

$$P_s = \frac{R_s \varepsilon_o \ell k_o^2 k_y^2}{4 \mu_o \alpha_x k_x^2 k_o^2} \left[k_x^2 \{ e^{-2\alpha_x d} - e^{-2\alpha_x (h-d)} + 4\alpha_x (h-d) e^{-2\alpha_x h} \} \right.$$

$$\left. + \alpha_x \{ e^{-\alpha_x d} + e^{-\alpha_x (2h-d)} \} \{ g^2 d + \varepsilon_r \alpha_x \} \right] \tag{5.116}$$

and the losses in the shorting plates are

$$P_e = \frac{R_s \varepsilon_o b k_o^2 k_z^2}{4 \mu_o \alpha_x k_x^2 k_c^2} \left[k_x^2 \{ e^{-2\alpha_x d} - e^{-2\alpha_x d (h-d)} + 4\alpha_x (h-d) e^{-2\alpha_x h} \} \right.$$

$$\left. + \alpha_x \{ e^{-\alpha_x d} + e^{-\alpha_x (2h-d)} \} \{ g^2 d + \varepsilon_r \alpha_x \} \right] . \tag{5.117}$$

The dielectric losses are

$$P_d = \frac{\tan\delta}{4} \frac{\varepsilon_o b \ell k_o}{\sqrt{\mu_o \varepsilon_o}} \left[k_o^2 g^2 d - (k_x^2 - k_c^2) \alpha_x \right] \frac{\sinh^2(\alpha_x [h-d])}{k_x^2 k_c^2} \tag{5.118}$$

The presence of the conducting plane above and below the dielectric strip gives the additional losses

$$P_c = \frac{R_s \varepsilon_o b \ell k_o^2}{2 \mu_o k_c^2} e^{-2\alpha_x h} \tag{5.119}$$

Then the Q-value of the side walls and the shorting plates are respectively for the modes of interest

$$Q_s = \frac{k_o \eta}{4 R_s} \quad b^3 \quad \frac{k_o^2 + \alpha_x^2}{\pi^2} \tag{5.120}$$

and

$$Q_e = \frac{k_o \eta}{4 R_s} \quad \frac{\ell^3}{n^2} \quad \frac{k_o^2 + \alpha_x^2}{\pi^2} \tag{5.121}$$

The Q-value of the dielectric is

$$Q = N/D \tag{5.122}$$

where $N=k_x^2\{e^{-2\alpha_x d}-e^{-2\alpha_x(h-d)}+4\alpha_x(h-d)e^{-2\alpha_x h}\}+4\alpha_x\{g^2 d+\varepsilon_r\alpha_x\}$

$e^{-2\alpha_x h}\cosh^2(\alpha_x[h-d])$,

and $D=4\alpha_x \tan\delta \left[g^2 d- \frac{\alpha_x}{k_o^2} (k_x^2-k_c^2)\right]e^{-2\alpha_x h}\sinh^2(\alpha_x[h-d])$.

The additional Q-value of the conducting plane is

$$Q_c= \frac{k_o \eta}{8 R_s} \frac{1}{k_x^2 \alpha_x} \left[k_x^2\{e^{2\alpha_x(h-d)} -e^{-2\alpha_x d}+4\alpha_x(h-d)\} + \right.$$

$$\left. \alpha_x \{g^2 d+\varepsilon_r\alpha_x\} \{e^{-\alpha_x d}+e^{-\alpha_x(2h-d)}\}^2 e^{2\alpha_x h}\right] . \tag{5.123}$$

The Q-value of the closed H-guide is

$$\frac{1}{Q} = \frac{1}{Q_s} + \frac{1}{Q_e} + \frac{1}{Q_d} + \frac{1}{Q_c} . \tag{5.124}$$

The resonant frequency is determined by the solution to the simultaneous equations

$$k_o^2 \varepsilon_r = k_x^2 + k_y^2 + k_z^2 \tag{5.125}$$

and

$$k_o^2 = -\frac{k_x^2}{\varepsilon_r^2}\tan^2(k_x d)\coth^2(\alpha_x[h-d]) + k_y^2 + k_z^2 . \quad (5.126)$$

5.6 Comparison of Resonators

A major difference in the two types of resonator guides is the H-field. The H-field normal to the dielectric strip is identical zero for the H-guide resonator, but for the rectangular resonator, a component of the H-field is only zero for modes where m or n is zero, i.e. the eigenvalue is zero. The important result of this feature of the H-guide is that the mating of sections or the shorting plates produce no current flow across the joints. By proper choice of modes in the conventional rectangular resonator, the same condition can exist.

The fields within the H-guide resonator decrease exponentially with distance from the dielectric strip. This is beneficial for the case of the closed H-guide resonator since the field strength at the conducting planes above and below the dielectric strip is greatly decreased. In terms of power, the power losses in the conducting plane is small compared to the other losses and greatly reduces the power losses that could possibly radiate through wall joints at these conducting planes.

The resonant frequencies of the conventional rectangular resonator as given by (5.51) is dependent upon the

mode and dimension of the resonator and obviously can take on an infinity number of values. The resonant frequency of the open H-guide is limited. The solution to the transcendental equation is illustrated in Figure 5.4. For most practical usage, the dielectric strip of the H-guide is less than one millimeter in thickness, or for d less than one-half of a millimeter. For purposes of illustration, a practical value of d, 0.025 cm and a much thicker strip for which d is 0.2 cm are used to show the effect of increasing thickness of the dielectric strip. The obvious result is that an increasing thickness will cause an increasing number of intersections. However, the thickness of the strip does no affect the characteristic equation as formulated for the dielectric region. For the practical case, there is only one value of k_x that satisfies the equations, and thus a limited number of k_x values are possible in the H-guide resonator. The resonant frequency of the closed H-guide has similar characteristics but the increased complexity of the simultaneous equations makes an iterative solution necessary.

The expressions for the Q-values of the side walls and the shorting plates are identical for both the open and the closed H-guide resonators. The presence of the additional conducting planes affects the dielectric Q-value and creates the additional Q-value of these conducting planes. A direct comparison is not possible since the position of the

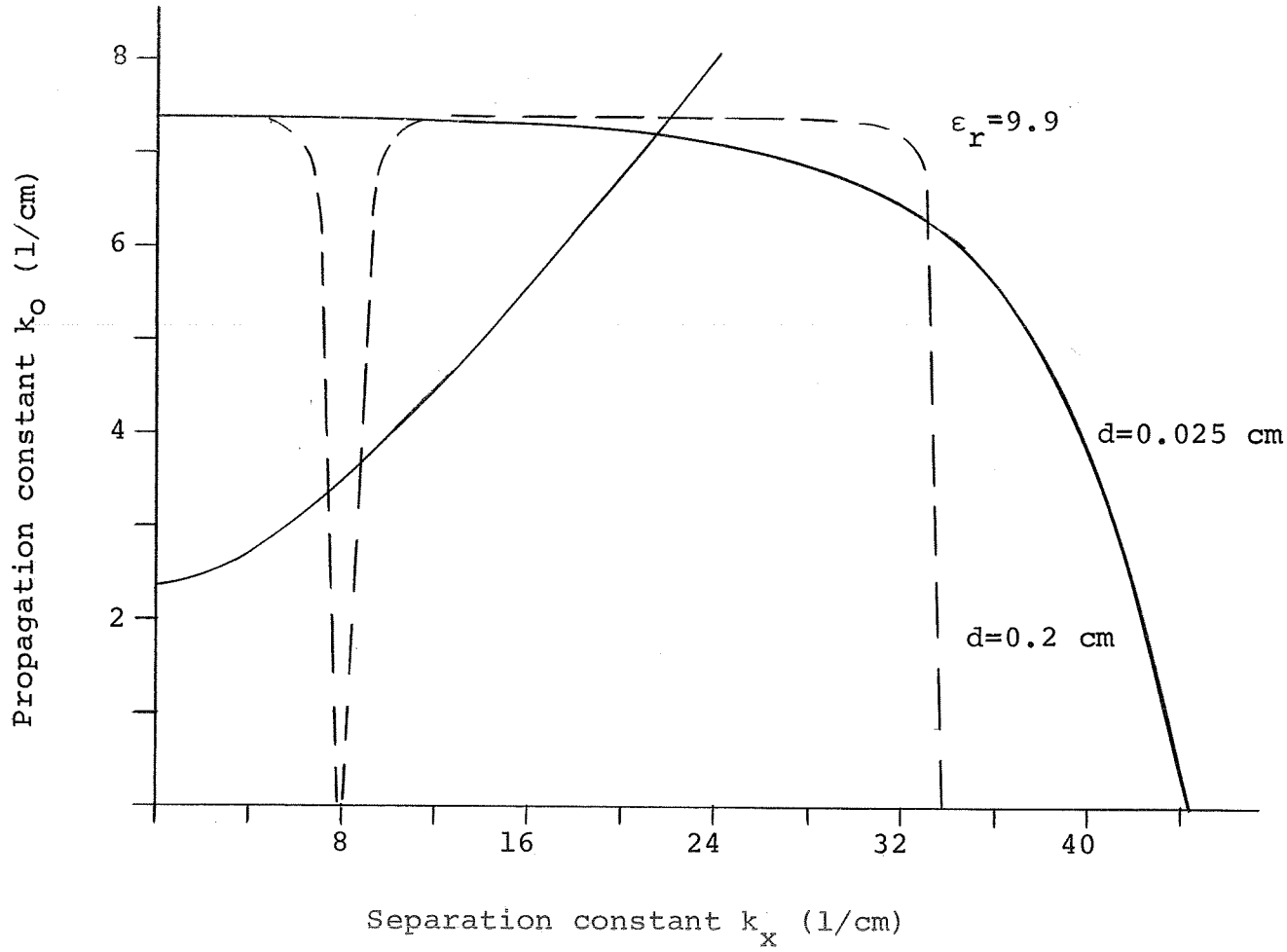

Figure 5.4. Graphic solution of resonant frequency of H-guide resonator

additional planes affect all of the field parameters. However, if h is large as compared to d the effects of the additional plane is minimized. In the limit as h goes to infinity, the open and closed H-guide parameters are in complete agreement.

The effect of the position of the additional conducting plane is illustrated in Figure 5.5. The position of the conducting plane is shown on the figure.

5.7 Loss Factors

The conventional rectangular resonator loss factor is the surface resistivity. The surface resistivity is given by

$$R_s = \sqrt{\frac{\pi f \mu}{\sigma_c}}$$

where σ_c is the conductivity of the material. For hard drawn copper σ_c is 5.65×10^7 mhos per meter and for the 30 to 40 GHz frequency range, the surface resistivity is 0.046 to 0.053 ohms. This loss factor is based on the frequency and the bulk property of the material. The skin depth for this frequency range is 0.387 to 0.335 microns for 20 to 40 GHz respectively.

The losses in the H-guide resonator are dependent upon both the surface resistivity of the metal walls and the dielectric loss tangent. If the parameter α_x is normalized with respect to k_o, then the individual Q-values can be rewritten as

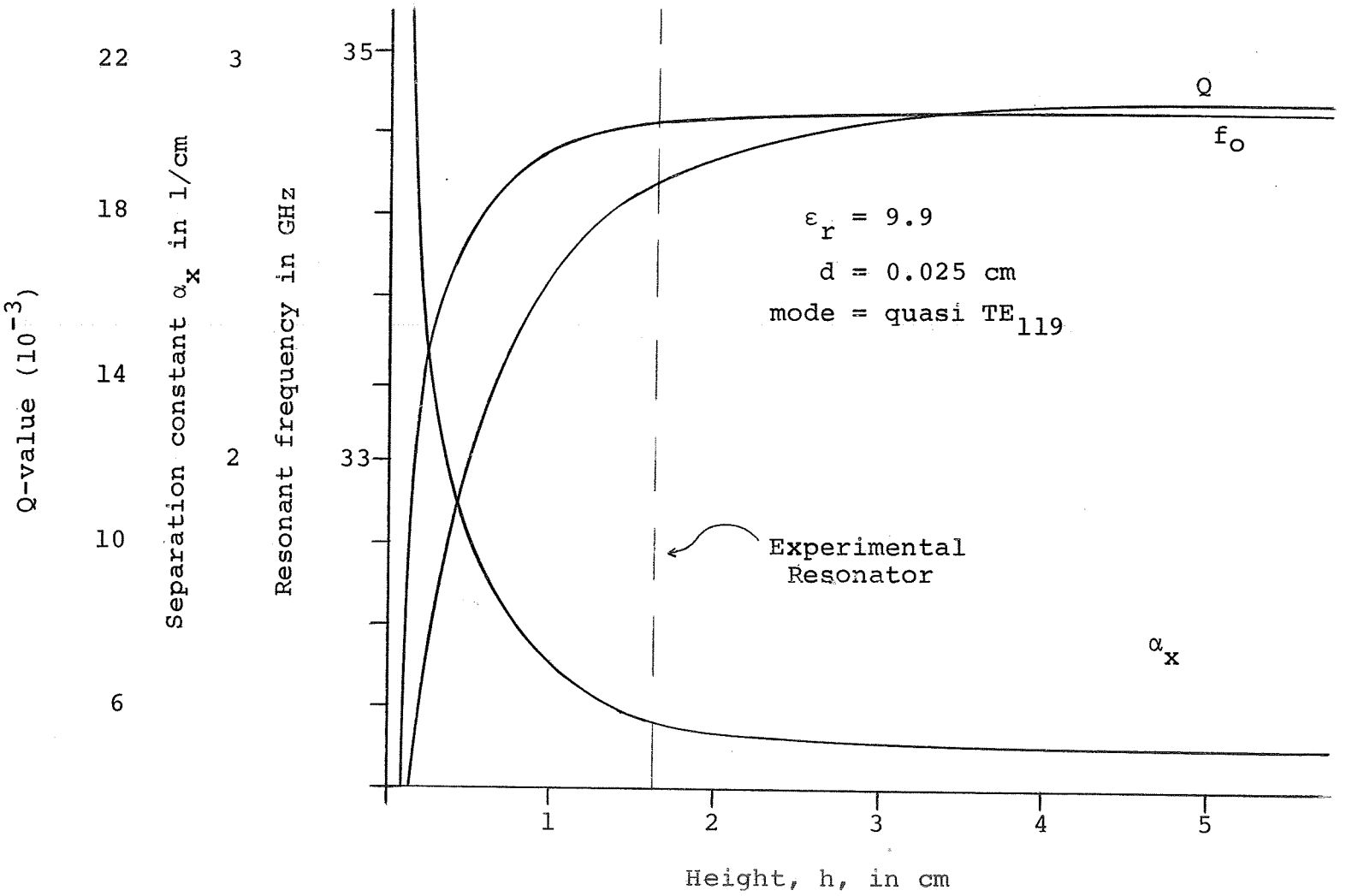

Figure 5.5. Effects of the position of the upper and lower walls on the closed H-guide resonator parameters

$$Q_s' = Q_s \frac{R_s}{b'^3} = \frac{\eta}{4} \frac{1+p^2}{\pi^2} \tag{5.127}$$

$$Q_e' = Q_e \frac{n^2 R_s}{\ell'^3} = \frac{\eta}{4} \frac{1+p^2}{\pi^2} \tag{5.128}$$

and

$$Q_d' = Q_d \tan\delta = \frac{\varepsilon_r - 1}{p} \frac{1+pd' + p^2 + p^3 d'(\varepsilon_r+1)}{[\varepsilon_r-1][p^2(\varepsilon_r+1)+1]d' - p(\varepsilon_r - 2p^2 - 2)} \tag{5.129}$$

where $b'=k_o b$, $\ell'=k_o \ell$, $d'=k_o d$, and $p=\alpha_x/k_o$.

Using these normalizations, the Q of the resonator can be found from the relationship

$$\frac{1}{Q} = \frac{1}{Q_s} + \frac{1}{Q_e} + \frac{1}{Q_d} \quad . \tag{5.130}$$

Rearranging

$$\frac{1}{Q'} = \frac{1}{Q} \frac{b'}{R_s(1+n^2 b'^3/\ell'^3)} = \frac{1}{Q_s'} + \frac{B}{Q_d'} \tag{5.131}$$

where

$$B = \frac{\tan\delta \quad b'^3}{R_s(1+n^2 b'^3/\ell'^3)} \ .$$

Thus, B illustrates the effects of the losses in the H-guide resonator. The normalized Q-value for a material having a relative dielectric constant of 10.0 is given in Figure 5.6.

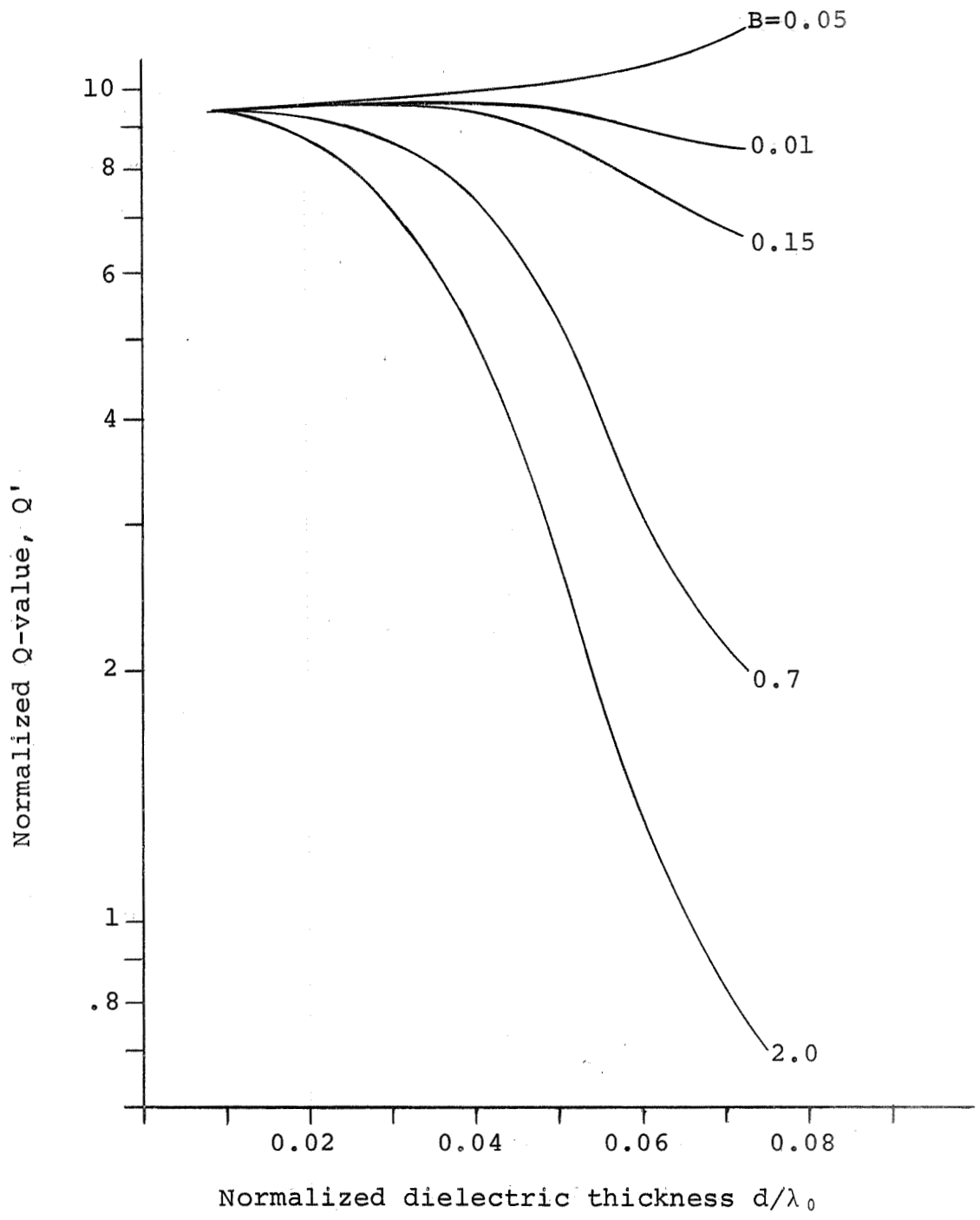

Figure 5.6. Effects of the normalization factor, B, on the normalized Q of the H-guide resonator for $\varepsilon_r = 10.0$

6. EXPERIMENTAL SURFACE LOSS MEASUREMENTS

6.1 Introduction

With the basic concepts introduced in Chapters 3 and 5, the theory was implemented by experimental work that was carried out by use of high frequency equipment. A resonator was constructed that could be used in its conventional modes as well as a closed H-guide resonator.

Since equipment is not readily available for reliable measurements of frequency at the millimeter wavelengths, a scheme was developed for using X-band signals and frequency multiplication to indicate the frequency of the A-band source that was used to generate the millimeter waves. The system allowed for an easy method for determining loaded Q-values. A derivation is shown for converting the loaded Q to the unloaded Q by an evaluation of the insertion loss.

The basic considerations of the resonator needed for a detailed study of the surface losses are discussed in Sections 6.6 and 6.7. The results of measurements of the effects of surface roughness for both mechanical and chemical polishing are shown subsequently.

6.2 Description of the Resonator

The rectangular resonator of the transmission type coupled by circular irises between two sections of rectangular waveguide was used throughout the experiments.

The inside width of the resonator was made equal to the inside width of the standard A-band waveguide (RG 96/U) to insure that only modes of one-half period sinusoidal variation in that direction would be present. The inside height was 3.12 cm and the longitudinal length was 4.78 cm.

Coupling to the waveguide was accomplished by circular holes centered in the resonator end plates. During all of the measurements, irises of 1.854 mm diameter were used since smaller diameters increased the insertion loss to an extent that the signal amplitude has approximately the amplitude of the noise level.

The resonator was constructed of 0.635 cm thick side walls and 1.435 cm thick upper and lower walls. The 0.683 cm thick end plates are permanently attached to the upper and lower walls. All walls are made of copper. The end plates have the coupling hole in an insert which has a 0.068 cm thickness. A detailed view of one end can be seen in Figure 6.1, the other end being identical.

This design allowed for the removal of the side walls without disturbing the remainder of the apparatus. A photograph of the resonator with a dielectric strip is shown in Figure 6.2. For changes made on the side wall surfaces, the side walls were removed and ground to have various degrees of surface roughness. To assure that the side walls return to the same position at the replacement, a flat plate was forced against the bottom of the resonator

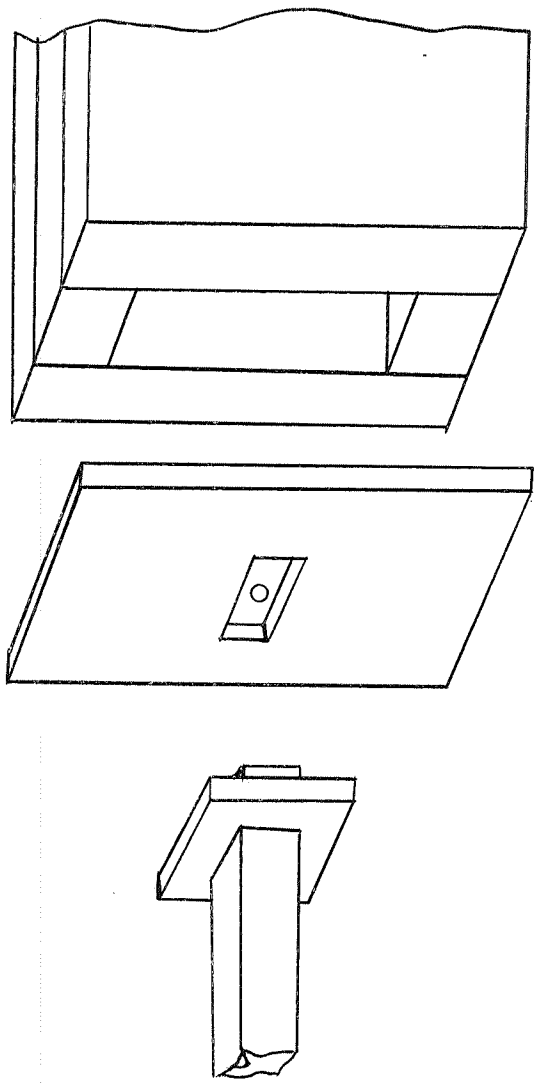

Figure 6.1. Assembly view of resonator end section

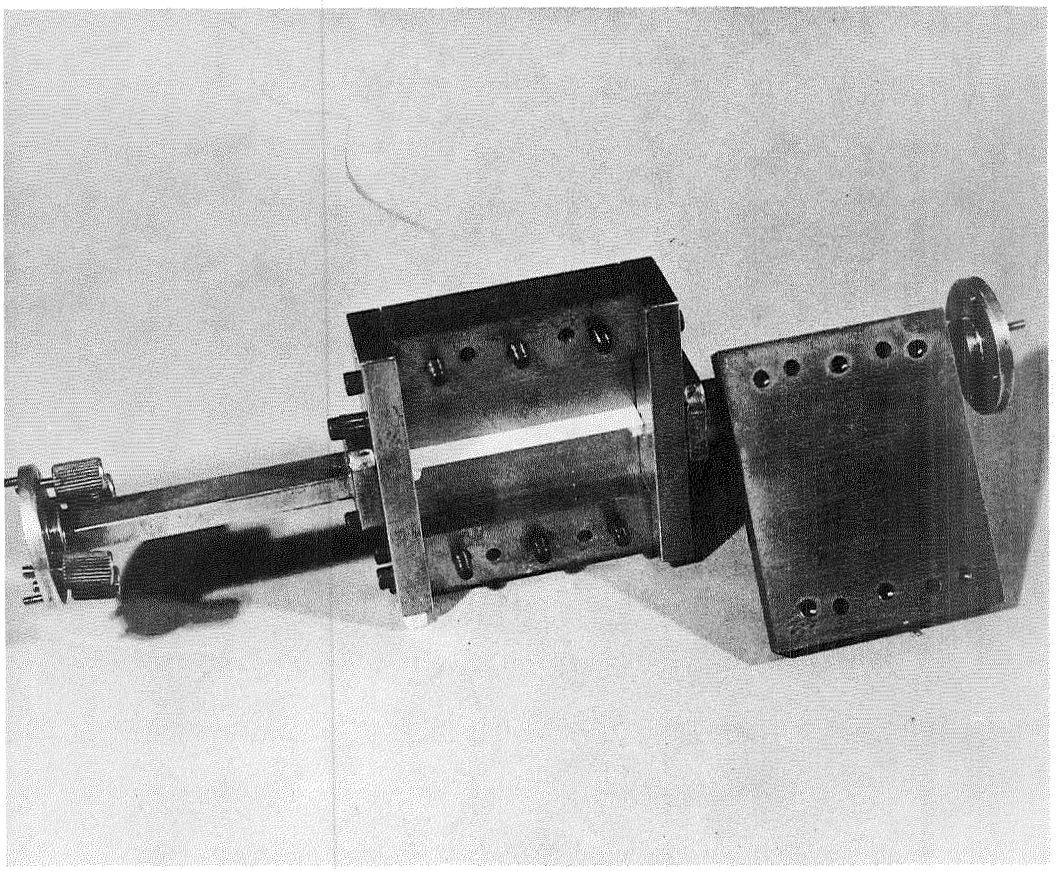

Figure 6.2 Closed H-guide resonator with a side wall removed

causing the bottom surfaces of the side walls to lie in the same common plane. The pressure of the screws on the side walls was held constant by torquing the screws to fifteen inch pounds at each assembly and subsequent measurement.

6.3 Roughness of the Walls

For the preparation of the side walls, the procedure described in Section 4.2 was used. The roughness of the end surfaces, upper and lower walls, all of which were polished to the 600 grit abrasive paper, was held constant throughout the measurements. The side walls were ground to the various abrasive paper levels and then their roughness was determined optically. The final grinding of each side wall left the grooves created by the grains of the abrasive in parallel with the long dimension of the resonator or the z-direction. The grooves were so oriented so that the current present on the side wall would flow transverse to the grooves. The technique for the optical measurements was described in Chapter 4. The walls were then inserted and fastened in the resonator for the Q-value measurements. When not in use the resonator and the walls were stored in a dessicator jar filled with dry nitrogen. The storage prevented oxidation of the surfaces and changing the chemical composition of the surfaces by chemical reactions.

6.4 Test Bench for Q Measurements

The bench set-up as shown in Figure 6.3 has a 35 GHz A-band klystron as the signal source. Power is supplied to

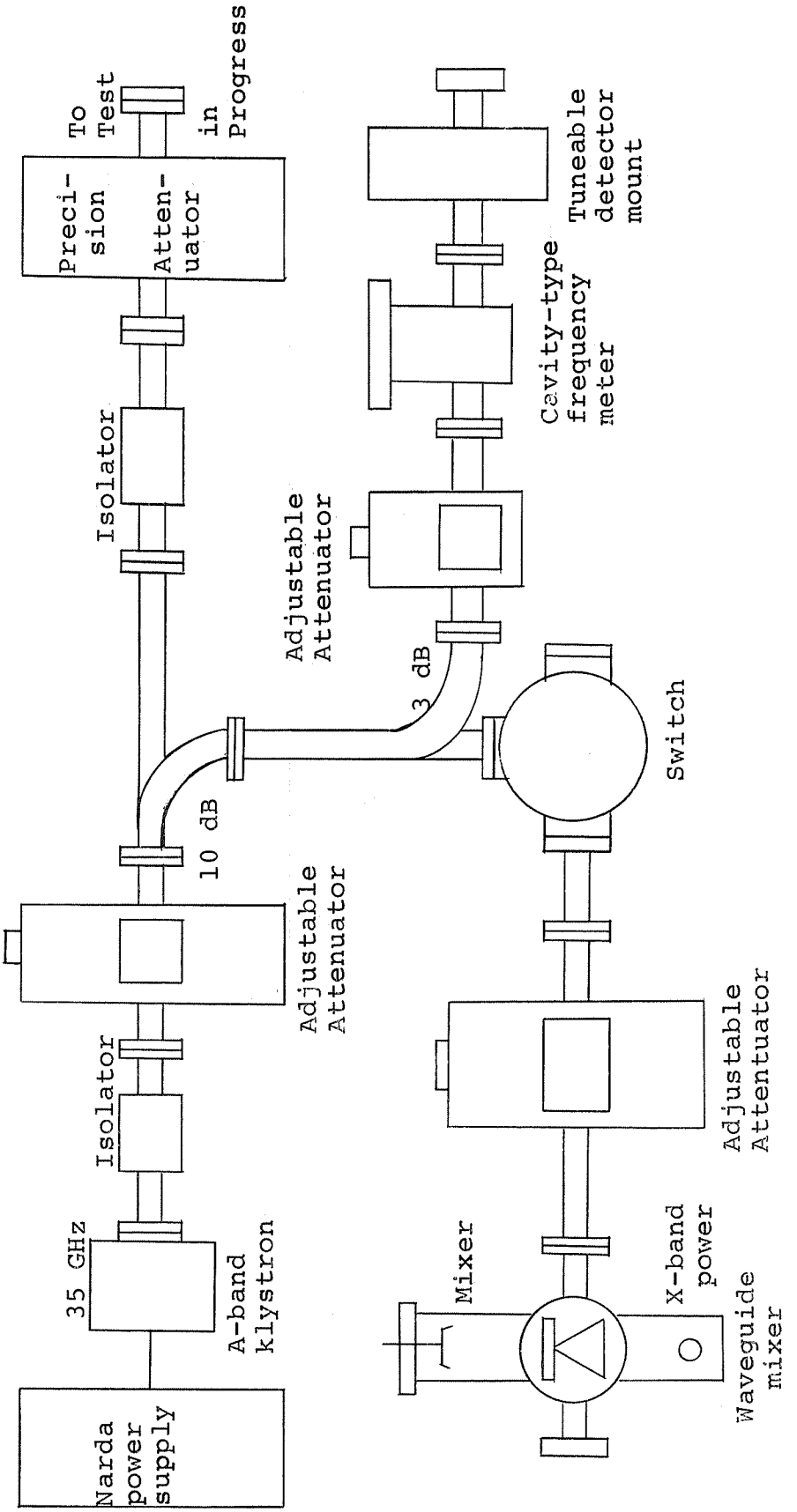

Figure 6.3. Diagram of test bench for Q measurements

the A-band signal source by a Narda 62A1 power supply. The klystron signal is fed through an isolator, an adjustable attenuator and a 10 dB directional coupler. From the main guide of the coupler, the signal travels through an isolator to a precision attenuator and then into the resonator under investigation. The secondary guide of the 10 dB directional coupler is fed into a 3 dB directional coupler which serves as a power divider. The signal of the secondary arm of the 3 dB coupler is fed through an adjustable attenuator and a cavity-type frequency meter to a tunable detector mount. The main arm of the 3 dB coupler is connected to a waveguide switch. The signal from one of the switch positions is fed through an adjustable attenuator into a waveguide mixer. The other switch position may be used for other experiments.

Since no frequency measurement equipment is presently available for frequencies up to 100 GHz, a special set-up was developed for these measurements.

For swept frequency operation the repeller plate of the A-band klystron is modulated with a 60 Hz sawtooth waveform generated by a Model 540 A function generator by Exact Electronics. This makes the klystron signal vary in frequency in proportion to the amplitude of the sawtooth voltage. The sawtooth voltage is also used as the input to the horizontal deflection plate of the HP 1200B oscilloscope. This allows the horizontal deflection of the oscilloscope to be, as an approximation, proportional to frequency. When the klystron

signal is displayed on the oscilloscope (as a function of the repeller voltage), each position of the trace represents a frequency. By one of the traces the mode pattern is monitored and compensated for nonsymmetry and nonlinearity in the wave mode at the Q-value measurements.

In order to know the frequency which corresponds to each horizontal position of the deflected beam the hetrodyne principle is used. A constant CW signal of known frequency (within the range of the display, and with the frequency found by use of a cavity-type frequency meter) is mixed with the operational A-band signal. The operational A-band signal changes linearly in frequency if the amplitude of the modulating sawtooth is kept relatively small. The constant CW signal is the result of frequency multiplication within the mixer and originates in an X-band source that can be adjusted to have its harmonic frequency within the range of that of the swept A-band signal. A Varian X-13 X-band klystron is used as the X-band source and its signal fed into a Demornay Bonardi DBGD-350 crystal multiplier-mixer. The frequency of the X-band source is monitored by an HP 5245 A frequency counter. The other input signal to the crystal mixer is the sawtooth-modulated A-band signal. Variable shorts on the crystal mixer permit adjustments for optimum frequency multiplication and mixing. The crystal current is limited to a maximum of 50 μA.

The output signal of the crystal mixer is amplified in an ac amplifier (10 Hz to 1.4 MHz) and fed into a RC-filter. The output is capacitively coupled to the line connecting the crystal detector to channel B of the oscilloscope for monitoring the klystron mode. On the screen of the oscilloscope, the mode pattern is then displayed with an interference signal superimposed on it. The interference signal is a sine wave with a frequency equal to the difference between the instantaneous A-band frequency which is swept linearly by the sawtooth voltage and the constant-frequency harmonic of the X-band signal frequency. A zero beat occurs at a specific position of the swept beam when the known harmonic of the X-band signal is equal to the unknown A-band signal. The frequency of the swept operational A-band generator at this specific position of the beam is then known also.

If the reflector voltage of the X-band source is modulated by an HP Signal Generator 606A with a sine wave, the X-band-signal will consist of the carrier and two or more side-frequencies ΔF apart, where ΔF is the modulation frequency. The indication of the scope has then the form as shown in Figure 6.4. Because the fourth harmonic is used, the first sideband indication on the scope is one fourth of the frequency on the scope. The beat-frequency spectrum displayed on the oscilloscope is then used to measure the difference frequencies between points on the trace of the scope.

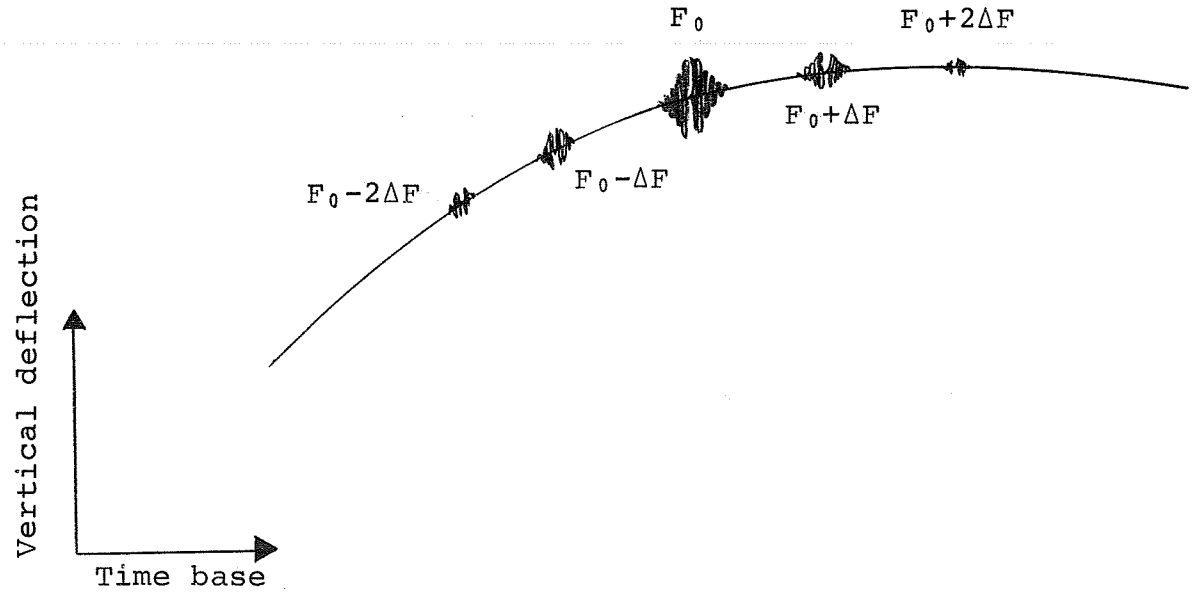

Figure 6.4. Beat signal superimposed on mode signal as observed on the oscilloscope

To measure the Q-value, the test resonator is inserted into the experimental branch of the general set-up. The signal from the A-band klystron is transmitted through the resonator and the resonance curve of the output is displayed on channel B of the oscilloscope. On channel A the mode pattern of the klystron is displayed. The two displays are first aligned without the resonator to coincide. This is accomplished by adjustments of the attenuators and tunable detector mounts. The reading of the precision attenuator is registered. With the test resonator reinserted into the circuit, the mode signal is placed on top of the resonance curve so that the peak of the resonant curve coincides with the klystron mode curve (as indicated in Figure 6.5) by adjusting the precision attenuator. The difference between the two readings of the precision attenuator is the insertion loss in dB. The power into the resonator is then increased by removing 3 dB of attenuation making the intersection of the two curves to be at the half-power points of the resonant curve. Turning on next the beat-frequency spectrum caused by the modulation of the reflector voltage of the X-band klystron and aligning the first sidebands with the intersections of both curves as shown in Figure 6.6, the difference of the half-power frequencies is found. An alternate method consists of measuring the frequency of each intersection and taking the difference between the two frequencies. This method is less accurate, however, due to the time lag between

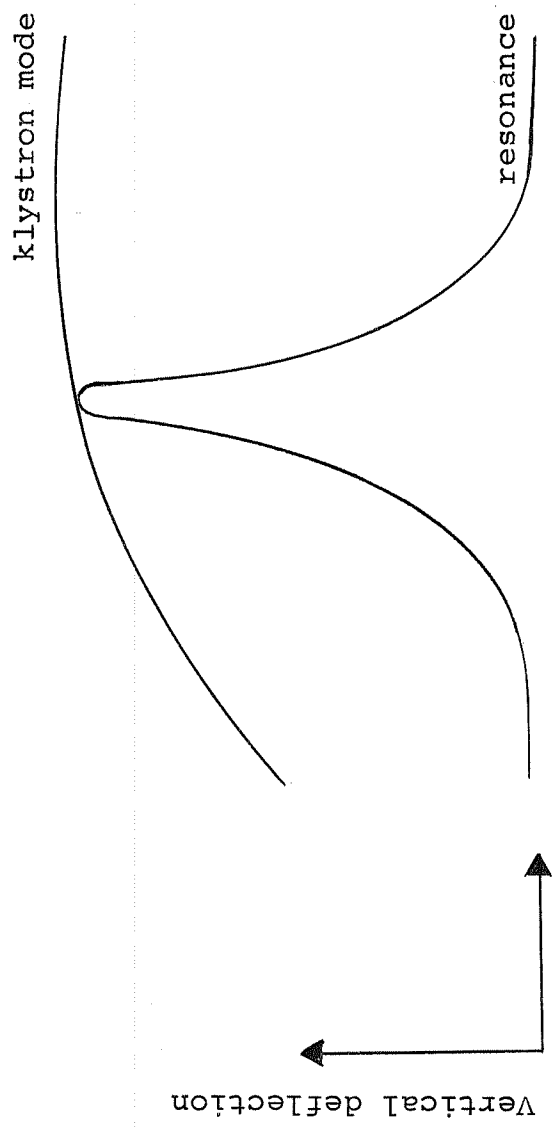

Figure 6.5. Resonance curve aligned with klystron mode curve as observed on the oscilloscope

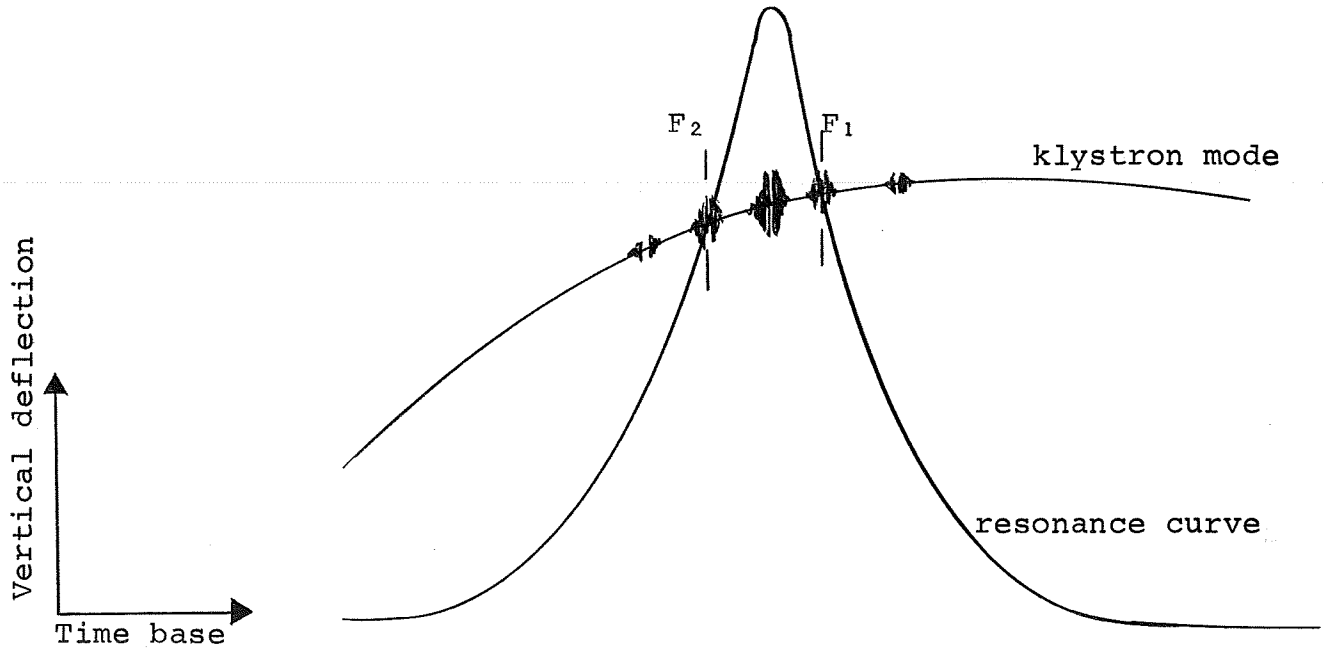

Figure 6.6. Resonance curve increased by 3 dB with interference pattern superimposed on mode curve

the two frequency measurements. Since the carrier frequency as displayed on the oscilloscope is that of the X-band source, the correct frequency (because the fourth harmonic is used) is four times that of the X-band signal. The first sideband frequency is doubled to get the total frequency difference (note that the first sideband frequency displayed on the scope is one-fourth the frequency of the modulating signal). With points F_1 and F_2 corresponding to the half-power frequencies, the loaded Q is $F_o/(F_2-F_1)$. The unloaded Q can be determined from the loaded Q and the insertion loss.

6.5 Theoretical Approach for Determination of the Unloaded Q-values

Montgomery [16] considered the transmission resonator in terms of lumped circuit parameters; an equivalent circuit for the resonator is shown in Figure 6.7. In the general case, the input and output would be different but the symmetrical case is considered since the input and output irises are identical. Ideal transformers represent the irises with turn ratio n:1. If the equivalent circuits of the transformer are utilized, Figure 6.7 becomes Figure 6.8.

The loaded Q, Q_L, for the circuit in Figure 6.7 is given by

$$Q_L = \frac{\omega_o L}{R+n^2(R_G+R_L)} \quad , \tag{6.1}$$

where ω_o is the resonant frequency under consideration. Then (6.1) can be written in terms of the unloaded Q, Q_u, as

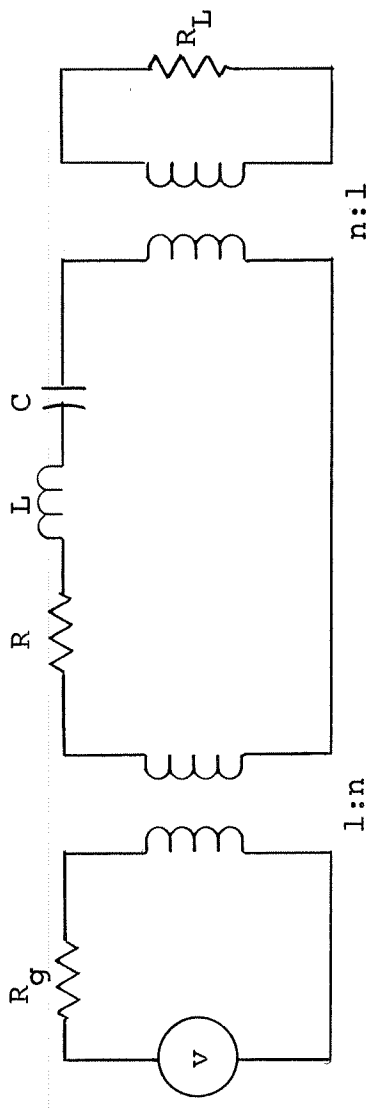

Figure 6.7. Equivalent circuit of transmission resonator with coupling irises shown as ideal transformers

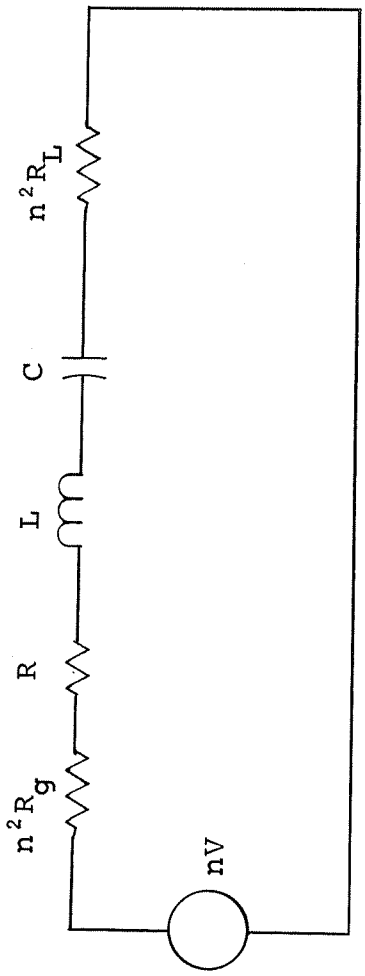

Figure 6.8. Alternative for the circuit shown in Figure 6.7

$$Q_u = Q_L \left[1 + \frac{n^2}{R} (R_G + R_L)\right]. \tag{6.2}$$

If the system is matched ($R_G = R_L$), which can be accomplished by making the voltage standing wave ratio, VSWR, small in both directions, then (6.2) becomes

$$Q_u = Q_L(1 + 2\beta), \tag{6.3}$$

where the coupling parameter, β, has been defined as

$$\beta = \frac{n^2 Z_o}{R} \tag{6.4}$$

and $Z_o = R_L = R_G$. The current for the loop in Figure 6.8 can be written in the form

$$I = \frac{n V}{R\left[(1+2\beta) + j Q_u \left(\frac{\omega}{\omega_0} - \frac{\omega_0}{\omega}\right)\right]}, \tag{6.5}$$

since

$$\omega_o^2 = \frac{1}{L C}. \tag{6.6}$$

The real power deliverd to the load impedance is given by

$$P_L = |I|^2 n^2 Z_o, \tag{6.7}$$

or in terms of β as

$$P_L = |I|^2 \beta R. \tag{6.8}$$

Substituting from (6.5) into (6.8) the power becomes

$$P_L = \frac{V^2 \beta^2}{Z_o\left[(1+2\beta)^2 + Q_u^2 \left(\frac{\omega}{\omega_0} - \frac{\omega_0}{\omega}\right)^2\right]}. \tag{6.9}$$

If the generator were to see a matched load, as in Figure 6.9, the power delivered to the load would be given by

$$P = \frac{V^2}{4 Z_o}. \tag{6.10}$$

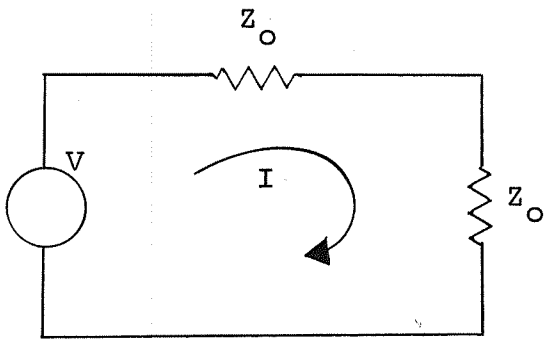

Figure 6.9. Generator, V, feeding a matched load Z_o

A transmission function, $T(\omega)$, defined as P_L/P, can be found from (6.9) and (6.10), that is

$$T(\omega) = \frac{4\beta^2}{[(1+2\beta)^2 + Q_u^2(\frac{\omega}{\omega_0} - \frac{\omega_0}{\omega})^2]}, \tag{6.11}$$

which becomes at resonance

$$T(\omega_0) = \frac{4\beta^2}{(1+2\beta)^2} \tag{6.12}$$

or for β in terms of $T(\omega_0)$ as

$$\beta = \frac{T(\omega_0)}{2[1-\sqrt{T(\omega_0)}]} . \tag{6.13}$$

Upon measuring $T(\omega_0)$ (insertion loss in dB can be transformed to its decimal equivalent), (6.13) yields β, and then (6.3) specifies Q_u after Q_L is measured.

6.6 Basic Considerations for the Resonators

Theoretical predictions of Section 5.3 indicated that the conventional resonator has a resonant frequency of 35.2 GHz for the TE_{109} mode. This mode has strong coupling when the waveguide is excited in the TE_{10} mode. This mode also gives the desired effects, that is, current flow on the side walls are only in one direction. The closed H-guide resonator has a resonant frequency of 34.7 GHz when a strip of dielectric (Lucalox, General Electric Company) having a thickness of 0.05 cm and a permittivity of 9.9 is used. The modes of the closed H-guide resonator are hybrid and this is the quasi TE_{119} mode. The values of the field distribution constant of the air region (α_x) and the wave propagation

constant in the dielectric region (k_x) are 1.36 per cm and 21.7 per cm respectively. This gives a value of the field strength at the upper and lower walls of 0.133 of the value at the center of the resonator or the power flow has decreased to 1.8 per cent. Therefore losses on these walls are negligible. Also, losses and uncertain connections at the intersections of the upper and lower surfaces with the side wall are practically eliminated.

The walls of the resonator were ground to the smoothest finish possible by the test abrasive papers. The procedure outlined in Section 4.2 was used, and as a final step the 600 grit abrasive paper was used. The conventional resonator under these conditions had a measured unloaded Q-value of 11,700. The theoretical Q-value of the TE_{109} mode is 17,800 and the surface loss parameter based on the dc conductivity is 0.049 ohms. Based on the experimental Q-value the surface loss parameter was 0.072 ohms. The handbook [22] value of the dc conductivity is given as 5.65×10^7 mhos per meter for hard drawn copper. A small strip (1.05 mm by 6.16 mm by 47.0 mm) was then cut from one of the side walls and the dc conductivity was measured. The experimental value of dc conductivity was 5.52×10^7 mhos per meter. Based on the experimental value of dc conductivity the surface loss parameter was 0.050 ohms. An excess-loss factor of 1.44 was thus measured under these conditions.

To determine the effects of chemical films on the loss, the side walls of the conventional resonator were polished with the 600 grit abrasive paper and then dipped into several chemical solutions. After the side walls were dry, the walls were assembled on the resonator structure and Q measurements made. The standard condition used throughout the experiments was to wash the walls with rapidly flowing water, followed by blowing a stream of air with sufficient force to remove residual water left on the surface. The Q-values, measured after dipping the side walls in the different chemical solutions, were compared to the water-washed walls. The following solutions gave Q-values which were within five per cent of the Q-value (10,550) of the water-washed walls: trichloroethylene; Oakite 131, a commercial cleaner manufactured by Oakite Products, Incorporated; an electrolytic polishing solution (Orthophosphoric acid with specific gravity of 1.3 to 1.4); an acid dip (by volume, 30% phosphoric acid, 65% glacial acetic acid, 5% concentrated nitric acid); a chemical polishing solution (by volume, 50% concentrated nitric acid, 25% glacial acetic acid, 25% concentrated orthophosphoric acid; 0.625 gm per liter sodium nitrate, 0.625 gm per liter ammonium chloride). Methanol, however, reduced the Q-value by 11.5 per cent and acetone by 32 per cent. Methanol and acetone are commonly used as cleaning agents of surfaces but were avoided when the effects of increased losses were observed.

A dimensional analysis of the two resonators for the modes investigated was made. Replacement of the side walls may have been the only possible cause of a dimensional change since the other walls were permanently attached during all of the experiments. However, by applying a torque to the screws of the side walls at each assembly, the same force was placed on the walls each time, and was believed to have kept dimensional changes to a minimum. If a dimensional change occurred, it certainly was less than 0.1 mm. For the conventional resonator a 0.1 mm change in displacement of the side walls from each other would give a 1.7 per cent change in the Q-value. A 1.2 per cent change in the Q-value and 0.5 per cent change in resonant frequency would result for the same dimensional change in the closed H-guide resonator.

6.7 Basic Loss Factors

As indicated in Section 6.6 the experimental value of the surface loss parameter was larger than predicted by theory for the conventional resonator. Using the value found experimentally (0.072 ohms) and experimentally measuring the Q-value of the closed H-guide resonator with a Lucalox dielectric strip (0.05 cm thick), the loss tangent for the dielectric was found to be 1.9×10^{-3} at 34.6 GHz. This value is much in excess of the manufacturers' specifications at 1 GHz (loss tangent equal to 0.25×10^{-4}). A second dielectric (1422 Rexolite, American Enka Corporation) strip was used which had a thickness of 0.084 cm and a permittivity of 2.54.

The measured value of the loss tangent was 1.4×10^{-3} at 34.6 GHz (manufacturers' value was 0.7×10^{-3}). A solid block of Rexolite was placed in the conventional resonator and again the loss tangent was determined. The loss tangent of the solid block was 1.1×10^{-3}. Although there exists a difference, surface films on the strip can contribute to the losses and thus increase the loss tangent. Other experimenters[1] have found the loss tangent of Rexolite to be in the neighborhood of 1.2×10^{-3}. There were no solid blocks of Lucalox available for making loss tangent measurements, therefore the loss tangent of Lucalox was accepted as 1.9×10^{-3}.

The possibility of additional losses in the coupling holes was considered also. The losses related to the coupling holes were so small that it was not feasible to measure the contribution quantitatively.

The Q of the closed H-guide resonator can be rewritten as

$$\frac{1}{Q_{total}} = \frac{1}{Q_s} + \frac{1}{Q_t} + \frac{1}{Q_e} + \frac{1}{Q_d} \qquad (6.14)$$

where Q_s = side wall Q-value,

Q_t = upper and lower wall Q-value,

Q_e = end plates Q-value,

Q_d = dielectric strip Q-value.

---

[1]Personal communication with Ray Johnson.

Based on the following values (Lucalox strip)

$$\varepsilon_r = 9.9,$$

$$2d = 0.05 \text{ cm},$$

$$\tan\delta = 1.9\text{x}10^{-3};$$

surface loss parameter = 0.072 ohms,

the following Q-values were found for the quasi TE_{119} mode:

$$Q_t = 269{,}900 , \tag{6.15}$$

$$Q_e = 72{,}180 , \tag{6.16}$$

$$Q_d = 37{,}320 , \tag{6.17}$$

$$Q_s = 17{,}630 , \tag{6.18}$$

$$Q_{total} = 9{,}895 . \tag{6.19}$$

From this it is evident that the major contribution to the losses results from the side walls.

If the surface of the side walls is altered, then the only individual Q-value to change would be that of the side walls. Then from an experimentally measured Q_{total} of the closed H-guide resonator the change of the Q_s of the side walls can be found. The following relation was employed for determining Q_s of the side walls:

$$\frac{1}{Q_s} = \frac{1}{Q_{total}} - \frac{1}{Q_t} - \frac{1}{Q_e} - \frac{1}{Q_d} . \tag{6.20}$$

When (6.15) through (6.17) are used in (6.20) the equation becomes for the quasi TE_{119} mode

$$Q_s = \frac{Q_{total}}{1 - .444\, Q_{total}\, 10^{-4}} \tag{6.21}$$

where Q_{total} is the measured Q-value. The same procedure was followed for the conventional resonator and for the TE_{119} mode

$$Q_s = \frac{Q_{total}}{1 - .302\, Q_{total}\, 10^{-4}} \quad . \tag{6.22}$$

6.8 Data Evaluation and Representation

Specific methods of data evaluation and representation were developed tailored to the project. The evaluation was carried out to derive the most important data relevant to those measured in the other phases of the study. The representation of the results was done in a form most useful to the reader. For example, the representation permits comparison of data for walls prepared in different ways as well as for slight material differences. Optical reflectance measurements were used to determine the statistical parameters of the rough surfaces. The reflected intensity normalized with respect to the intensity with the angle of reflectance equal to the angle of incidence was considered an appropriate measure of "roughness" when plotted as a function of the angle of reflectance. From a plot of the normalized reflected intensity versus angle of reflectance, the angular spread was measured as the angular difference between points for the magnitude of the reflectance of 0.6 of the maximum value. This is illustrated in Figure 6.10. It was shown theoretically in Section 3.3 that such normalization would give a

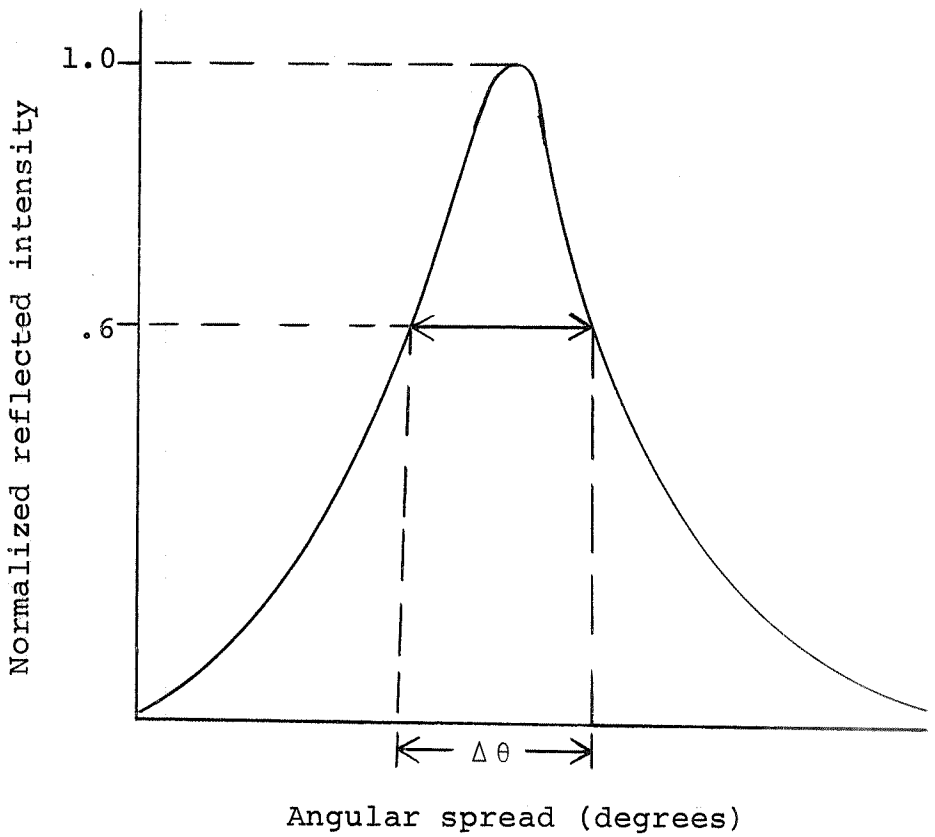

Figure 6.10. Normalized reflected intensity as a function of angular spread

reflectance formula dependent on only one of the statistical parameters of the surface, namely the correlation factor β. Therefore using (3.24), the value of β could be determined from the angular spread. Also by use of the curve in Figure 4.26, and use of the reflected intensity data, a rms height variation could be determined.

The relative changes in surface losses were determined by Q-value measurements of the resonators. To improve the repeatability of the Q-value measurements, the structure described in Section 6.2 was designed. This arrangement allowed for easy removal and reliable reassembly of the side walls. Thus the Q-value measurements (Q_{total}) took into consideration only changes in the Q of the side walls. This Q of the side walls denoted by Q_s was found from the Q_{total} by use of (6.21) or (6.22); the choice was governed by the type of the resonator used. The closed H-guide resonator was used because of the reduction of possible losses at the interface of the upper a lower walls with the side walls. The conventional resonator was then used as a check to verify the indications of loss variations with "roughness" as determined by the closed H-guide resonator. Two sets of walls could have slight material difference, therefore, a normalization process was used in order that the two sets of data could be compared. The normalization process had the additional feature that it gave a relative change of Q_s to the maximum Q_s-value. Recalling that the Q_s-value was

inversely proportional to the surface losses and using the assumption that the stored energy remains constant, the reciprocal of the values of the normalization gives the relative change in the surface loss to the minimum surface loss. To illustrate the normalization process, arbitrary points as would be typical of measured values on two sets of surfaces are shown in Figure 6.11 for the Q_s-values as a function of the angular spread. Once the data points were plotted, a curve was drawn through the points of each data set (one side wall set) and extended to intersect the vertical axis (corresponds to $\Delta\theta=0$). This intersect was then used as the maximum Q_s-value and all data used for that curve was normalized with respect to that maximum Q_s-value. Therefore two different sets of side walls could be compared by this technique. The result of the normalization is illustrated in Figure 6.12 and thus shows how the data then compare.

6.9 Q Measurements of the Side Walls

A series of experiments was made using both the conventional and the closed H-guide resonator configurations. The results for various surface finishes are given in Table 6.1 and 6.2. The values of Q_{total} were measured as described in Sections 6.4 and 6.5. The values of Q_s were calculated by use of (6.21) and (6.22). The angular spread was taken from the optical measurements and was the angular displacement

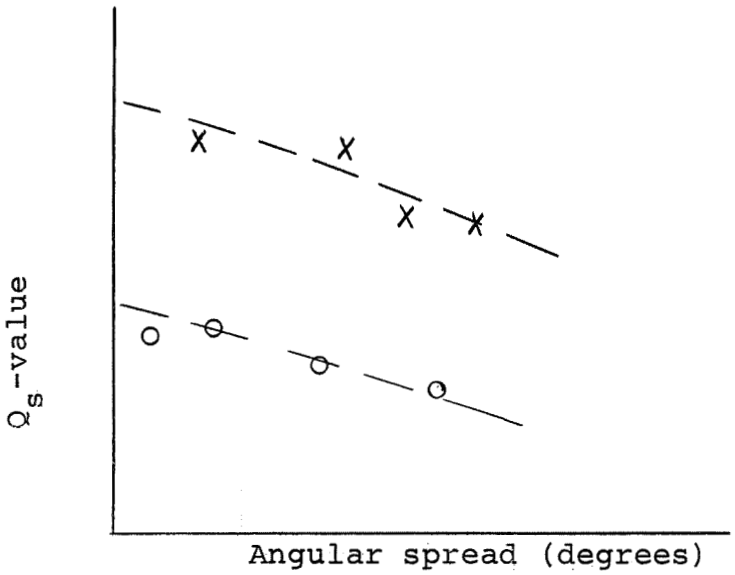

Figure 6.11. Typical Q-values of the side walls plotted for corresponding angular spread

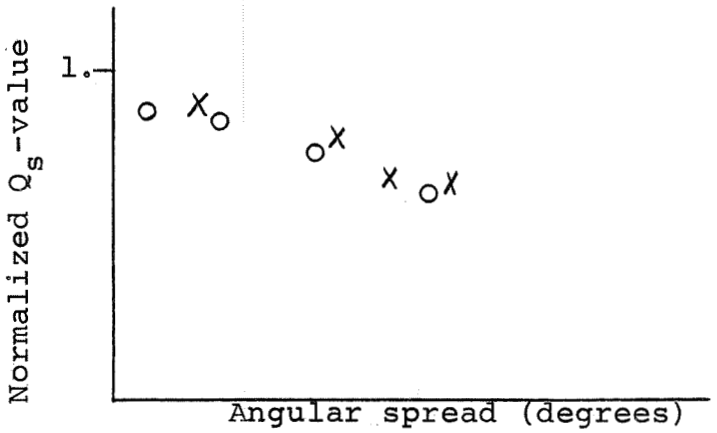

Figure 6.12. Normalized Q-values of the side walls versus angular spread

Table 6.1 Tabulated experimental results of the conventional resonator

Wall set	Data point	Angular spread	Q_u	Q_s	Normalized Q_s
1	C-1	2.50	9961	14247	0.996
1	C-2	7.50	10021	14370	1.005
1	C-3	39.50	9685	13689	0.957
1	C-4	21.50	9909	14141	0.989
1	C-5	40.50	9357	13043	0.912
1	C-6	3.25	10279	14906	1.042
1	C-7	8.50	9930	14184	0.992
1	C-8	28.00	9195	12730	0.890
1	C-9	44.25	9095	12452	0.871
1	C-10	2.25	9614	13547	0.947
1	C-11	8.75	9569	13458	0.941
1	C-12	26.25	9137	12619	0.884
1	C-13	24.50	9150	12644	0.884
1	C-14	38.00	9161	12665	0.886
1	C-15	35.50	8727	11850	0.829
2	C-16	13.00	11405	17397	0.967
2	C-17	25.25	11321	17202	0.955
2	C-18	38.00	11045	16573	0.921
2	C-19	39.50	10510	15397	0.855
2	C-20	40.00	10346	15048	0.836
2	C-21	15.00	11512	17647	0.980
2	C-22	13.00	11655	17986	0.999
2	C-23	18.00	10834	16103	0.894
2	C-24	36.00	10306	14963	0.831
2	C-25	35.00	10713	15837	0.879

Table 6.2 Tabulated experimental results of the closed H-guide resonator

Wall set	Data point	Angular spread	Q_u	Q_s	Normalized Q_s
2	H-1	2.00	9813	17376	1.007
2	H-2	21.00	9487	16379	0.950
2	H-3	24.00	9560	16598	0.962
2	H-4	37.00	8887	14669	0.850
2	H-5	31.75	9080	15203	0.881
2	H-6	3.00	9509	16445	0.953
2	H-7	14.25	8843	14550	0.843
2	H-8	28.25	9109	15284	0.886
2	H-9	39.00	8367	13305	0.771
2	H-10	3.00	9740	17148	0.994
2	H-11	9.75	9622	16786	0.973
2	H-12	31.25	9365	16019	0.929
2	H-13	21.75	9144	15383	0.892
2	H-14	28.75	9004	14991	0.869
1	H-15	5.00	8736	14262	1.004
1	H-16	5.25	8671	14090	0.992
1	H-17	14.00	8360	13287	0.936
1	H-18	21.25	8286	13036	0.918
1	H-19	37.25	7881	12116	0.853
1	H-20[a]	4.75	6944	16873	1.004
1	H-21[a]	6.50	6902	16639	0.990
1	H-22[a]	20.50	6870	16443	0.978
1	H-23[a]	17.50	6619	15075	0.896
1	H-24[a]	35.50	6522	14581	0.868

[a] Data points of the closed H-guide resonator with a Rexolite strip, all others with Lucalox strip

between the 0.6 points of the normalized reflected intensity curves.

In Table 6.1 the results of the conventional resonator are given for two different sets of side walls. Two sets of walls were used to check the consistency of the data. The characteristics of the two sets are slightly different as shown in Figure 6.13. The normalization as shown in Figure 6.14 was the result of taking the projected average Q_s for each set of walls at the zero scattering angle, $\Delta\theta=0$, and dividing the value into each Q_s (projected Q_s for first set of walls was 14,300 and 18,000 for the second set).

The results of Table 6.2 are based on two different closed H-guide resonators, one with a Lucalox strip and the second with a Rexolite strip. Each have the same resonant frequency with slightly different field constants (Lucalox α_x=1.36 per cm, k_x=21.7 per cm; Rexolite α_x=1.42 per cm, k_x=8.85 per cm). The resonator with the Lucalox strip was used with two different sets of walls. Again the difference in walls was observed as shown in Figure 6.15. Also shown on Figure 6.15 are the results of the Rexolite strip. The normalization of Q_s as shown in Figure 6.16 was carried out as for the conventional resonator (the averaged projected Q_s of the Lucalox resonator was 14,200 for the first wall set and 17,250 for the second wall set and for the Rexolite resonator, 16,800).

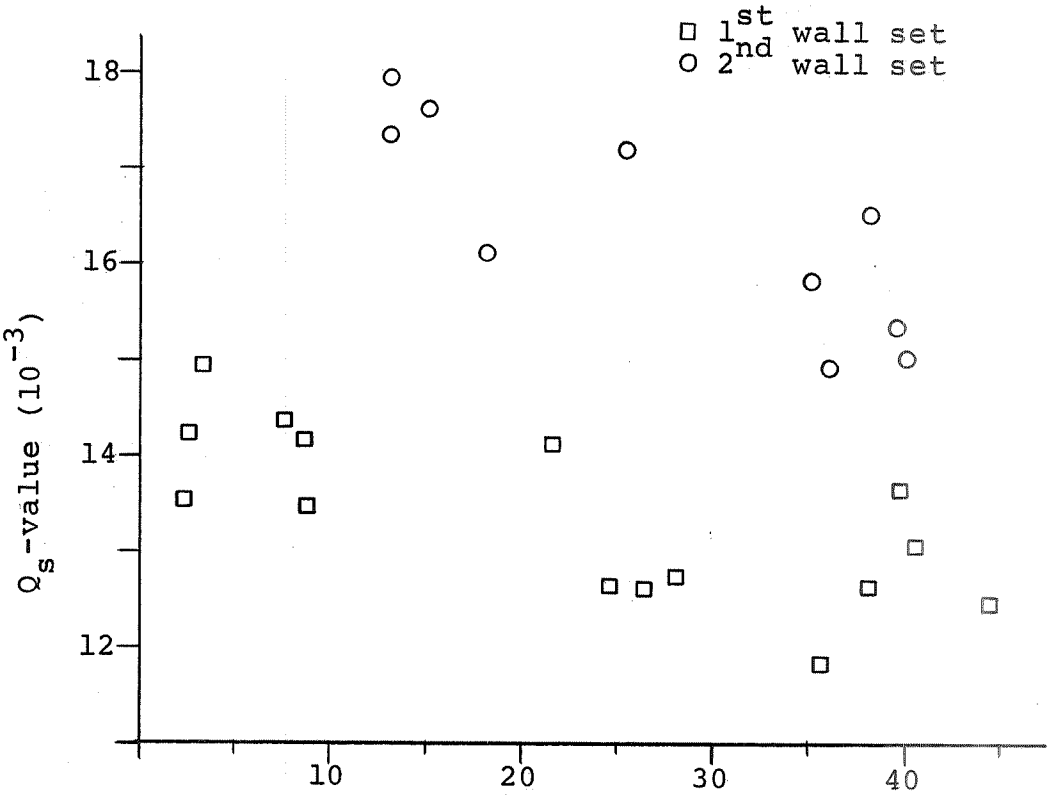

Figure 6.13. Q_s-values of the conventional resonator as a function of the angular spread

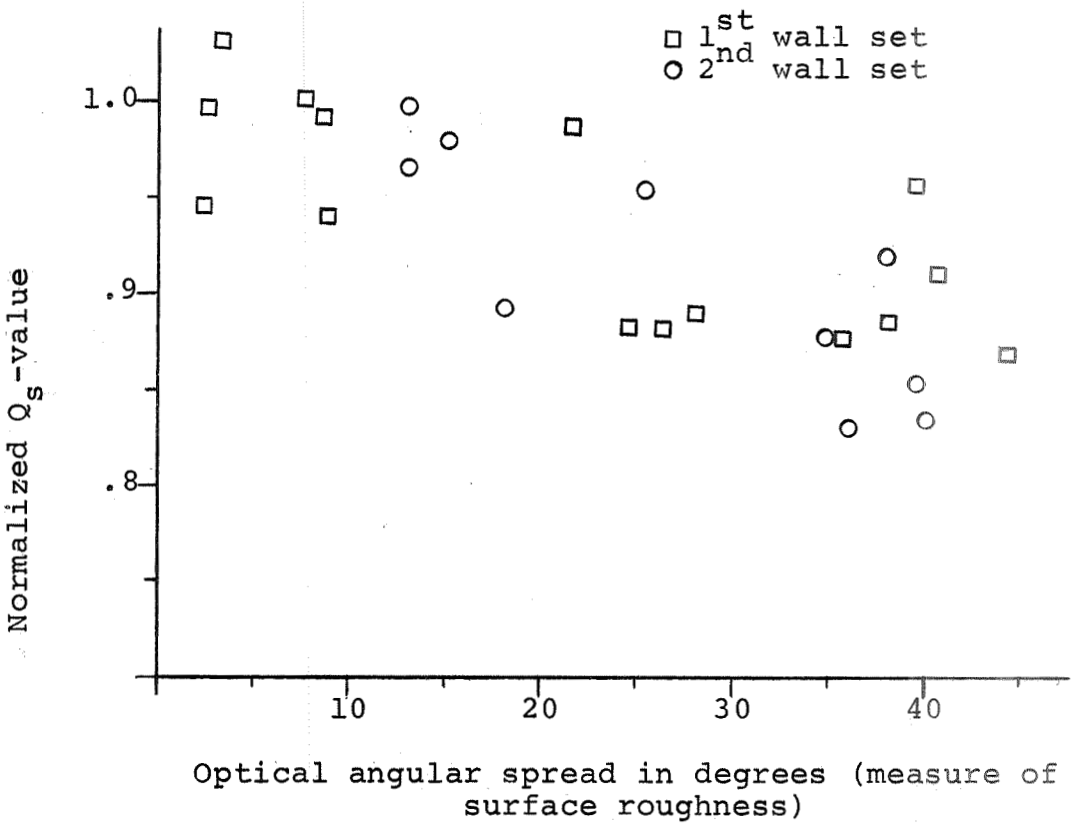

Figure 6.14. Normalized Q_s-values of the conventional resonator as a function of the angular spread

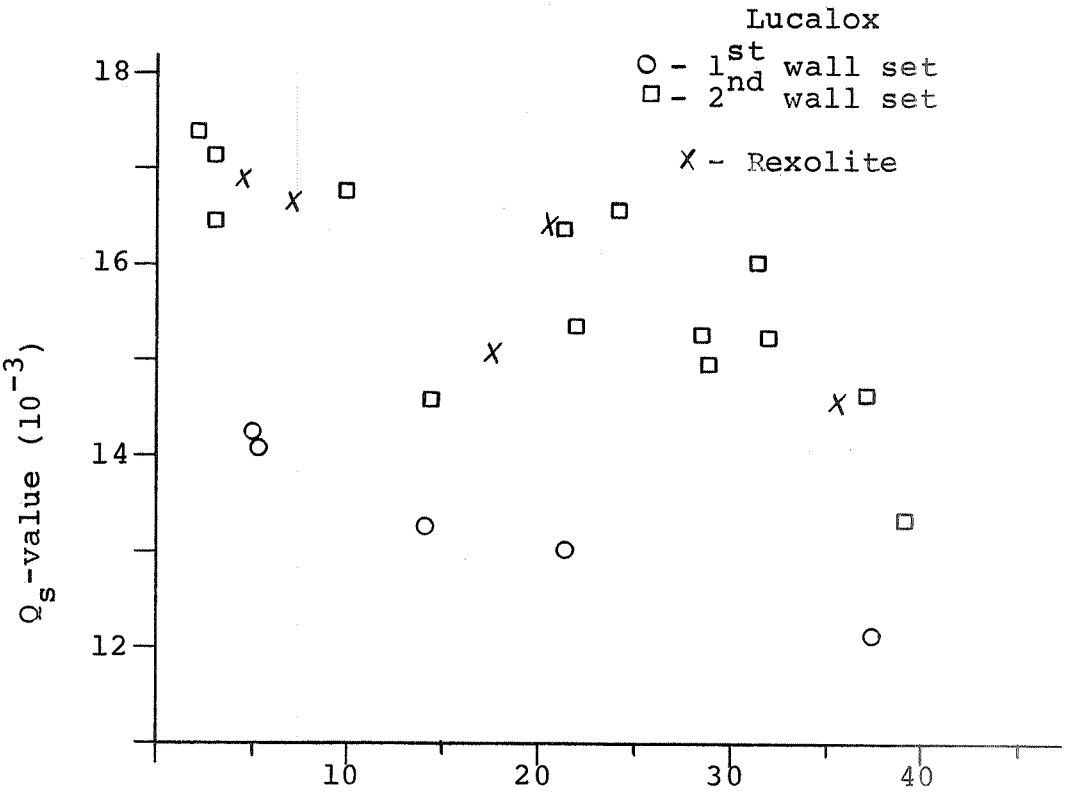

Figure 6.15. Q_s-values of the closed H-guide resonator as a function of the angular spread

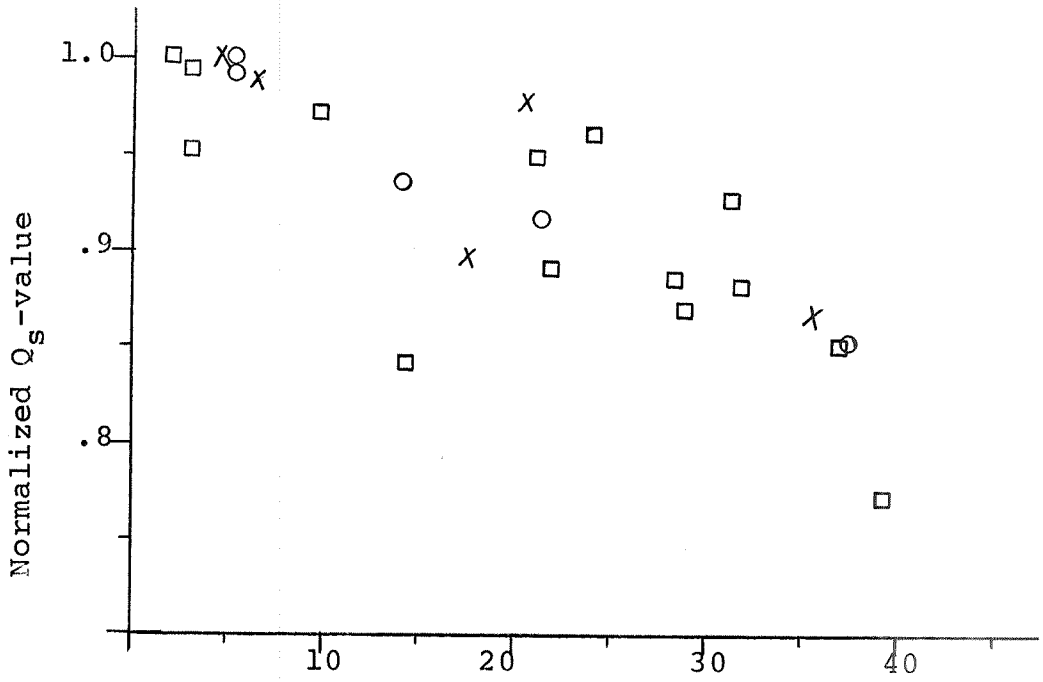

Figure 6.16. Normalized Q_s-values of the closed H-guide resonator as a function of the angular spread

The normalized results of Figure 6.14 and 6.16 shows the fractional decreases of Q_s for increasing surface roughness. Recalling that the Q-value is inversely proportional to the surface losses, the trend of Figures 6.14 and 6.16 indicate increasing surface losses with increasing surface roughness. The angular spread conversion to the correlation factor β is obtained through use of (3.24). The normalized Q_s as a function of β is shown in Figures 6.17 and 6.18.

From the normalized reflected intensity curves of Chapter 4, the correlation factor was found from the experimental data of the side walls. The graph of Figure 4.24 gives the reflected intensity (in volts and at the position $\theta=\psi$) as a function of $\sigma^2\beta$; therefore, by knowing the magnitude of the reflected intensity the rms roughness, σ, can be determined. The results of the data reduction is given in Table 6.3. The tabulated data were put in graphical form to illustrate the effects of each factor, Figures 6.13 through 6.22.

6.10 Mathematical Models

From Figures 6.14 and 6.16, the normalized Q_s showed a decrease with increasing angular spread. Mathematical models were proposed to illustrate the trend and to give the magnitude of the data scattering. Two models were considered, linear and exponential. The first model was the exponential

$$Q_{sn}(\gamma,\Delta\theta) = e^{-\gamma(\Delta\theta)^2} \qquad (6.23)$$

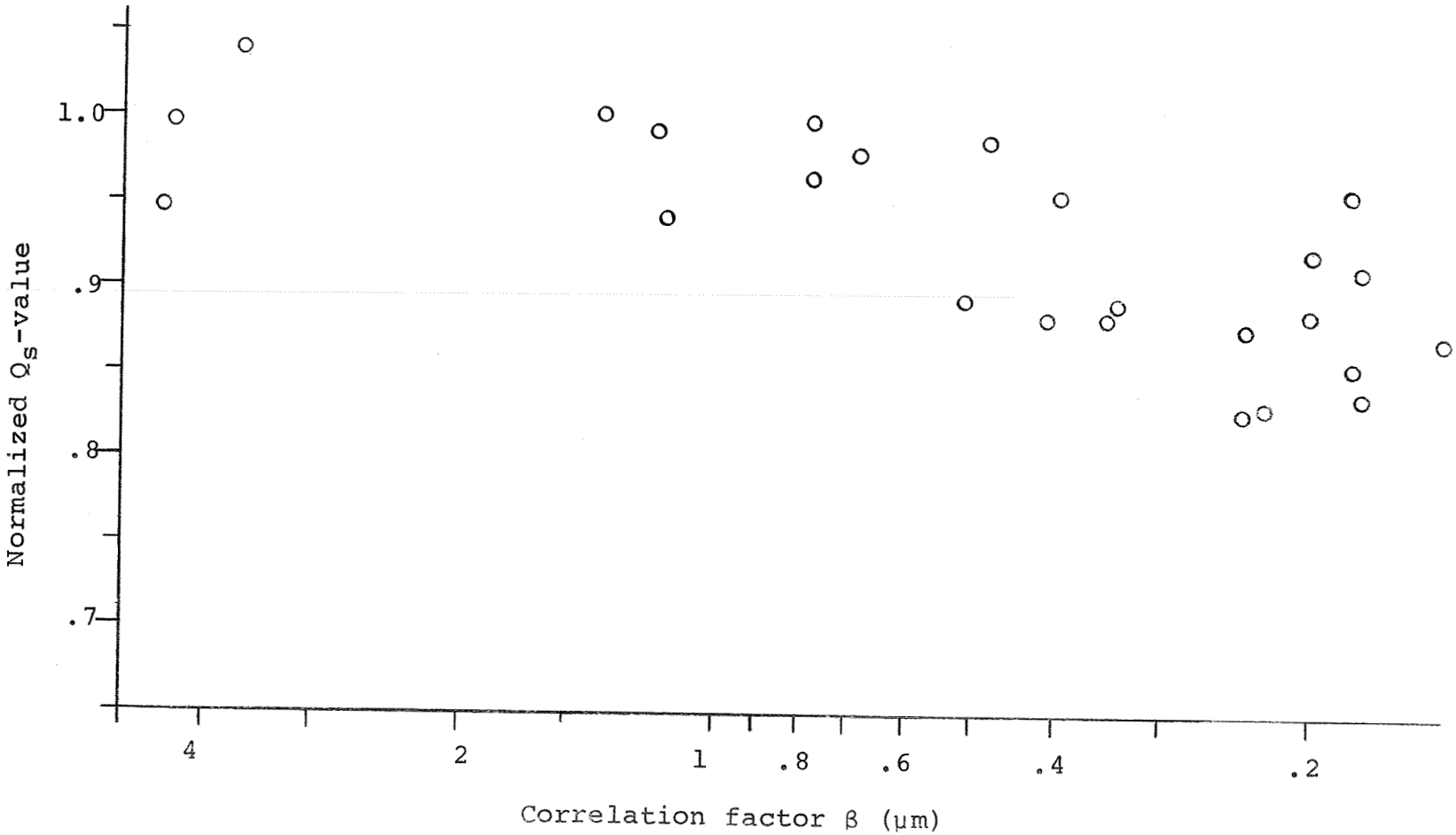

Figure 6.17. Normalized Q_s-values of the conventional resonator as a function of the correlation factor, β

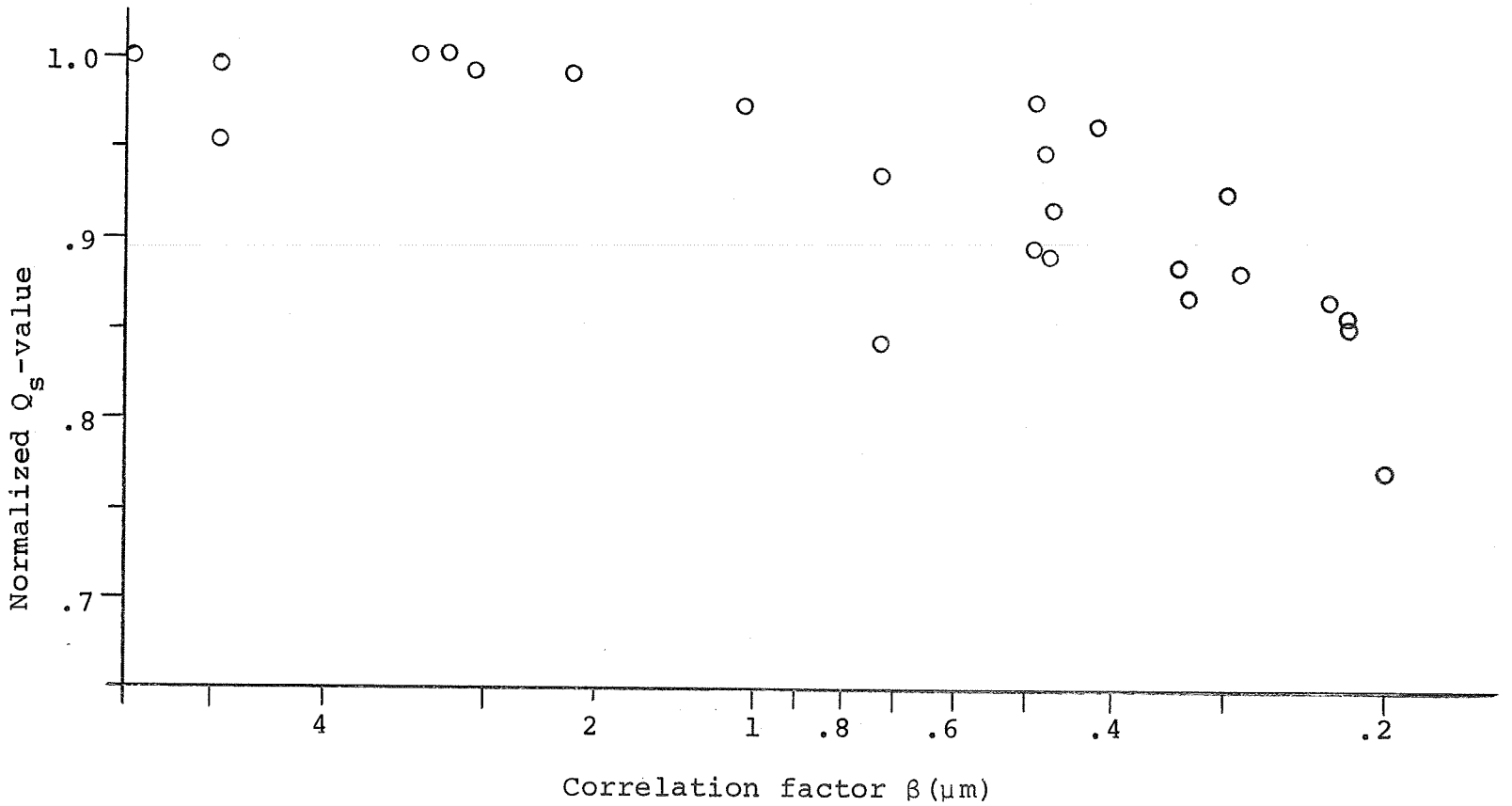

Figure 6.18. Normalized Q_s-values of the closed H-guide resonator as a function of the correlation factor, β

Table 6.3 Tabulated surface factors for the side walls of Tables 6.1 and 6.2

Data point	$\beta x10^{6}$ in m	σ $x10^{6}$ in m	σ^2 $\beta x10^{19}$ in m^3
C-1	4.370	0.870	33.07
C-2	1.360	0.972	12.84
C-3	0.180	1.394	3.50
C-4	0.470	1.119	5.89
C-5	0.175	1.296	2.94
C-6	3.625	0.691	17.33
C-7	1.180	0.982	11.37
C-8	0.340	1.182	4.75
C-9	0.140	1.360	2.59
C-10	4.500	0.609	16.69
C-11	1.150	0.942	10.21
C-12	0.350	1.097	4.21
C-13	0.410	1.116	5.11
C-14	0.200	1.420	4.03
C-15	0.240	1.467	5.16
C-16	0.775	0.917	6.51
C-17	0.398	1.038	4.29
C-18	0.200	1.330	3.52
C-19	0.180	1.342	3.24
C-20	0.175	1.242	2.70
C-21	0.680	1.010	6.89
C-22	0.775	1.000	7.81
C-23	0.510	0.979	4.89
C-24	0.226	1.271	3.65
C-25	0.240	1.070	1.07
H-1	5.000	0.664	22.01
H-2	0.480	1.111	5.93
H-3	0.420	1.058	4.70
H-4	0.220	1.214	3.24
H-5	0.290	1.029	3.07
H-6	3.950	0.949	35.57
H-7	0.725	1.036	7.78
H-8	0.340	1.000	3.40
H-9	0.200	1.063	2.26
H-10	3.950	0.842	28.03
H-11	1.025	1.082	12.00
H-12	0.300	1.155	4.00
H-13	0.470	1.103	5.72
H-14	0.330	1.116	4.11
H-15	2.200	0.815	14.63
H-16	2.050	0.841	14.49
H-17	0.725	0.912	6.03
H-18	0.470	1.126	5.96

Table 6.3 (continued)

Data point	$\beta x10^{6}$ in m	$\sigma x10^{6}$ in m	$\sigma^{2}\ \beta x10^{19}$ in m^{3}
H-19	0.220	1.126	2.79
H-20	2.375	0.814	15.74
H-21	1.600	0.909	13.22
H-22	0.499	0.984	4.83
H-23	0.590	0.941	5.22
H-24	0.230	1.063	2.60

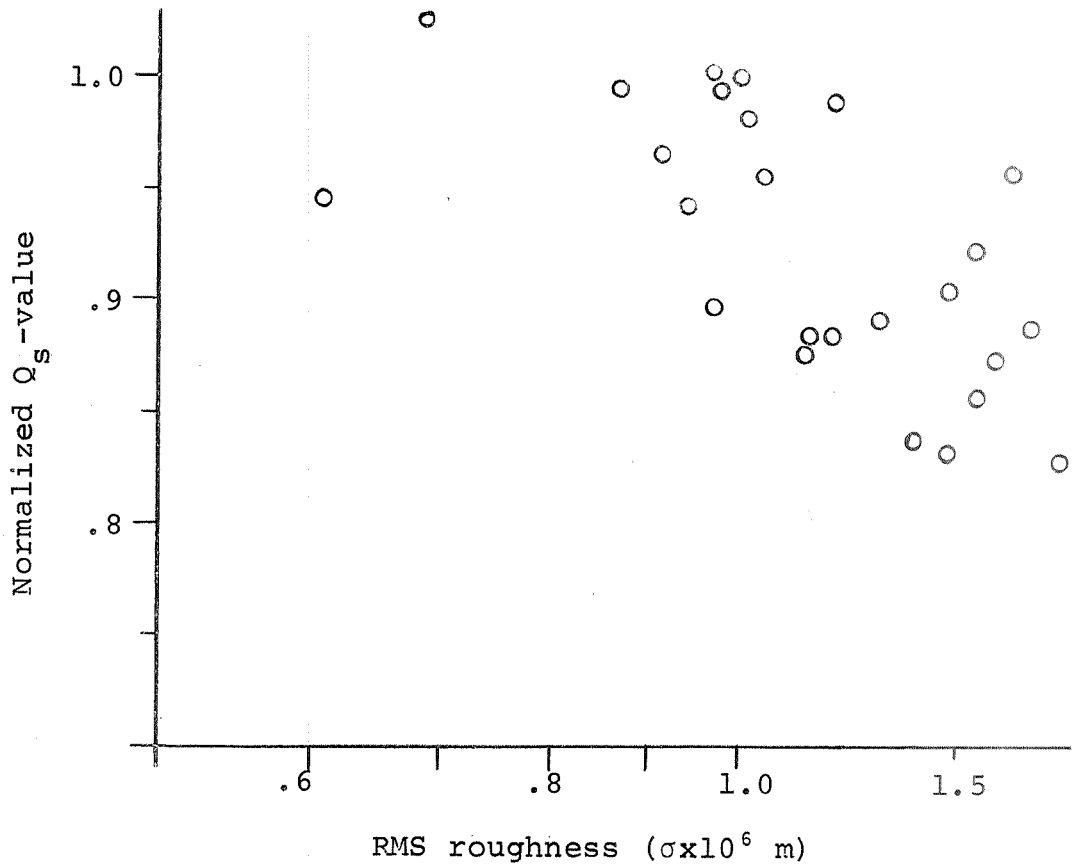

Figure 6.19. Normalized Q_s-values of the conventional resonator as a function of the rms height variation, σ

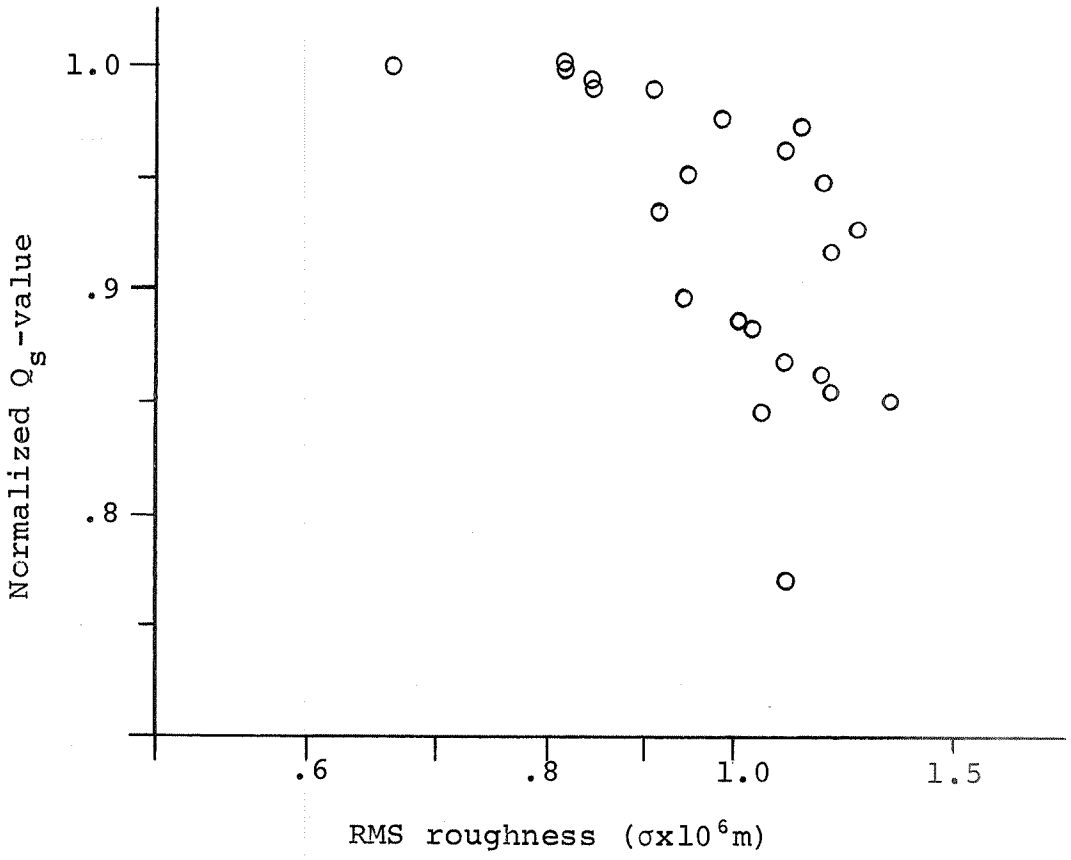

Figure 6.20. Normalized Q_s-values of the closed H-guide resonator as a function of the rms height variation, σ

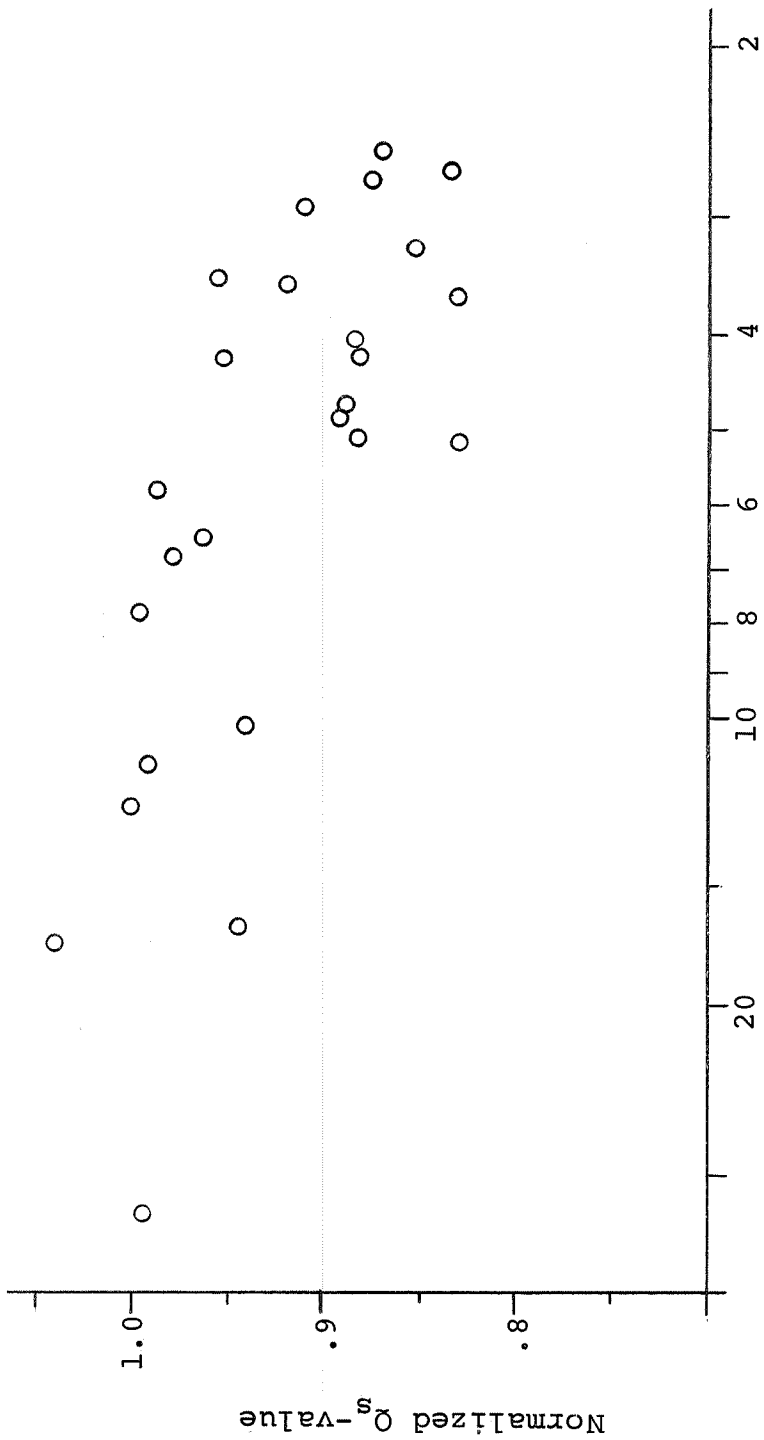

Figure 6.21. Normalized Q_s-values of the conventional resonator as a function of the surface parameter, $\sigma^2\beta$

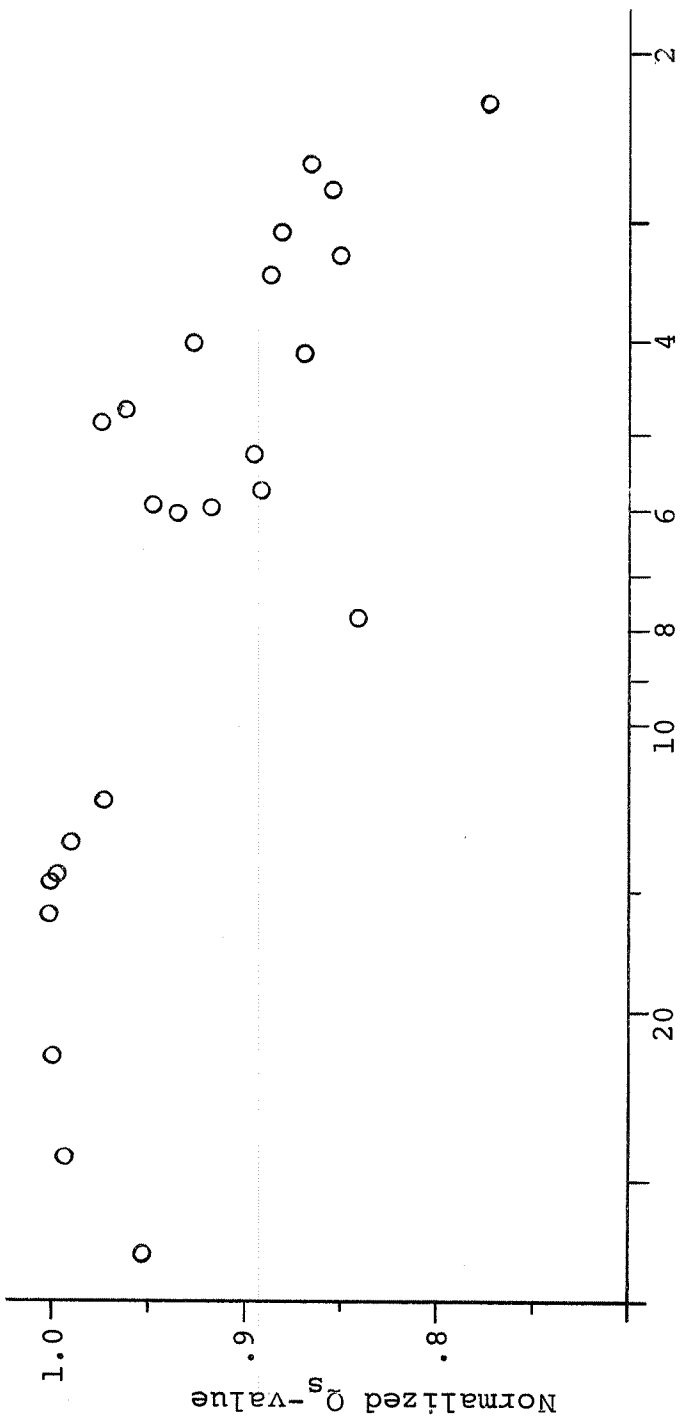

Figure 6.22. Normalized Q_s-values of the closed H-guide resonator as a function of the surface parameter, $\sigma^2\beta$

and the second was linear

$$Q_{sn}(m,\Delta\theta) = 1 - m\ (\Delta\theta) \qquad (6.24)$$

where γ and m are arbitrary constants used to match the data.

The procedure used to match the arbitrary constants to the data was to minimize the rms deviation. The form of the rms error deviation was

$$\text{rms error} = \left[\frac{1}{N}\sum_{i=1}^{N}\{M_i - Q_{sn}(\Delta\theta_i)\}^2\right]^{1/2} \qquad (6.25)$$

where N is the number of data points

M_i is the normalized Q_s at $\Delta\theta_i$

$\Delta\theta_i$ is the angular spread of the i-th datum point

Q_{sn} is the mathematical value for either the linear or the exponential function.

Different values of γ and m were substituted into (6.25) until the rms error was minimized, and then this value of γ or m was considered the best constant for the data.

Using this technique for determining the minimum rms deviation, the arbitrary constants for the conventional resonator were:

$\gamma = 0.92\text{x}10^{-4}$ per square degree with a standard deviation of 0.043, and

m = 0.0031 per degree with a standard deviation of 0.039.

For the closed H-guide, the results were:

$\gamma = 1.34\text{x}10^{-4}$ per square degree with a standard deviation of 0.039, and

m = 0.0039 per degree with a standard deviation of 0.036. As expected the closed H-guide resonator gave less scatter. The best mathematical representation for the data was the linear model for this range of angular spread.

From Figures 6.17 and 6.18 the normalized Q_s-values showed a decrease with decreasing values of the correlation factor β. A mathematical model was proposed to illustrate the trend and to give the magnitude of the data scattering. The model was

$$Q_{sn}(A,\beta) = 1 - e^{-A\,\beta^{1/2}} \qquad (6.26)$$

where A was an arbitrary constant used to match the data.

The procedure of minimizing the rms deviation was again used by the variable $\Delta\theta_i$ in (6.25) was replaced by β_i. Different values of A were substituted into the new expression for (6.25) until the rms error was minimized, and then this value of A was considered the best constant for the data.

Using this technique for determining the minimum rms deviation, the arbitrary constants were:

for the conventional resonator

$A = 3.88 \times 10^3$ per $m^{1/2}$

error = 0.036

for the closed H-guide resonator

$A = 4.62 \times 10^3$ per $m^{1/2}$

error = 0.044

However if several points which appear to be separated from the trend of the data are removed the resulting trend

for the two resonators are in better agreement. The following data points were discarded: C-3, C-5, C-9, C-18, H-6, H-7, and H-9. The minimization of the rms error procedure was repeated with the following results:

for the conventional resonator

$A = 4.11 \times 10^3$ per $m^{1/2}$

error = 0.033

for the closed H-guide resonator

$A = 4.06 \times 10^3$ per $m^{1/2}$

error = 0.022

The difference between the two mathematical models for this relationship of Q_s and the correlation factor is insignificant and the results can be considered the same if the above mentioned data points are removed.

6.11 Effects of Electrolytic and Chemical Polishing

There are many methods and chemical solutions used for electrolytic polishing. The solution used in this investigation was orthophosphoric acid diluted with water until a specific gravity of 1.35 was obtained. The displacement between the cathode and anode (surface to be polished) was approximately 2.5 cm. The polishing duration was two minutes at five volts and one-half of an ampere. This condition resulted in excessive pitting of the surface (referred to as "orange peel" in the literature). A copper sheet perforated with 5 mm diameter holes was placed one centimeter in front

of the surface to be polished and with this arrangement the "orange peel" disappeared. Using this arrangement for electrolytic polishing, the following procedure was used. First the surface of the side walls were polished with the abrasive papers as described in Section 4.2. The Q of the resonator with the side walls in place was measured; then the side walls were electrolytically polished, and the Q-value measurement repeated. The results for several cases are given in Table 6.4. The normalized results are superimposed on the accumulated results of Section 6.9 where the solid line connects the results before and after electrolytic polishing (Figure 6.23 and 6.24).

The optical measurements of the surface parameters after electrolytic polishing cannot be considered as reliable (although the results appear to be very good) as that obtained after mechanical plishing. Although the electrolytic polishing leaves visible parallel grooves, the chemical reaction at the boundaries of the copper grains create variations or grooves transverse to the mechanically created grooves. Thus, a portion of the reflected light is scattered in all directions but the majority is still reflected in the same direction as in the case of the mechanical polishing.

Attempts at chemical polishing were not successful. Chemical reaction with the surface was very rapid and difficult to control. The results gave a pitted surface similar

Table 6.4 Tabulated results of Q-value measurements illustrating effects of electrolytic polishing

Polished	Data point	Angular spread	Q_u	Q_s	Normalized Q_s
MECH.	HP-1	17.50	6050	8272	0.827
ELECT.	HP-1	7.50	7219	10624	1.062
MECH.	HP-2	20.50	6510	9157	0.872
ELECT.	HP-2	7.00	7073	10311	0.982
MECH.	HP-3	3.00	6627	9390	0.939
ELECT.	HP-3	2.25	7358	10928	1.090
MECH.	CP-1	20.50	9581	13482	0.843
ELECT.	CP-1	7.00	11108	16715	1.045
MECH.	CP-2	17.50	9455	13234	0.792
ELECT.	CP-2	7.50	10881	16207	0.970
MECH.	CP-3	2.25	10155	14647	0.915
ELECT.	CP-3	2.00	11099	16695	1.043

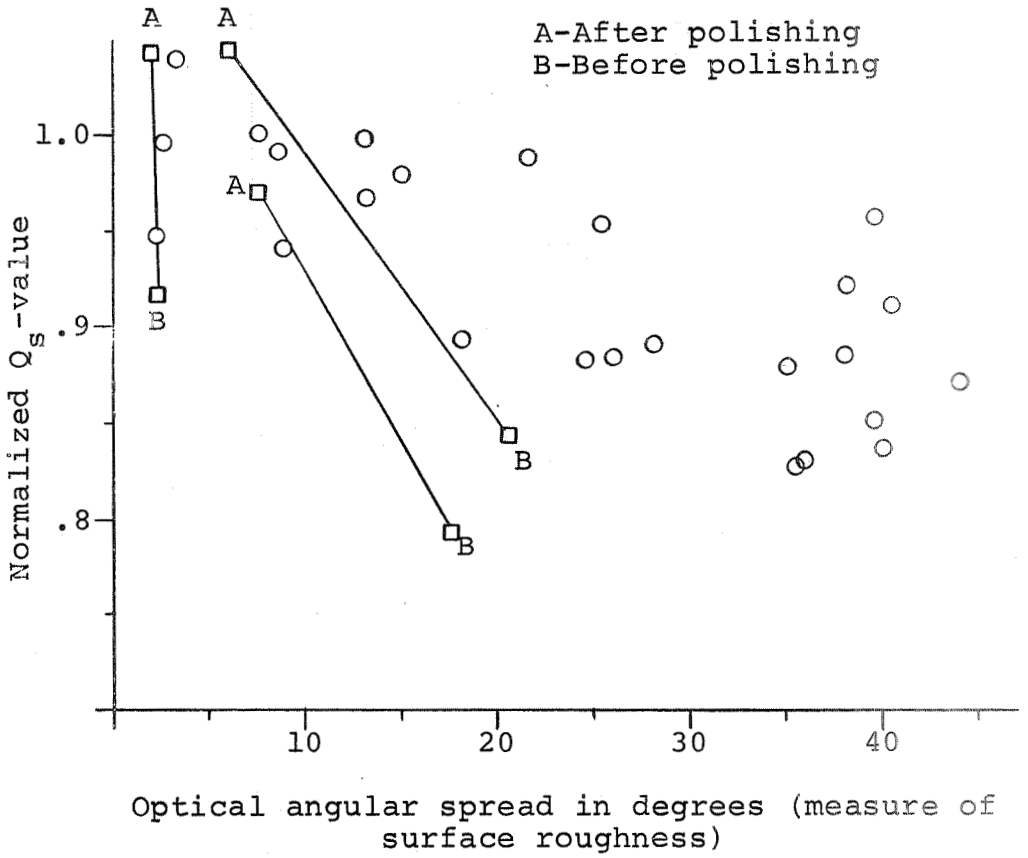

Figure 6.23. Effects of electrolytic polishing on the normalized Q_s-values for the conventional resonator

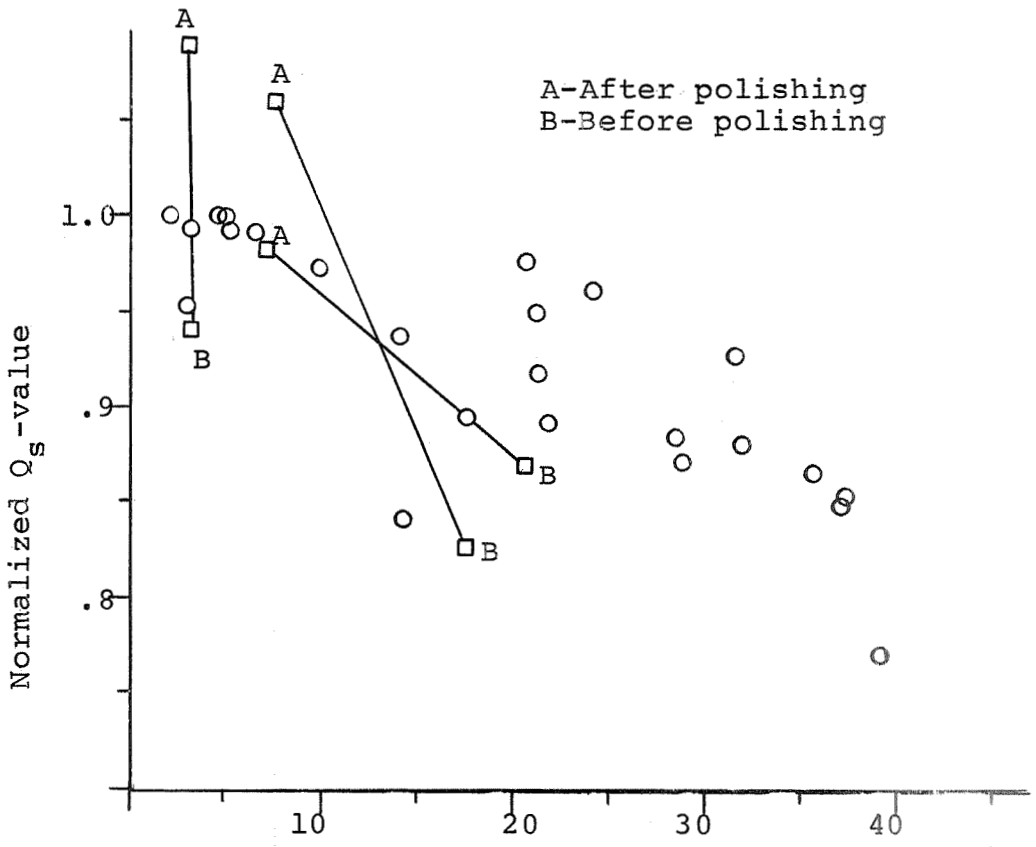

Figure 6.24. Effects of electrolytic polishing on the normalized Q_s-values for the closed H-guide resonator

to the "orange peel" of the electrolytic polishing and the rapid etching of the surface left large separations between the side walls and the end plates. This resulted in unreliable values of Q; therefore, chemical polishing was abandoned.

7. CONCLUSION

7.1 Discussion

The technique developed for optical measurements gives an excellent scheme for determining the statistical parameters of a rough surface. When the parameters were taken from a rough copper surface and used in the theoretical derivation, the agreement with the measured reflected intensity was very good. The quality of the model for predicting reflectance decreases as the rms height variation increases (note Figure 4.20). Therefore the results given for small values of the correlation factor β are not as accurate as for the larger values.

The theoretical surface model was a flat, one-dimensional rough surface and the derivation of the reflected intensity was limited to small height variations. Although this may seem of rather limited use, most practical waveguides or other machined surfaces polished by abrasive paper techniques leave the surface with small, parallel grooves. Therefore for such surfaces, this technique gives an easy, nondestructive method for reliably measuring the parameters of surface roughness.

Although not the principle intent of this investigation, several areas gave new and interesting results. The H-guide resonator was shown to have a lesser number of excited modes than the conventional resonator. The reduction of modes is

directly related to the thickness of the dielectric strip present in the H-guide resonator. The H-guide resonator had the additional feature that the magnetic field intensity normal to the dielectric strip is identically zero; thus no current flows across the mating sections. The uncertainty of the measurements is therefore reduced. The exponential decrease of field strength with the normal distance from the dielectric strip gave a large reduction of power flow at the upper and lower walls of the closed H-guide resonator. The power flow reduction gave a lesser possibility of leakage and disturbance at these walls.

The data from the closed H-guide had less scatter, indicating that removal and replacement of the side walls produced less effects than for the conventional resonator. Another possibility for data scatter was the variation of side wall positioning but this was minimized by the procedure outlined in Section 6.2. Chemical films were also known to affect the surface losses but the same cleaning procedure was followed for each experiment so that the effects of the chemical films remained constant. Filling the cavity with dry nitrogen eliminated atmospheric effects and the effects of water vapor. Results of electrolytic polishing showed that the normalized Q_s-values with an electrolytic polishing film present on the side walls were larger than those of water washed walls with similar surface roughness. This was

expected since the walls dipped in the electrolytic solution gave Q-values of approximately five per cent higher than the water washed walls. This is in agreement with the results shown in Figures 6.23 and 6.24.

The results of the closed H-guide resonator measurements gave the clearer indication of the effects of the surface parameters. As a result of this investigation, the surface losses appear to be highly dependent on the correlation factor β. The Figures 6.19 and 6.20 show too much scatter to give any conclusive indication of dependence of surface losses on the rms height variations.

As for further studies it is recommended that investigations be carried out to determine the effects at higher frequencies. Also of interest would be the effects of frequency on losses for a given roughness. The investigation presented was limited to frequencies near 35 GHz. Another area of extreme importance is the effect of chemical films on the surface properties. It would be of interest to determine if the power losses due to chemical films change with either increasing frequency or time.

7.2 Summary

In the study of surface effects on the losses in waveguides, reliable methods of measuring both surface roughness and losses are needed. Previous mechanical methods could not reliably measure rms height variations of the order of a

few microns. By use of a scattering theory, it was shown that light reflected from rough surfaces contains information that could be used to determine the statistical parameters of the surface. By the use of a laser beam and a light detector, a scheme was used to measure the reflected intensity of one dimensionally rough surfaces. It was shown by a microscopic examination of the surface that the statistical parameters could be reliably measured by the reflectance technique and were in agreement with a theoretical model based on the use of a Laplace correlation function.

The Q-values of resonators were measured to determine the change in losses for various surface roughnesses. A closed H-guide resonator was shown to have advantages, for a demountable resonator, over the conventional rectangular resonator. The surface irregularities were shown by Q-value measurements to have a great effect on surface losses. The rms height variation in the way of this evaluation did not show a distinct relationship to the Q-values. The correlation factor β on the other hand, produced a strong effect on the losses. Changes of 20 per cent in Q-values were noted for the "roughest" surfaces. The Q-value measurements were made for both types of resonators whose side walls were either mechanically or electrolytically polished.

8. LIST OF REFERENCES

1. Allison, J., and F. Benson. 1955. Surface Roughness and Attenutation of Precision-drawn, Chemically Polished, Electropolished, Electroplated and Electroformed Waveguides. Proc. I. E. E. 101 III:251-259.

2. Beck, A., and R. Dawson. 1950. Conductivity Measurements at Microwave Frequencies. Proc. I. R. E. 38:1181-1189.

3. Bennett, H. 1963. Specular Reflectance of Aluminized Ground Glass and the Height Distribution of Surface Irregularities. J. Opt. Soc. Amer. 53:1389-1394.

4. Bennett, H., and J. Porteus. 1961. Relation between Surface Roughness and Specular Reflectance at Normal Incidence. J. Opt. Soc. Amer. 51:123-129.

5. Benson, F. 1953. Waveguide Attenuation and its Correlation with Surface Roughness. Proc. I. R. E. 100 III:85-91.

6. Birkebak, R., and E. Eckert. 1965. Effects of Roughness of Metal Surface on Angular Distribution of Monochromatic Reflected Radiation. J. Heat Transfer 87:85-94.

7. Davies, H. 1954. The Reflection of Electromagnetic Waves from a Rough Surface. Proc. I. R. E. 101:209-214.

8. Gevers, M. 1951. Measuring the Dielectric Constant and the Loss Angle of Solids at 3000 Mc/s. Phillips Technical Review. 13 No. 3:61-70.

9. Hofman, H. O. 1924. Metallurgy of Copper. McGraw-Hill Book Company, Inc., New York.

10. Horner, F., T. A. Taylor, R. Dunsmuir, J. Lamb, and W. Jackson. 1946. Resonance Methods of Dielectric Measurements at Centimetre Wavelengths. J. Inst. El. Engrs. 93 III:53-68.

11. Kohl, G. L. 1949. The Principles of Metallographic Laboratory Practices. McGraw-Hill Book Company, Inc., New York.

12. Kuhn, S. 1946. Calculation of Attenuation in Waveguides. J. Inst. El. Engrs. 93 III A:663-678.

13. Lending, R. 1955. New Criteria for Microwave Component Surfaces. Proc. of the National Electronic Conference. XI:391-401.

14. Marcuvity, N. 1951. Waveguide Handbook. (Vol. 10, Massachusetts Institute of Radiation Laboratory Series). McGraw-Hill Book Company, Inc., New York.

15. Maxwell, E. 1947. Conductivity of Metallic Surfaces at Microwave Frequencies. J. Appl. Phys. 18:629-637.

16. Montgomery, C. G., R. H. Dicke, and E. M. Purcell. 1948. Principles of Microwave Circuits. (Vol. 8, Massachusetts Institute of Technology Radiation Laboratory Series). McGraw-Hill Book Company, Inc., New York.

17. Morgan, S., Jr. 1949. Effect of Surface Roughness on Eddy Current Losses at Microwave Frequencies. J. Appl. Phys. 20:352-362.

18. Newton, J., and C. L. Wilson. 1942. Metallurgy of Copper. John Wiley and Sons, Inc., New York.

19. Propst, R. H. 1967. A Study of H-Guides with Artificial Dielectrics. Unpublished Master thesis, Department of Electrical Engineering, North Carolina State University at Raleigh, Raleigh, N. C.

20. Rabinowicz, E. 1968. Polishing. Scientific American Vol. 218 No. 6:91-99.

21. Ramo, S., J. R. Whinnery, and T. VanDuzer. 1965. Fields and Waves in Communication Electronics. John Wiley and Sons, Inc., New York.

22. Stratton, J. A. 1941. Electromagnetic Theory. McGraw-Hill Book Company, Inc., New York.

23. Thorp, J. 1954. R. F. Conductivity of Copper at 8 mm Wavelengths. Proc. I. E. E. 101 III:357-359.

24. Tischer, F. J. 1953. A Waveguide Structure with Low Losses. Archiv der Elektrischen Ubertragung 7:592-596.

25. Tischer, F. J. 1959. Properties of the H-guide at Microwave and Millimetre-wave Region. Proc. I. E. E. 106 B Supplement 13:47-53.

26. Torrance, K., and E. Sparrow. 1965. Biangular Reflectance of an Electric Nonconductor as a Function of Wavelength and Surface Roughness. J. Heat Transfer 87:283-292.

A P P E N D I X

9. APPENDIX

A set of copper samples similar to those used in Section 4.4 were measured for rms height variations with a Profilometer (Bendix Corporation Type QB Amplimeter and Type LK Tracer). The samples were also measured by the optical technique. The results are tabulated below where β is the correlation factor and σ is the rms height variation.

Table 9.1. Comparison of Profilometer and optical results

Grade of abrasive paper	Profilometer rms values	Optical parameter σ	Optical parameter β
G-2	22-24 μ in.	51.0 μ in.	4.9 μ in.
G-1	17-19 μ in.	59.7 μ in.	3.9 μ in.
240	13-16 μ in.	40.4 μ in.	13.0 μ in.
320	13-16 μ in.	37.1 μ in.	14.2 μ in.
400	4-5 μ in.	35.4 μ in.	41.3 μ in.
600	4-5 μ in.	36.6 μ in.	49.2 μ in.

The Profilometer results indicate smoother surfaces than those obtained optically. This is expected since the Profilometer's needle, of which the up and down motion is used for measuring the rms value, would not be able to follow the surface profile at every point on the surface. The needle has a radius of 500 μ in. and for very rapid varying surfaces the needle could not reach the bottom of the grooves. A comparison of two surfaces which were observed and measured microscopically (data reduction from photographic enlargements) are as follows:

Table 9.2. Comparison of Profilometer and measured surface parameters

Grade	Profilameter rms	Photo rms	Optical rms	Optical β
G-1	17-20 μ in.	71 μ in.	118 μ in.	0.39 μ in.
240	15 μ in.	48 μ in.	44.9 μ in.	11.80 μ in.

The optical technique was known (see Chapters 3 and 4) to lose accuracy for very rough surfaces such as G-1 but the range is still good. For smoother surfaces such as 240 the results illustrate that the optical technique is very good. This result also indicates that the Profilometer does give smaller rms values than the actual values obtained from the surface measured microscopically. From these results it is evident that the optical technique developed for measuring surface parameters for the range of this study is an improvement over such devices as the Profilometer.